DEVELOPMENT AND OPTIMIZATION OF A THERMOLUMINESCENT DOSIMETER (TLD) ANALYZER SYSTEM FOR LOW-DOSE MEASUREMENTS UTILIZING PHOTON COUNTING TECHNIQUES

by

DONALD WADE HANNA

B.S., Kansas State University, 1978

A MASTER'S THESIS

submitted in partial fulfillment of the

requirements for the degree

MASTER OF SCIENCE

Department of Nuclear Engineering

KANSAS STATE UNIVERSITY
Manhattan, Kansas

1979

Approved by:

Major Professor

TABLE OF CONTENTS

TABLE OF CONTENTS (Continued)

LIST OF FIGURES

LIST OF FIGURES (Continued)

LIST OF FIGURES (Continued)

List of Tables

List of Tables continued

1.0 Introduction

As society progresses further into the nuclear age, it increasingly concerns itself with the effects of radiation and demands an effective means of monitoring it. In the area of personnel dosimetry, the photographic emulsion (the film badge) was long the mainstsy of the nuclear industry. Its dominion, however, is rapidly diminishing since the advent of thermoluminescent dosimetry. Thermoluminescent dosimeters (TLDs) are evoking this change because of the many advantages obtained through their use instead of film bsdges. Among these are dose range, precision, reproducibility, energy response, dosimetry information stsbility, and cost (1). With the continuation of this trend as motivation, the instrumentation and techniques detailed in this work were developed as a means by which the most popular TLD, LiF, could be used to make low-dose measurements with good accuracy and precision.

TLDs are dielectric crystals capable of storing the energy imparted to them by a radiation field and relessing this energy in the form of light when heated. The exact mechanisms involved in the thermoluminescence (TL) process are not presently fully understood although isolated phenomena hsve been successfully modeled. It is generally accepted that the interaction of ionizing radiation within the crystal produces free charges which become trapped. When the crystal is heated, these charges are freed from the traps which results in the emission of photons.

In all commercial TLD analyzer systems, the detection of TL is accomplished exclusively through the use of photomultiplier tubes (PMTs). The discrete nature of the PMT's signal allows two methods by which the signal can be measured; either integration of charge (dc method) or direct counting of charge pulses (photon counting). Both of these methods were recognized when the PMT was introduced some 40 years ago.

Photon counting has been utilized extensively in recent years for making low-level light measurements for a number of applications. It has seen only limited use, however, in conjunction with TL measurements. Most investigators involved in this area report that photon counting has significant advantages over the dc method for low-level light detection. Aitken et al. (2) illustrated the greatly reduced effect of large noise pulses and groups of time correlated pulses on the photon counting system they assembled for TL detection in archaeological pottery samples. However, Spanne (3), attempting to account for the differences in readout units, concluded that the precision of low-dose TL measurements could theoretically be improved by a factor of two utilizing photon counting techniques and demonstrated an experimental increase of a factor of only 1.4. A few investigators have reported on the performance of their photon counting TLD analyzer systems. Schneider et al. (4) reported that their system was linear over a wide exposure range extending to fractions of an mR. They used extremely large (370 mg) LiF crystals (TLD-100) and did not report quantitative data on reproducibility. Additionally, the pulse-height discriminator level in their system was adjusted to maximize

signal-to-noise ratio (SNR) with no consideration of system stability. Lasky et al. (5), through investigations with their photon counting TLD analyzer system, concluded that the use of photon counting permitted an order of magnitude improvement in SNR over dc techniques. Niewiadomski (6) reported that he was able to detect 0.5 mrad with a reproducibility of 30% utilizing LiF (TLD-100) high sensitivity ribbons, although his system's linearity extended to only 1 rad. This investigator recognized the importance of a highly stable apparatus but did not consider the adjustment of pulse-height discriminator or PMT applied voltage to optimize this, instead adjusting to maximize only SNR. Schlesinger et al. (7) compared the sensitivity and accuracy of a photon counting system and conventional dc system. They reported a standard deviation of 50% for their commercial dc system compared to 6% utilizing photon counting at an exposure of 25 mR and concluded that no quantitatively meaningful results could be obtained on the commercial system for exposures belows 20 mR. The techniques described in this work were developed to maximize both the stability of a photon counting TLD analyzer system and its sensitivity. Both are considered equally important since the maximization of only SNR leads to reduced system stability.

2.0 Theory of Thermoluminescence

2.1 Energy Deposition and Storage

The interaction of ionizing radiation in a crystalline material such as LiF induces a transfer of electrons from the valence band to the previously unpopulated conduction band. The number of electrons involved in this transfer is directly related to the amount of energy expended in the material by the incident radiation. In the specific case of gamma radiation, this ionization is primarily the result of Compton scatter, photoelectric absorption and pair production. The degree of ionization depends upon the energy of the gamma-ray, but each of these processes produce ionization and excitation in the crystal. The free electrons and holes produced by the interaction travel through the crystal until they either recombine or are trapped at some metastable state resulting from a lattice defect or impurity site. These trapped charges enable the crystal to record the passage of ionizing radiation.

2.2 Thermoluminescence

The classification of a material as a TLD is indicative that the radiation released charges remain trapped until the time at which the TLD is heated. Identically this requires that the trapping levels in the material be sufficiently deep within the crystal's forbidden region that thermal excitation at room temperature releases an insignificant number of trapped charges. As the temperature of the TLD is

elevated during the readout process, trapped charges are released which recombine to give up a portion of their excitation energy as photons. The basic mechanism involved in TL emission has been modeled by Randall and Wilkins (8). This model illustrates the dependence of photon emission from a heated crystal on the trap depth as well as temperature and heating rate. The application of heat to the crystal gives rise to a number of peaks in the glow curve (a plot of light output as a function of time or temperature). Each glow peak corresponds, in the simplest sense, to releases from traps residing at a certain energy level. Both the total TL emission and the height of the glow peak are proportional to the number of charge carriers liberated from the valence band during irradiation. It is the process of capturing these released charges which is important as the mechanism for such phenomena as nonlinearity, the sensitization factor, and the irradiation temperature effect of TL sensitivity (9). A typical glow curve for LiF (TLD-100) is shown in Fig. 1.

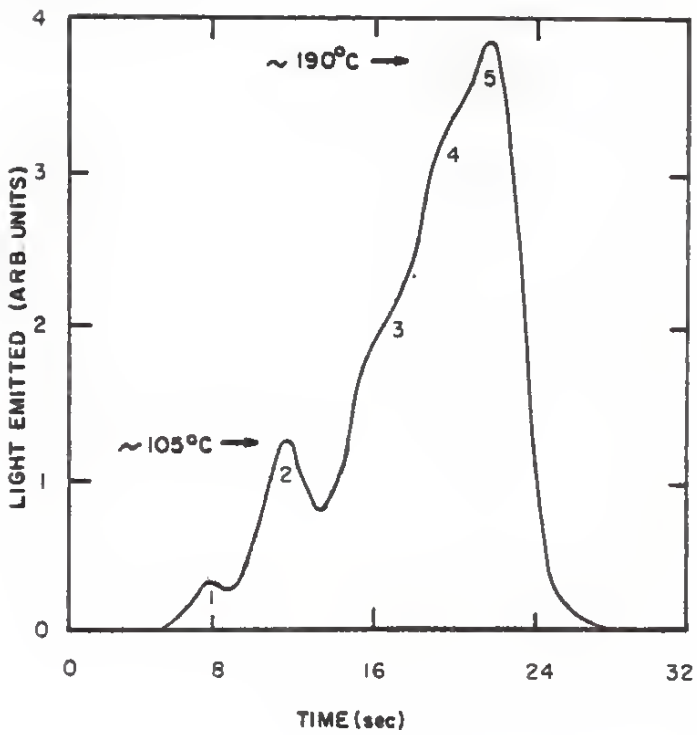

Fig. 1. Typical glow curve of LiF (TLD-100) immediately after irradiation illustrating the commonly identified peaks.

3.0 Measurement of Emitted Thermoluminescence

3.1 Detection of Light

The detection of light has long been an essential capability in such diverse areas as scintillation counting, archaeological dating, astronomical measurements, and thermoluminescent dosimetry. Because of the large differences in light characteristics encountered in these areas, a number of light sensitive devices have been developed. Many of these are unique detectors designed only to meet the requirements necessary to make a single type of measurement. It was the advent of the photoconductive device which introduced the technology required for the production of a number of these detectors such as the simple photodiode detector (10), the photoconductive multiplier (11), and the photosil detector (12). Virtually all of the available light sensitive devices do, however, have a common characteristic. Their operation is dependent upon the concept of the photon. It was the discovery of the photoelectric effect which provided the initial impetus for this description of light in the particle sense. It subsequently became the basis for Einstein's photoelectric equation (13). Despite this similarity in these detectors, they have little capacity for interchangeability because of their narrow scope of measurement capabilities. A notable exception is the photomultiplier tube (PMT). This light sensitive device exhibits relatively good sensitivity over a wide spectral range. By judicious choice of the materials used in its construction, its response can be well matched to the emission wave-

lengths of different light sources. Additionally, the wide dynamic range of the PMT permits measurement of light intensities which vary over several orders of magnitude.

3.2 Photomultiplier Tubes

3.2.1 General Characteristics

The PMT is a relatively simple device consisting of an evacuated chamber containing the photocathode, dynodes, an anode, and associated structural materials (see Fig. 2). The photocathode is the light sensitive portion of the PMT. It is manufactured of a photosensitive material which, through the photoelectric effect, emits electrons when illuminated by a photon source. Even though the photoelectric effect is a relatively efficient process on a per quantum basis, the primary photocurrent due to individual photon interactions is much too small for practical use. Hence, some means of electron multiplication is necessary. The dynodes in the PMT supply this amplification and are capable of producing electron gains of up to 10^6.

Dynodes consist of materials which emit several low-energy secondary electrons per incident primary electron. This secondary emission occurs in much the same manner as does photocathode electron emission. The difference between these two processes is that an impacting electron causes emission of dynode electrons rather than the interaction of an incident photon (14). If the electrons emitted from the dynodes have sufficient energy to overcome the work function (or electron affinity) of the surface, they are emitted into the vacuum of the PMT

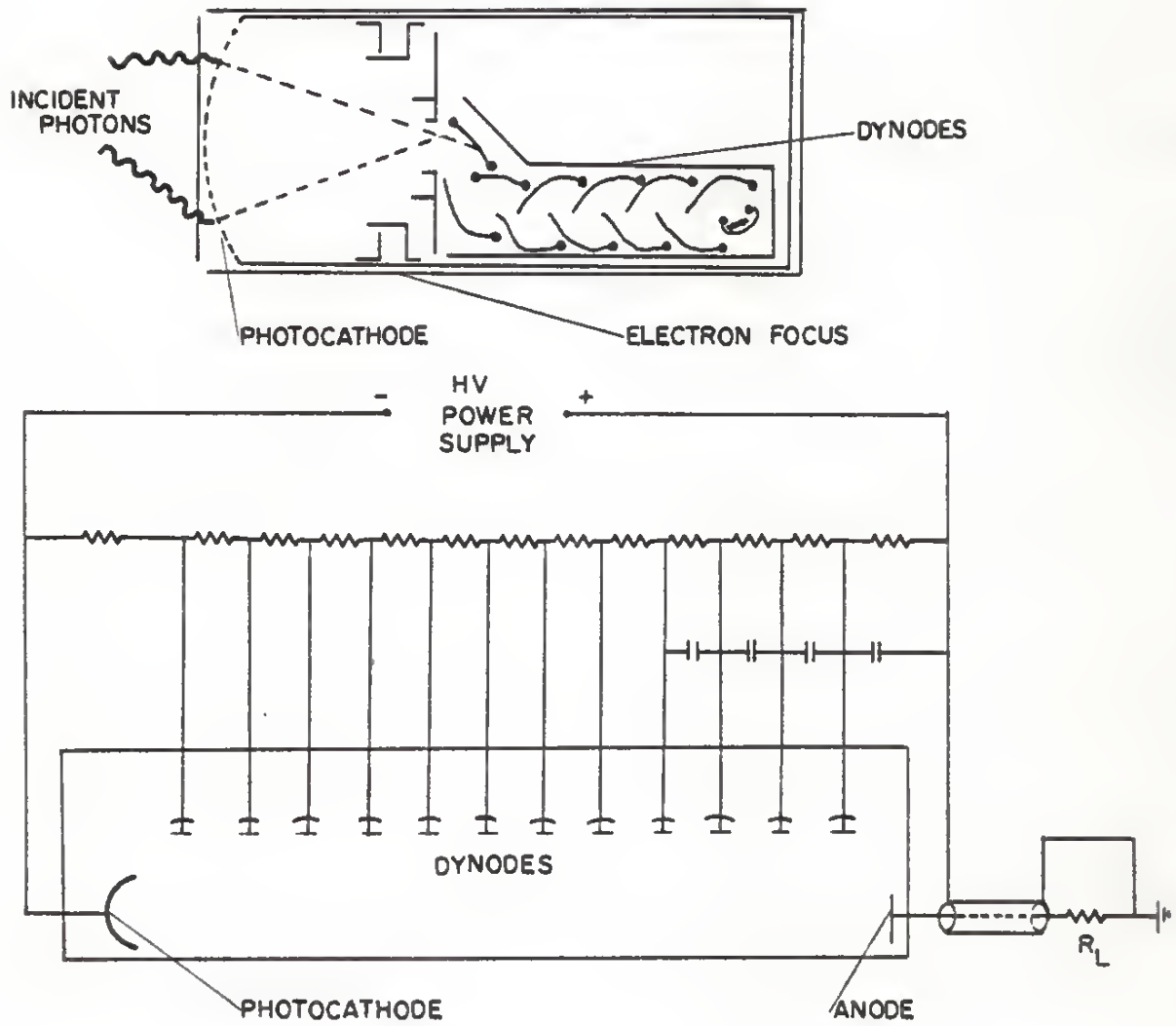

Fig. 2. Diagram showing the basic components of a PMT and its associated voltage divider network.

and accelerated by an electric field to the next dynode. This electric field is supplied by a voltage divider network. As shown in Fig. 2, this circuit consists of a series of resistances across which the PMT operating voltage is applied. The dynodes are held at increasingly positive potentials with respect to the photocathode. At the anode, the electrons are collected as a charge pulse which is then available as a signal for external instrumentation. Therefore, due to dynode induced internal electron multiplication, a photon incident on the PMT's photocathode produces a measureable charge pulse at the anode.

The amount of charge contained in each photon-induced anode pulse depends upon a number of parameters. Many of these are PMT-type dependent since they are related to the materials utilized in construction of individual PMTs. However, for a given PMT, it is important to consider the dependency of the charge pulse size on the PMT operating voltage. As this voltage is increased, two processes tend to produce an increase in the amount of charge contained in the output pulse. The first of these is an increase in the electron collection efficiency between dynodes. At low PMT voltages, electron gain is lost due to electron collisions with non-dynode structures. Electrons also skip dynode stages due to poor interdynode electric field focusing. These deleterious effects are minimized by increasing the PMT's voltage. The second effect is related to an increase in the average number of secondaries emitted from the dynodes per primary interaction. As the energy of this primary is increased, i.e., the accelerating electric field strength increased due to a higher PMT operating voltage, the number of secondaries

emitted tends to increase. Therefore, the charge pulse also increases in size. It would seem that, because of these two processes, the stability of a system utilizing a PMT would be highly dependent on the regulation of the high voltage power supply. In general, this is the case. However, once a sufficiently high voltage is reached, additional increases only slightly affect the size of the charge pulse. This occurs when the PMT voltage supplies sufficient electric field strength between the dynodes that an insignificant number of electrons are lost. Adding to this is the limitation which occurs concerning the number of secondaries emitted per primary interacting at the dynodes. For higher energy primaries, this number becomes relatively constant because their greater penetration depths decrease the probability that the secondaries produced reach the surface of the dynode to be emitted. These effects combine to establish what is referred to as the PMT voltage plateau characteristic.

In addition to the voltage/amplitude relationship discussed above, PMT output pulses also vary for a fixed value of high voltage. These output pulses exhibit a wide range of amplitudes because of the variance in the amount of charge contained in individual pulses. This arises primarily from the statistical nature of secondary emission from the dynodes, i.e., fluctuations in the number of secondary electrons emitted per incident primary (15). This provides for a definite distribution in the pulse-heights of photon-induced signals at the anode. This pulse-height distribution is also due in part to non-photon related pulses referred to as PMT dark noise.

3.2.2 Photomultiplier Tube Dark Noise

Dark noise refers to the signal emerging from the anode of an unilluminated PMT. Differentiation between this signal and the desired photon-induced signal is especially important in situations like low-dose TL dosimetry which require low-intensity light measurements. Under conditions such as these, it is imperative that the dark noise component of the PMT's output signal be minimized. Once this has been achieved, it is possible to establish improved sensitivity limits for the system. Many types of PMT dark noise arising from the mechanisms discussed in this section can be distinguished from the photon-induced output signal, thus presenting the possibility of their removal.

Thermionic emission of electrons from the photocathode and dynodes constitutes the major component of dark noise in the PMT's output signal (4,16). Since spontaneous emissions from the photocathode cannot be distinguished from emissions due to photon interactions, the resulting pulse at the output does not differ from a photon-related output pulse. Reduction in photocathode area and PMT cooling are techniques routinely used to diminish this type of dark noise. Unfortunately, even though PMT cooling reduces the number of thermionic emissions, it can have a detrimental effect on the spectral response of the photocathode. In some instances, cooling can reduce the PMT's quantum efficiency for a given source of photons to the extent that this reduction far outweighs any improvement in dark noise levels (16). Generally the best technique for dark noise compensation is some method of background subtraction, although cooling to moderate temperatures is often utilized. Electrons

are also emitted thermionically from the dynodes. The resulting output signals tend to be of lower amplitude than photocathode-related signals since they do not experience full dynode-chain multiplication. These pulses can be essentially eliminated from the output signal through the use of a lower level pulse-height discriminator. This is especially valid in PMTs utilizing high gain first dynodes.

A less important portion of the dark noise in a PMT is generated by a mechanism referred to as x-ray emission afterpulsing (17). Electrons which have been accelerated by the interdynode electric field can cause a soft x-ray to be emitted when they strike a surface such as a dynode or the anode. If this x-ray interacts with the photocathode, it can cause the emission of an electron. The result would be an output pulse indistinguishable from a photon-related signal. This type of dark noise increases with the number of electrons traversing the dynode chain, hence background subtraction, although somewhat helpful, is not entirely sufficient to eliminate it.

Ohmic leakage, another form of PMT dark noise, can pose a serious problem if PMTs are cooled far below room temperature or operated at extremely low voltages (14,15,16). It is, in fact, the predominant source of dark noise at low PMT operating voltages. However, at normal operating voltages, ohmic leakage is typically obscurred by other sources of dark noise and hence is an insignificant addition to the total dark noise. In general, the use of modern PMT sockets and cooling only to moderate temperatures reduce its effect. However, the collection of condensed water vapor, oil, dirt, or grease on the outside of the tube

can significantly increase its contribution. These leakage currents usually manifest themselves as very large pulses.

In poorly evacuated tubes, a portion of the dark noise may be generated by another mechanism referred to as positive ion feedback (17). This occurs when an electron traveling between dynodes ionizes a gas molecule in the PMT. The resulting positive ion accelerates in the opposite direction under the influence of the electric field striking either the photocathode or a dynode. This relatively massive ion can cause the emission of several electrons when it hits the surface. If this interaction occurs near the anode, the resulting pulse will be small. If, however, the interaction occurs near the photocathode, the resulting pulse will be very large. Hence, ion interactions produce output pulses with a range of amplitudes, some of which will be indistinguishable from photon-related signals. For this type of dark noise, both upper and lower level pulse-height discrimination would be beneficial.

In certain instances, the interaction of ionizing radiation can contribute a significant portion of a PMT's dark noise. Most glasses, e.g., that in the PMT glass envelope, contain naturally occurring ^{40}K. Radioactive decay of this isotope can produce dark noise pulses either by direct interaction of the beta-particles in the photocathode or indirectly by causing Cerenkov light, scintillations, or phosphorescence in the glass envelope (14,16). Cerenkov light flashes produced by cosmic rays can create a fundamental noise limitation on which PMT

cooling has no effect (18). Even though the cosmic-ray induced PMT pulse rate may be as low as 1 or 2 $cm^{-2}min^{-1}$, individual pulses may contain a charge which is hundreds of times larger than from a single photon-induced pulse. The large magnitude of these pulses results from the Cerenkov radiation being emitted within the resolving time of the PMT. Since cosmic rays are directed downward and Cerenkov radiation emitted in a cone about the direction of the radiating particle, their effect on a PMT's dark noise can be minimized by orienting the tube face down.

The major sources of PMT dark noise have been examined in this section. However, others do exist. For example, the dark-noise pulse rate can be much higher than necessary if the shield surrounding the PMT is at a different potential than the photocathode. This shield prevents leakage currents which would otherwise flow through the PMT's glass enevelope and produce instability or noise due to flourescence or corona discharge effects. It should be noted that, as in any electrical system, there are always large numbers of small amplitude pulses which can arise from stray electrical noise and from external amplifiers. For PMTs operated in the pulse mode, this is routinely eliminated using lower-level pulse-height discrimination.

3.3 PMT Signal Conditioning

3.3.1 Direct Current Technique

The most obvious way to relate the PMT's output signal to the incident light intensity is to convert the charge pulses to voltage

pulses and use conventional counting instrumentation. However, when one considers that 3×10^{14} photons cross one square centimeter of a typical laboratory work surface per second, it is apparent that moderate light levels would quickly saturate even the most advanced counting system. Due to the need for measurements at these levels of intensity utilizing PMTs, an alternate direct current (dc) method is usually employed. This technique can be understood by considering that the amplitude and duration of the charge-pulse from the PMT are largely dependent upon the characteristics of the electrical circuit connected to the output of the PMT. This external circuit can be intentionally designed to widen the output pulse, without changing the charge contained in the pulse, to the extent that a significant degree of pulse overlap occurs even at very low signal rates. The result is an electron current proportional to the incident light intensity. Usually this current is passed to a capacitor whose charge is then determined by a electrometer measurement of the capacitor voltage. The readout from such a system is, therefore, charge with units of some fraction of a coulomb.

From the previous discussion of PMT characteristics, it is apparent that PMTs will introduce several inherent inaccuracies in light intensity data when used with a dc-type system. Consider first that a current measurement is reflective of the charge contained in each pulse. As discussed earlier, these pulses have a definite distribution of amplitudes and hence each pulse, although corresponding

to a single photon, will contribute unequally to the total current. Thus, the dc measurement is not perfectly representative of the incident light level. Secondly, consider the dc measurement technique as applied to low-level light detection. Of obvious concern is the SNR. In this type system, pulse-height discrimination is not applicable. Therefore, it cannot be used to eliminate any portion of the dark-noise level. The SNRs obtained are not as great as if photon counting with pulse-height discrimination were utilized. Moreover, recall that the PMT dark noise spectrum contains a certain percentage of very large pulses. These pulses will contribute a disproportionately large amount of charge to the dc measurement. Although current suppression circuits can be utilized to negate a constant value of the dc (essentially dark-noise subtraction) the variability and drift of the noise component limit their usefulness. Despite these drawbacks, at moderate to high levels of light where SNRs are not important, this technique enables the acquisition of data over a wide range of incident light intensities.

The magnitude of systematic errors in data obtained with a system utilizing a PMT in the dc measurement mode depends to a large extent on the stability of the PMT's gain characteristics with time. Since the current that is measured at the PMT's output is directly dependent on the charge contained in the amplified photoelectron pulses, any change in the amplification (gain) is directly related to a change in the current measurement. The strong dependence of this gain on such parameters as applied voltage, surface condition of dynodes, and history

of the PMT limit the stability that this type of system can achieve. Additional instabilities are introduced by changes in the baseline (dc drift) of the PMT dark current due to changes in leakage current, operating voltage, and temperature (17).

Another source of instability occurring in PMTs is associated with phenomena known as short and long term fatigue (14). This refers to the decrease in a tube's sensitivity because of decreasing gain upon exposure to a light source. It is highly dependent on output current, previous history, and type of dynode material. In general, this change becomes more prevalent as the output current increases. The exact mechanism by which fatigue occurs is not known, but is thought to arise through some change in the dynode surface material due to the impacting electrons. One possibility is the removal of dynode material during illumination of the PMT. The PMT usually recovers its original sensitivity if left in the dark for a period of time. This seems to imply a gradual return of the dynode material that was lost during illumination. Short term fatigue degrades the quality of virtually all measurements made with a PMT coupled to a dc-type system. Long term fatigue can be a major problem if measurements are made over long periods of time with a relatively intense light source. Fatigue characteristics are highly dependent on individual PMT properties.

3.3.2 Photon Counting

Since the PMT's ability to detect light is based on its discrete nature, digital processing techniques are readily applicable. Addition-

ally, there are many advantages (and disadvantages) of pulse-type operation over the dc measurement technique. At this point, an important distinction needs to be made between pulse counting as referenced to scintillation counting and what is termed photon counting. Photon counting, as the name implies, refers to the direct counting of individual photon interactions. This should be contrasted to scintillation counting which refers to the counting of individual interactions of radiation quanta in a scintillator such as a NaI(Tl) crystal. When radiation interacts within the scintillator, large numbers of photons are released in a very short time interval (depending on the decay characteristics of the particular scintillator used). The number of photons released is so large and the time interval short enough that the PMT cannot resolve the individual photons. Hence, the output consists of a single very large pulse which is counted as one interaction. This is reflective of the paralyzable nature of PMTs. More specifically, when two or more pulses arrive at the anode within the resolving time of the PMT (nominally 10 nsec) they combine to produce a single larger pulse of longer duration. For the duration of this pulse, no further transitions can be recognized at the output and counted by the instrumentation that follows. This effective deadtime will be extended indefinitely if pulses continue to arrive within the PMT's resolving time, hence the deadtime increases as the signal rate increases and the PMT becomes paralyzed. The output signal rate, therefore, decreases as the input rate increases, introducing

large errors. In contrast to a PMT, a pulse-height discriminator is a non-paralyzable device. This results from the discriminator's dead time being constant after the occurrence of each signal event, i.e., the deadtime does not increase as the input signal rate increases. The discriminator output rate follows the input until a maximum is reached (determined by the discriminator's resolving time) after which the output rate tends to remain constant. Therefore, a detection system which has been optimized for scintillation counting, may be considerably different than an optimized photon counting system. The count rate limitation for all but the fastest organic scintillators is set by the decay constant of the scintillator. For photon counting, the PMT and the associated electronics are the limiting components because individual photons are being measured directly.

In contrast to the dc technique for measuring light intensity, data collected with a photon counting system is directly correlated to the number of photon interactions which occur at the PMT's photocathode. It is readily apparent that pulse-height discrimination can be used to eliminate a large portion of the non-photocathode related noise spectrum discussed earlier. To a first approximation, the pulse-height distribution of photon induced output pulses is Poisson. This stems from the Poisson characteristics of secondary electron emission from the dynodes (19,20,21). In practice, there is generally a large number of small amplitude noise pulses at the lower end of the differential pulse-height distribution followed by a valley and then

a peak in the distribution due to photocathode related signals. Many PMTs do not exhibit this valley and are not very useful in photon counting applications. Tubes with high gain first dynodes, on the other hand, are extremely well suited since they exhibit a prominent valley. This valley results since thermonic dynode emissions undergo significantly less gain than photocathode emissions, resulting in pulses well below the photocathode related peak in the distribution. By using pulse-height discrimination, significant improvement in SNRs can be expected over those obtainable using the current measurement technique. These improvements have been reported to be on the order of 5 to 22% (22).

As important as improved SNRs, is the increase in system stability afforded by photon counting. For judicious discriminator level settings, gain changes have a markedly less profound effect on the output measurement when the signal is processed digitally. Hence, drifts in the PMT applied voltage as well as the fatigue phenomenon do not tend to limit system stability on the same order of magnitude as they do in a current measurement system.

Since the output pulse width will, to a large degree, determine the maximum counting rate in a photon counting system, it should be as small as achievable. This parameter is governed by two mechanisms, the RC time constant of the output circuit and the single photoelectron transit time spread. The transit time spread arises primarily from fluctuations in individual electron times of flight due to differing

trajectories and initial velocities (23). Generally, the amount of transit time spread depends on the tube geometry and the applied voltage. The importance of good tube design is realized by considering that unequal path lengths between dynodes as well as non-uniform electric fields add to the magnitude of the transit time spread (24).

In assembling a detection system for low-level light, it is necessary to achieve as high a SNR as possible in conjunction with good system stability. From the previous discussions, it appears that photon counting has a distinct advantage over dc measurement in both of these areas. Photon counting elicits high SNRs because of reductions in the noise spectrum using pulse-height discrimination and exhibits good stability due to the reduced effect of changes in gain and dark noise. Equally important is the improvement in fatigue characteristics achieved by photon counting. An additional advantage is high speed digital processing capability without the use of analog-to-digital conversion (25). The primary disadvantage of using photon counting techniques is its limited upper range. However, in a system where relatively low-level light is expected, photon counting should yield significant improvements over the conventional technique.

4.0 Description of TLD Analysis System

4.1 TLD Readout System

The TLD analysis system developed in this work consists of a commercial TLD analyzer modified by the addition of a photon counting TL detection system. A Harshaw model 2000A-B TLD analyzer was modified to function as the TLD heating unit. This dc-type system was selected because of its research grade design which utilizes a flexible TLD heating circuit. Modification included replacement of the original PMT assembly, optics, and calibration source with suitable photon counting instrumentation.

The PMT chosen for use in the photon counting system was an RCA Model 8850 PMT. This tube was designed for fast pulse-type operation and the actual unit employed was selected by RCA for its low-dark noise characteristics. It has a high-gain gallium-phosphide first dynode and as a result functions well in a system utilizing pulse-height discrimination to eliminate non-photocathode related pulses. The photocathode material is bialkali which exhibits a relatively good efficiency of 31% at the peak of its spectral response curve. Additionally, the tube's spectral response closely matches the emission spectra of LiF (TLD-100) as shown in Fig. 3. The photocathode and dynode materials used in this PMT are also characterized by low thermionic emission of electrons, hence, a low-dark noise pulse rate. This tube was used in conjunction with an Ortec Model 9201 PMT base and voltage divider network designed for fast pulse-type operation.

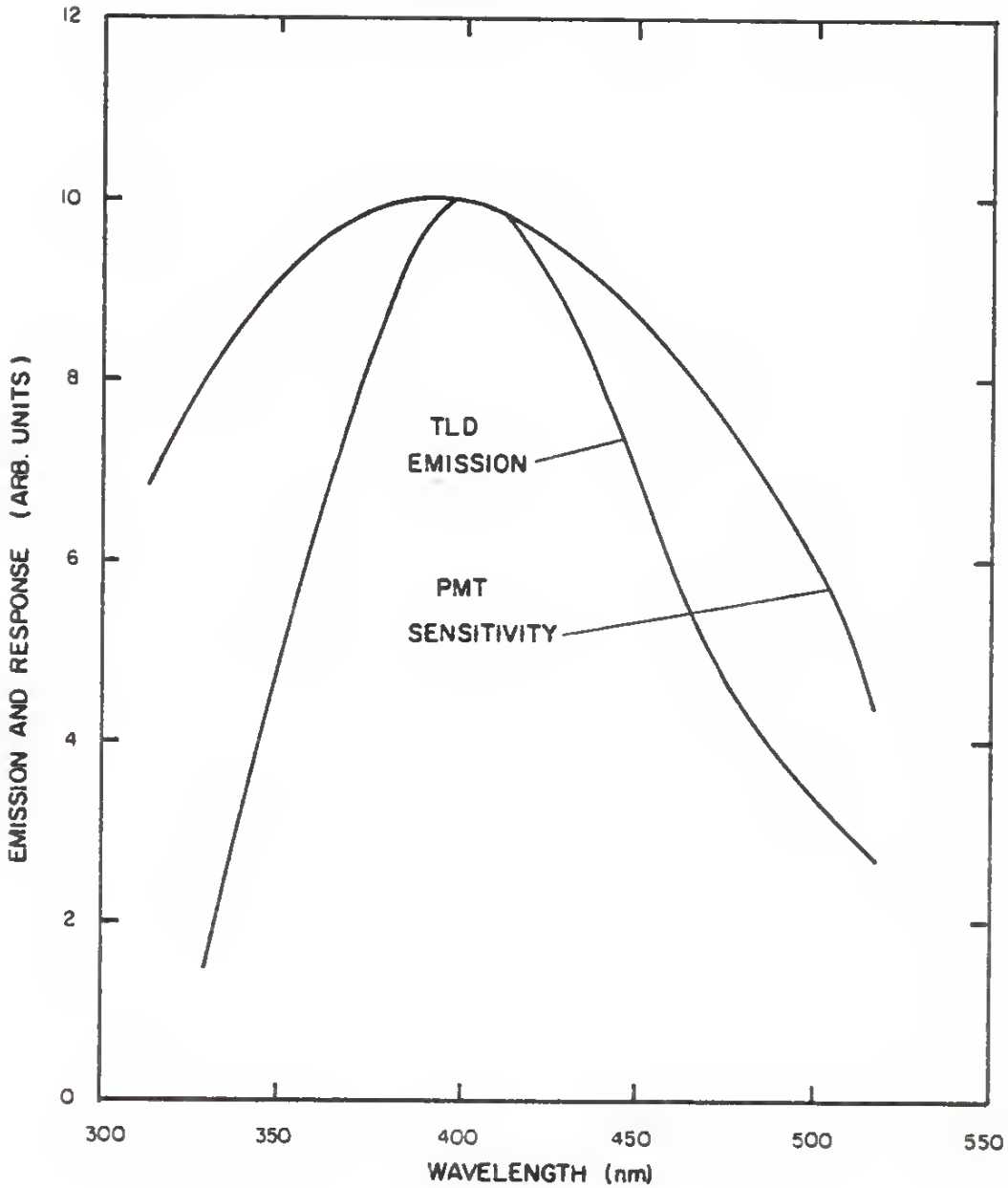

Fig. 3. Comparison of the spectral characteristics of thermoluminescence emission from LiF (TLD-100) and the RCA 8850 PMT's sensitivity.

The original PMT in the Harshaw system was mounted horizontally. A lens and mirror assembly directed the heated dosimeter's TL onto its photocathode. This assembly was removed and the new PMT mounted vertically, directly above the heating planchet on which the TLD rested. This reduced photon losses resulting from non-ideal lens transmission and mirror reflection. Moreover, it was discovered, upon removing the lens, that its natural flourescence had increased the measured PMT dark noise count by a factor of five. The original thermoelectric cooler was coupled directly to the PMT housing and adjusted to maintain a constant temperature of 10 °C. Besides reducing the PMT dark noise due to thermionic emission, this maintained the thermocouple reference junction, utilized by the planchet heating circuit, at a constant temperature. Finally, the Ra activated scintillation crystal mounted in the rear of the sample drawer was removed and replaced by an HP 5082-4984 green light emitting diode (LED). Although the original light source may have been suitable for the dc-type system, it did not model the effect of TL emission on the photon counting system. The scintillator emitted very large bursts of unresolvable photons. An LED, on the other hand, emits single photons and therefore was useful as a calibration and testing device for the photon counting system.

The need for an instrument with a wide dynamic range required the use of an extremely fast pulse-height discriminator and counter. The instrumentation chosen was manufactured by Princeton Applied

Research (PAR). Both the PAR Model 1121 pulse-height discriminator and the PAR Model 1109 photon counter are rated at nominally 10 MHz with a switch selectable 100 MHz prescale circuit. The PAR pulse-height discriminator also has a ratemeter circuit which supplies an analog signal proportional to the input pulse rate. Therefore, glow curves are obtainable using an analog recorder. Glow curves can also be measured in digital form. The PAR pulse-height discriminator has an output which supplies a -16 mA current pulse into a 50 Ω load whenever an input pulse exceeds the discriminator level. By directing this signal to an Ortec Model 450 research amplifier, it can be amplified and shaped to meet the input requirements of a TMC Model 402 multi-channel analyzer (MCA). Hence, digital glow curves were routinely measured by operating the MCA in the multiscalar mode. The components utilized in the photon counting TLD analyzer as well as their inter-connections are shown in Fig. 4.

4.2 Microprocessor Control System

A microprocessor was incorporated into the photon counting TLD analyzer to increase its flexibility and provide for better reproducibility. To achieve these ends, the microprocessor was programmed to provide the operator with audible notification (by means of a buzzer) concerning TLD removal from the sample drawer, initiate and terminate the readout cycle based on the heating planchet's temperature, and control the PAR photon counter integration period (length of time the counter was active). A Mini-Micro Designer 1 (MMD1) development system was selected

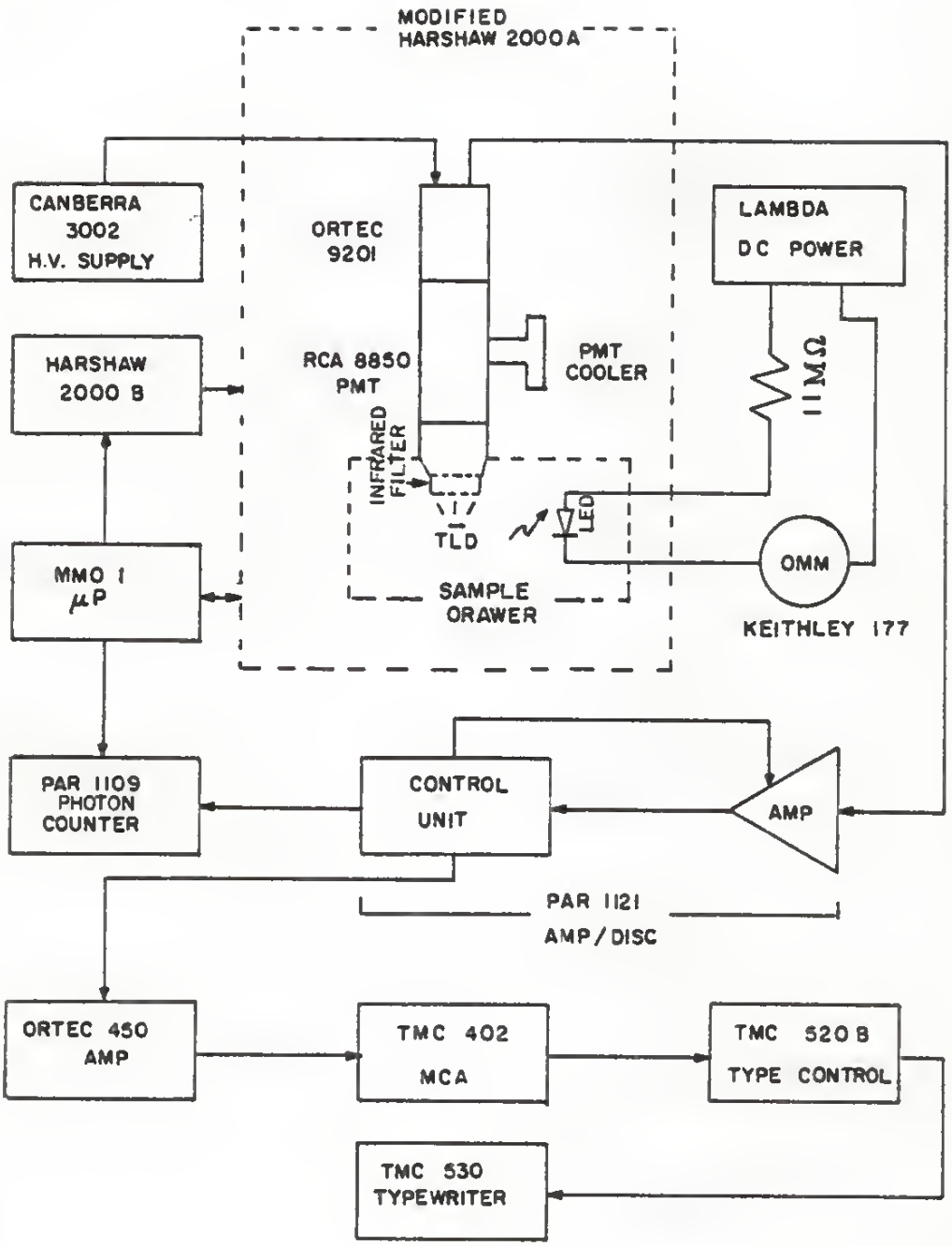

Fig. 4. System diagram showing the components and their interconnections utilized in construction of the photon counting TLD analyzer.

to provide this control. This microprocessor system, manufactured by E&L Instruments, Inc., contains an 8080A central processing unit (CPU) and has a user accessable data bus as well as various input and output control lines. Software programming was easily accomplished by inputing the instructions to random access memory (RAM) through an octal key pad.

The MMD1 system also has a number of output ports with latches available to the user. This eliminated the need for hardware which would otherwise have been necessary to permit the microprocessor to send control signals to any external circuitry. Hence, control of the PAR photon counter simply required connecting a number of these output latches to the counter's control inputs. Since these inputs were compatable with the TTL logic signals supplied by the MMD1 system, interface circuitry was not required. Additionally, the starting and stopping of the TLD heat cycle were accomplished by TTL signals from these output latches to the Harshaw system. Finally, operation of the buzzer required a transistor interface between it and the MMD1 output latch since it required more current than was available had a direct connection been made. The actual connections made to provide for microprocessor control of these various devices are shown in Fig. 5.

The control signal inputs to the PAR photon counter are either level or transition sensitive depending on the input being considered. Its HOLD function is activated by a logic 0. When this occurs, the counter stops its operation and displays the total accumulated counts

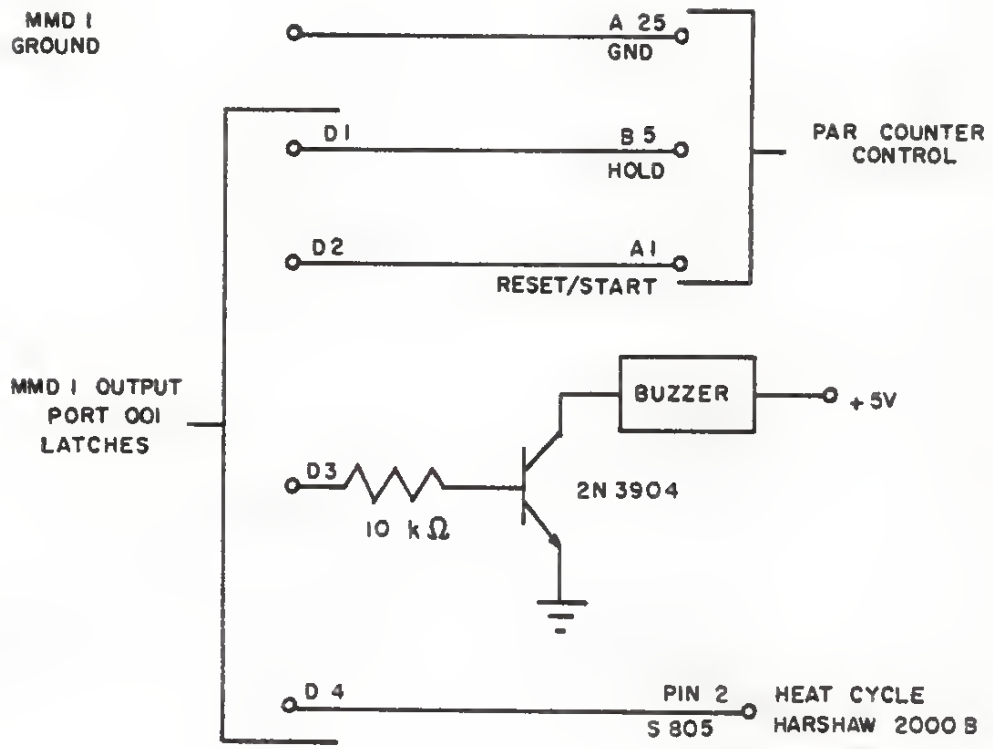

Fig. 5. MMDl microprocessor system interconnections to the photon counting TLD analyzer.

up to that point in time. When the logic level is returned to 1, the counter resumes operation without being reset to zero. The RESET/START function is triggered by a TTL Logic 0 pulse. When this occurs, the counter is reset to zero and its operation started. The 1-to-0 transition arms the start circuit with the actual RESET/START occurring on the 0-to-1 transition. The heat cycle on the Harshaw system is controlled in this same manner. It is started by a 0-to-1 transition and likewise is stopped by a 0-to-1 transition. The buzzer, on the other hand, is level sensitive and hence is on when a logic 1 is applied and off if the logic level is 0.

For the microprocessor to make decisions based on external occurrences, it must have some means of monitoring them. Since connections to its data bus are available, data may be received by the microprocessor through the use of 3-state buffers. The device select pulses to these buffers are generated through the use of a single logic gate and control signals available from the MMD1 system as shown in Fig. 6. The Harshaw System has a convenient output which supplies a voltage directly proportional to the temperature of the heating planchet. By comparing this voltage to reference voltages, the circuit shown in Fig. 6 provides necessary temperature information to the microprocessor. In this circuit, two operational amplifiers (IC1 and IC2) were utilizied, the one with more gain (IC1) was used for the temperature range 20 °C to 60 °C and the other for the range from 100 °C to 300 °C. Two ranges were utilized to speed the change in voltage with respect to time so that comparator

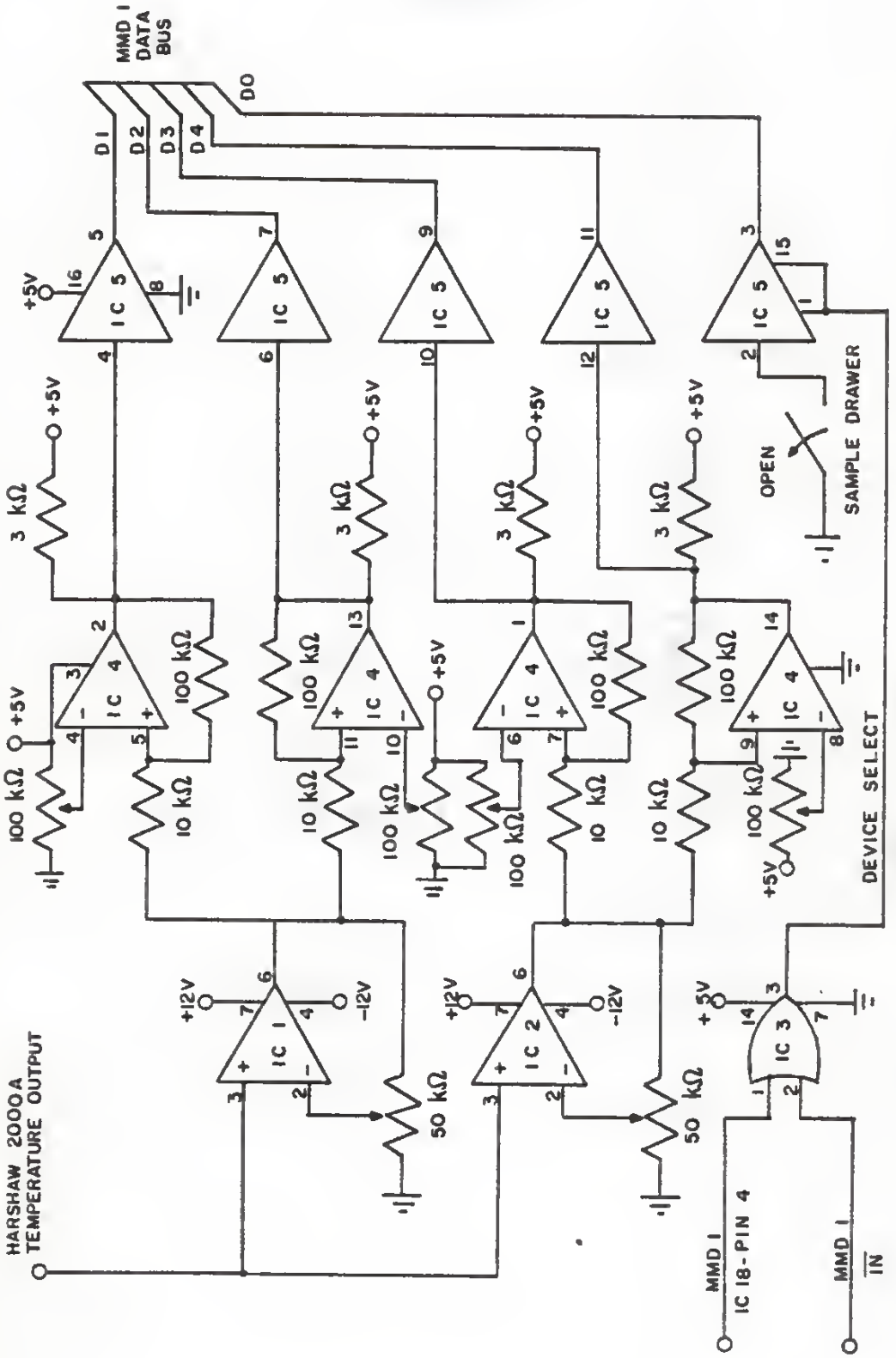

Fig. 6. Temperature comparator and buffer circuit utilized to input information to the MMDl microprocessor system. The integrated circuits are identified in Table I.

Table I. Identification of integrated circuits used in the circuit shown in Fig. 6.

INTEGRATED CIRCUIT IDENTIFICATION NUMBER	MANUFACTURER DEVICE NUMBER	DEVICE DESCRIPTION
IC 1	MC1741CP	Operational Amplifier
IC 2	MC1741CP	Operational Amplifier
IC 3	DM7432N	Quadruple 2-Input Positive-OR Gates
IC 4	LM339N	Quad Comparators
IC 5	SN74367AN	Hex Bus Drivers

oscillations were not as great a problem. Additionally, positive feedback was used in conjunction with the comparators (IC4) to further eliminate their oscillations due to the slowly varying input. The comparator reference voltages can be easily adjusted to correspond to a temperature range from 20 °C to 300 °C. Once the heating planchet's temperature exceeds that corresponding to the particular reference voltage being considered, that comparator's output swings to TTL logic level 1. This information, supplied to the microprocessor concerning the heating planchet's temperature relative to the four reference temperatures, was sufficient for its temperature based decision making process. The final information required by the microprocessor concerned the status of the TLD sample drawer. A microswitch mounted in the drawer provided a logic 1 if the drawer was open and a logic 0 if the drawer was closed.

The microprocessor aided in performing the TLD readout cycle in an extremely reproducible manner. This cycle was initiated once the planchet temperature cooled to 35 °C following the previous cycle. Since the microprocessor notified the operator to remove the TLD following the second readout (each dosimeter was heated twice) at 60°C, sufficient time was allowed for replacement of the TLD and filling the readout chamber with a nitrogen atmosphere. Hence, two of the reference temperatures remained fixed at 35 °C and 60 °C. The other references were adjusted to control the integration period of the counter. This period varied depending on the heating rate as will be discussed later.

Once the microprocessor program was initiated, further interaction by the operator was unnecessary. Information was automatically supplied to the microprocessor concerning TLD removal by the microswitch in the TLD sample drawer. The software flow diagram and listing are included in Appendix A.

5.0 Photon Counting System

5.1 Optimization Technique

To fully utilize the advantages that a photon counting system offers over conventional dc systems, careful consideration must be made concerning the PMT applied voltage and the threshold level of the pulse-height discriminator. These system operating levels primarily affect sensitivity and stability. In order to optimize these characteristics, parameters must be defined which adequately represent them and can be used to adjust the system operating levels. Sensitivity can be represented quite simply by some form of SNR since this usually defines the lower level of detectability. Stability, however, is somewhat more complex because of its many components.

Stability can be defined as the change in a system's output, i.e., its count rate, with respect to any change in its operating levels or characteristics. The most important of these are discriminator level, PMT applied voltage, and fatigue-induced PMT gain changes. Therefore, it is necessary to determine some parameter which can be used to evaluate the relative effects of these on the system's output. To do this, consider the PMT's output differential pulse-height distribution (PHD) with its valley and photocathode-related peak as discussed in Section 3.3.2. If the discriminator is set such that its threshold level corresponds to the valley region, essentially all of the photocathode-related pulses will cause a signal at the discriminator's output. This signal can then be registered by a counter. However, if

any shift occurs in either the discriminator level or the PHD, the count rate st the discriminator's output will change. This, then, is the mechanism by which system instability occurs. It is apparent that discriminator level drift, PMT applied voltage drift, and PMT fatigue must induce a change in the relative positions of the discriminator level and the PHD. This obviously occurs with drifts in discriminator level. However, changes in the relative position of the PHD occur at the onset of PMT applied voltage changes or PMT fatigue since these affect the amplitudes of the individual pulses. The magnitude of the change in count rate which occurs because of the instability mechanism is dependent upon the characteristics of the valley region in the differential PHD. If it is relatively wide and deep (i.e., a low differential count rate), a small change in the count rate measured at the discriminator's output will be observed upon changes in the discriminator level's relative position. If, on the other hand, this region is nsrrow and relatively high, large changes in count rate will be observed upon the occurrence of any such change. Therefore, a parameter which represents these valley characteristics would likewise be representative of system stability.

The valley in the differential PHD corresponds to a plateau-like region in the integral PHD. The width of this plateau corresponds to the width of the valley. However, the height of the valley corresponds to the slope of the plateau. Figure 7 illustrates several integral PHDs for the photon counting system. These were obtained by illuminating the PMT with an LED whose current wss 0.3 μA and subtracting the dark noise

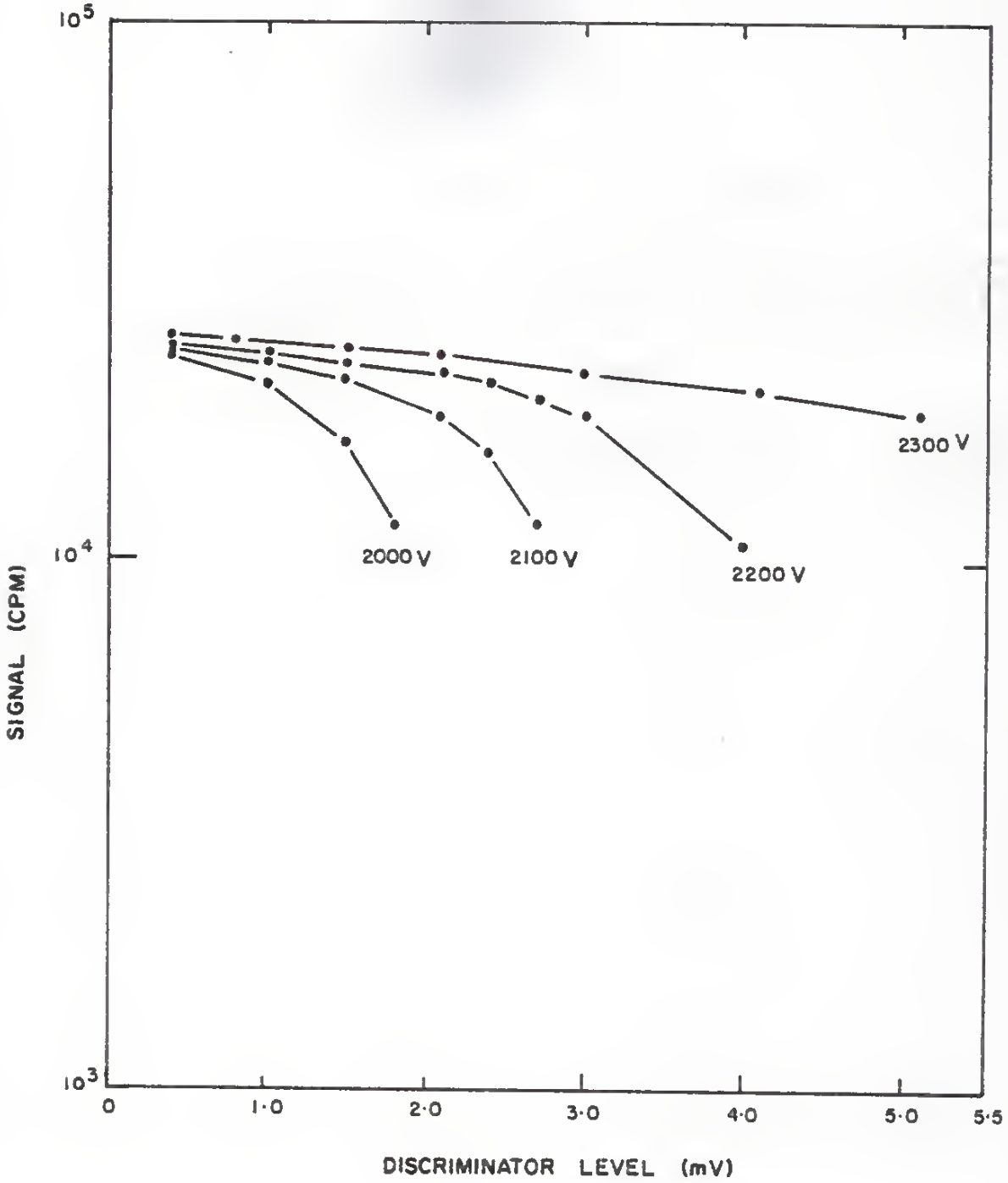

Fig. 7. Integral pulse-height distributions, obtained by subtracting the dark distribution from that obtained by a 0.3 μA LED illumination, measured for four PMT voltages (straight line segments added for visual clarity).

PHD from that which resulted. These are referred to as signal PHDs. It should be noted from these that, as the PMT voltage is increased, the width of the plateau increases while the slope decreases. Identically, the valley widens and becomes deeper. Since both of these are desirable occurrences, the trends in either one can be utilized as an indication of trends in the system's stability. Darland et al. (26) referred to the slope of the integral PHD as the system's relative discriminator level instability. It has been shown here that this is also representative of the overall system instability.

The location of the discriminator level in the differential PHD's valley affects both SNR and stability. A signal integral PHD is shown plotted on a linear scale in Fig. 8. Since fatigue induces downward shifts of the PHD, a discriminator level near the low end of this plateau would be advantageous. However, better SNRs are obtained when the discriminator level is at the upper end of this region since larger numbers of small amplitude noise pulses are discriminated against than photon-related pulses. Because these two discriminator level settings are diametrically opposed, it is reasoned that a setting in the center of the plateau is optimal.

Finally, the PMT applied voltage can be optimized utilizing sensitivity and stability as parameters. There is associated with any photon counting measurement an uncertainty or variance due to statistical fluctuation in the number of photons arriving at the detector (the PMT in this system). Photons do not, in general, obey the classical statistics of Boltzmann which gave rise to determination of the mean square deviation as simply the mean value of the measurements.

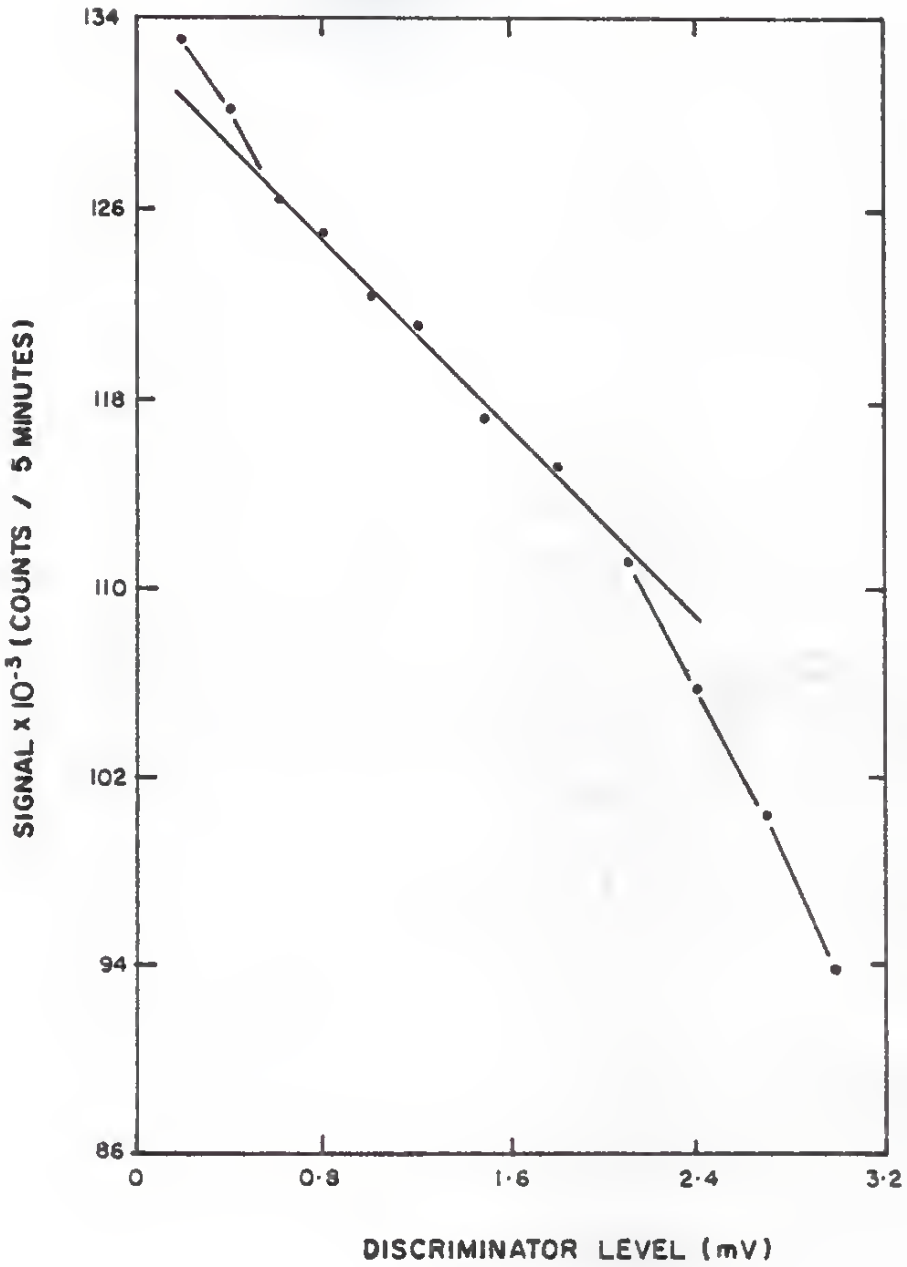

Fig. 8. Integral pulse-height distribution at a PMT voltage of 2200 V, obtained by subtracting the dark distribution from that obtained by a 0.3 μA LED illumination. The plateau region is characterized by a linear least-squares fit (straight line segments added for visual clarity).

Instead, they follow Bose-Einstein statistics. However, for photon energies higher than those corresponding to wavelengths of a few thousand nanometers, Bose-Einstein statistics reduce to the classical mean deviation (27). Schneider et al. (4) suggested optimizing sensitivity by maximizing the ratio of $(\text{signal})^2$ to background to give minimum variance at the lowest measurable signal. If the inverse of this quantity is defined as NS^2R (noise-to-signal squared ratio), an optimum sensitivity condition occurs when it is minimized. If discriminator level instability is minimized, an optimum stability condition occurs. Both of these quantities can be determined as a function of PMT applied voltage from least-squares fits to the plateau regions of the integral PHDs. Table II sumarizes the parameters determined for these fits as applied to both the signal and dark PHDs. Discriminator instability can be determined from these data as the percent change in counts per mV charge in discriminator level. This quantity is calculated by dividing the slope of the signal PHD plateau by the actual number of photons interacting at the photocathode. This can be determined as the signal axis intercept of the line resulting from a linear least-squares fit to the plateau region to be approximately 133,000 counts (for a 5 minute interval). Discriminator instability is shown in Fig. 9 as a function of PMT voltage. The sensitivity parameter, NS^2R, was also calculated from the data in Table II at the center of the plateau regions and plotted in Fig. 10. In an effort to determine the optimum PMT operating voltage, both the parameters in Figs. 9 and 10 must be considered. If both are weighted equally, their product can be formed (henceforth referred to as the PMT voltage product) and

Table II. Linear least-squares fit parameters for plateau regions of signal and dark integral pulse-height distributions.

PMT Voltage (volts)	Intercept (a_0)	Slope (a_1)	Coefficient of Determination (r^2)	Source of Data
1950	130,997	-32,495	0.993	
2000	132,030	-26,171	0.993	
2050	133,938	-22,806	1.000	
2100	132,237	-16,214	0.998	Signal Integral
2150	132,608	-13,007	0.990	Pulse-Height
2200	132,472	- 9,980	0.984	Distribution
2250	134,228	- 8,944	0.996	
2300	135,081	- 7,787	0.988	
1950	16,850	- 6,767	0.93	
2000	18,194	- 6,240	0.92	
2050	19,040	- 4,731	0.96	
2100	19,051	- 3,359	0.99	
2150	21,653	- 3,904	0.95	Dark Integral
2200	21,710	- 2,778	1.00	Pulse-Height
2250	24,165	- 2,791	0.92	Distribution
2300	27,191	- 2,983	0.89	

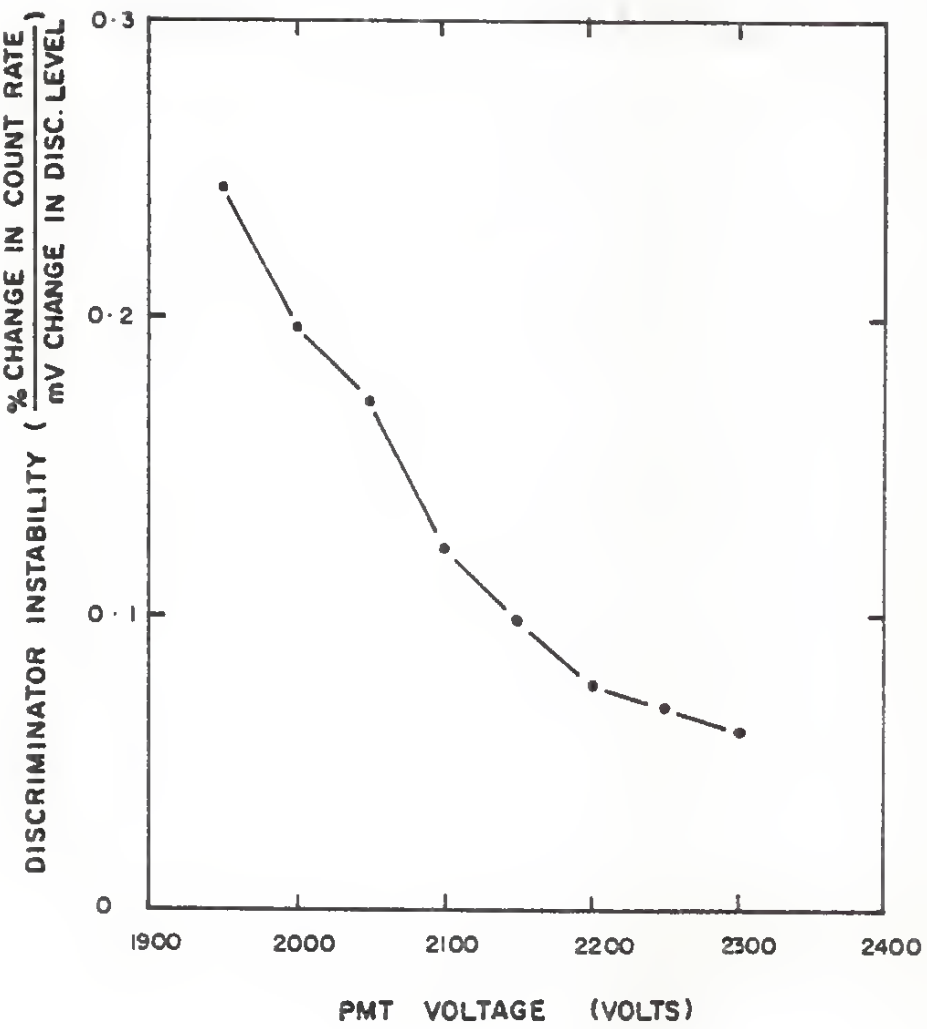

Fig. 9. Variation of count rate instability with respect to discriminator level drift, calculated from the slope of the plateau in the integral pulse-height distribution, as a function of PMT voltage (straight line segments added for visual clarity).

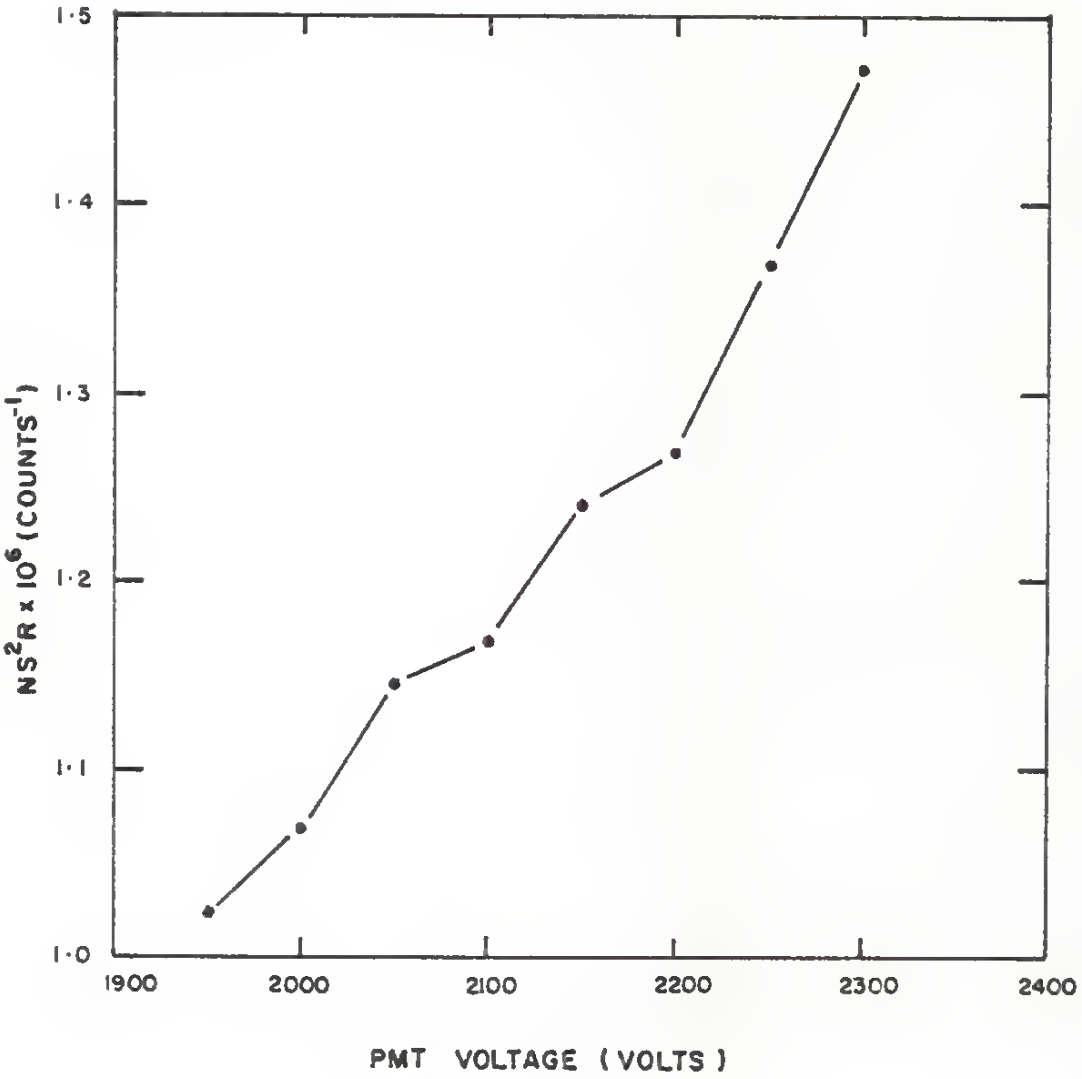

Fig. 10. Variation in the ratio of dark noise to the square of the signal, obtained by a 0.3 μA LED illumination, as a function of PMT voltage (straight line segments added for visual clarity).

minimized to determine the optimum PMT voltage. The resulting data are listed in Table III and plotted in Fig. 11. Note that the curve plateaus above 2200 V. Since lower PMT voltages tend to extend the life of the PMT (due primarily to fewer dynode property changes because of less current through them), 2200 V was selected in conjunction with a discriminator level setting of 1.35 mV as the optimum system operating levels.

5.2 Linearity

Linearity is one of the major characteristics in a photon counting system which must be investigated because of the limitation on its upper range by pulse pile-up. Although the PAR instrumentation utilized in this system is rated at nominally 100 MHz, the actual range over which its response is linear is somewhat less because of the random nature of photon emission. The process of photon emission is essentially the same in TLDs and LEDs, i.e., both emit light when an electron falls from the conduction band into the valence band. Additionally, these devices are both assumed to emit photons as uncorrelated events. Hence, the LED should serve as a reasonable model which emulates the effect of TL emission on the photon counting system.

The relationship between light released from and current through an LED is linear except for currents below the mA region. Unfortunately this is the region which must be used to investigate the photon counting system's linearity. However, since this region of the LED's light output curve has a relatively slowly changing slope it can still be utilized. Figure 12 illustrates the relationship between LED

Table III. Calculation results for photon counting system optimization (from linear least-squares fits to the integral pulse-height distributions).

PMT Voltage (volts)	Optimum Discriminator Level (mV)	NS^2R^* x 10^6 ($counts^{-1}$)	Disc Instability ($\frac{\%\text{ change in C.R.}}{\text{mV change in disc}}$)	Voltage Product x 10^6 (Arb. units)
1950	0.50	1.023	0.244	0.250
2000	0.60	1.068	0.197	0.210
2050	0.85	1.144	0.171	0.196
2100	1.00	1.166	0.122	0.142
2150	1.20	1.240	0.098	0.121
2200	1.35	1.268	0.075	0.095
2250	1.50	1.369	0.067	0.092
2300	2.70	1.471	0.058	0.086

*NS^2R refers to the ratio of noise to the square of the signal.

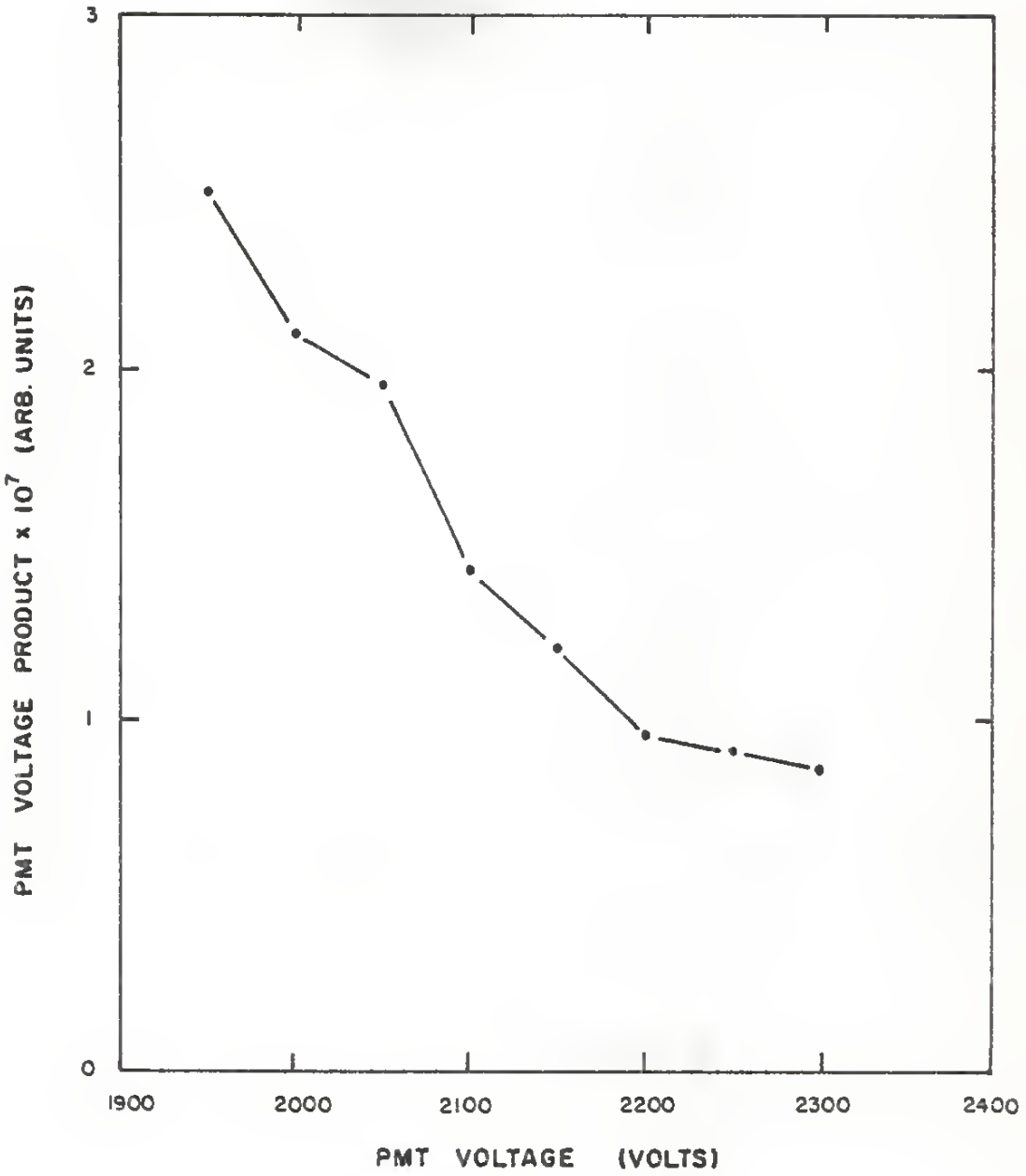

Fig. 11. Optimization parameter versus PMT applied voltage (straight line segments added for visual clarity).

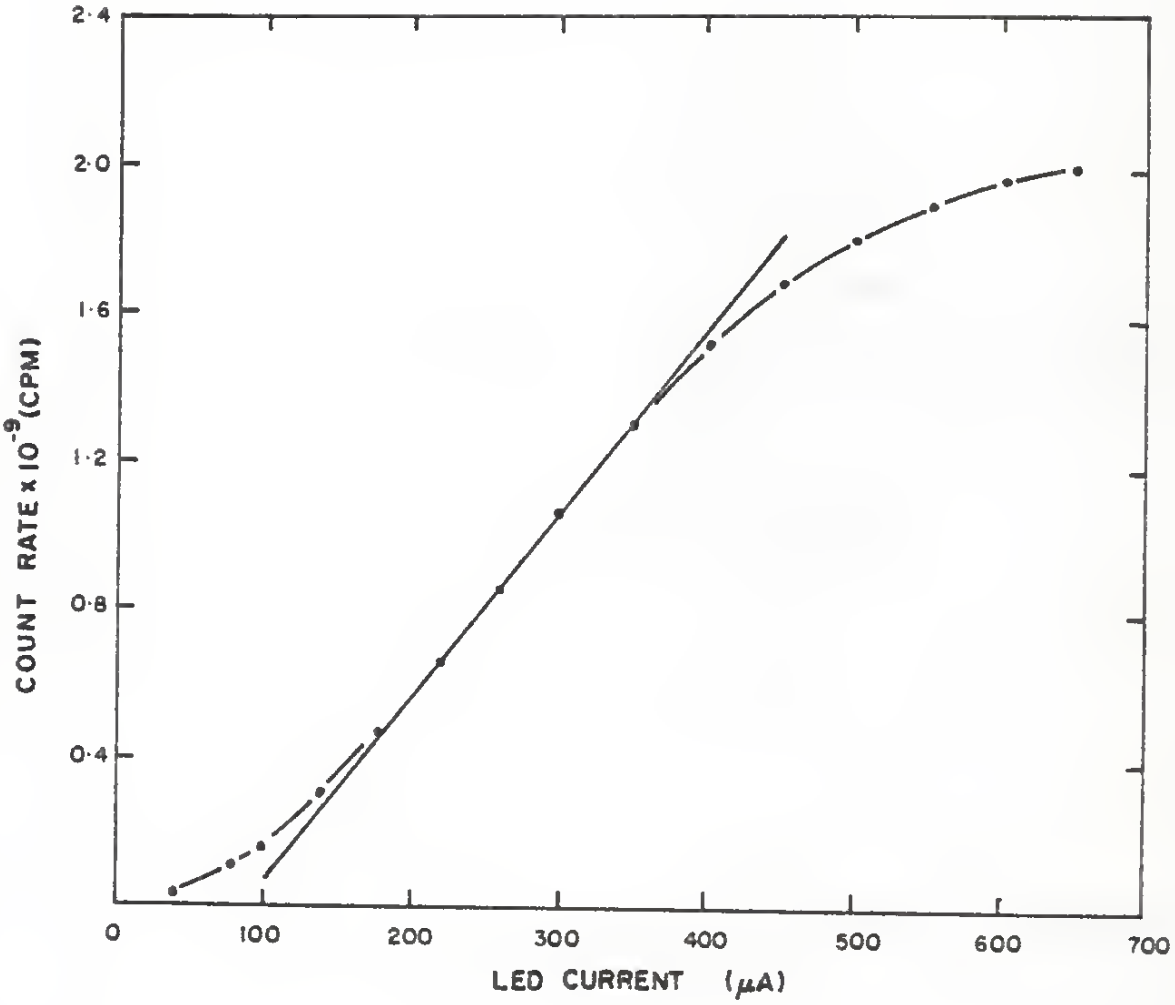

Fig. 12. Illustration of system non-linearity due to pulse pile-up at high signal rates (linear least-squares line identifies linear region).

current and the photon counting system's count rate. Since the slope of the LED's light output curve increases slowly in this region, it can be expected that the photon counting system loses linearity slightly before that count rate indicated by the photon counting system's departure from linearity as determined by Fig. 12. Therefore, the approximate count rate at which the system can be expected to become nonlinear is nominally 20 MHz. Hence, TLDs which result in count rates above this value when readout have been given doses outside the system's linear range.

5.3 Fatigue Characteristics

The LED was used to investigate the effect of PMT fatigue on the photon counting system. A constant voltage was applied across the LED and resistor to produce a constant photon output which was monitored by the photon counting system. Count rate as a function of time was recorded over an eight hour period from the time the LED was turned on. Due to the voltage regulation capabilities of the Lambda DC Power Supply and the slight variability in the ambient air temperature, the current through the LED, and hence its photon emission, could not be held perfectly constant. The LED current tended to vary slightly about an average value. The three values of current used in this investigation, 150 μA, 250 μA, and 350 μA corresponded to count rates of 5.5 MHz, 13.3 MHz, and 21.8 MHz, respectively. For each of the three investigations, there appeared no trend for the count rate to diminish with time. The standard deviation about the mean count rate was 0.13%, 0.22%, and 0.10%, respectively. From these results, it is apparent

that fatigue had negligible effects on the photon counting system for count rates up to 21.8 MHz (actually beyond its maximum linear count rate). This illustrated the effectiveness of the optimization procedure utilized to set the system's operating levels.

6.0 Thermoluminescent Dosimetry Techniques

Procedures utilized in the handling, preparation, and readout of TLDs have a significant effect on the accuracy and precision of the resulting measurements. This subject has been addressed by a number of investigators including Robertson and Gilboy (28) and Simons and Huntsman (29). These authors concluded that reproducibility in TLD measurements depends primarily upon consistency in thermal pre-treatment (annealing) and readout procedures.

Prior to their use as radiation dosimeters, TLDs are annealed at a high temperature to empty the traps filled by previous irradiations. The manner in which this annealing procedure is applied affects both the total area under the glow curve and the relative heights of its peaks. In general, the area under this curve tends to be reduced for TLDs annealed at high temperatures for long periods of time (30). Hence, the TLD becomes less sensitive. The area under the glow curve is also significantly affected by the rate at which the TLD is cooled after it is removed from the annealing oven. This affects the relative height of the individual glow peaks as well (31,32). Therefore, it is apparent that any deviation from an established annealing procedure affects the sensitivity of individual TLDs. This, in turn, reduces the reproducibility of subsequent measurements. For these reasons, Harshaw Chemical Co. (a major TLD supplier) recommends a standard pre-irradiation anneal for one hour at 400 °C followed by two hours at 100 °C. Harshaw also recommends a post-irradiation anneal for ten minutes at 100 °C to com-

pensate for the fading phenomenon.

Fading refers to a decrease in the area under a TLD's glow curve as a function of time following irradiation. During irradiation, substantial filling occurs in the low temperature traps corresponding to peaks 1 and 2 (see Fig. 1). At room temperature these peaks have half lives of 10 minutes and 10 hours, respectively (30). Thus, their contribution to the area under the glow curve decays rather rapidly. By annealing in the prescribed manner following irradiation, these traps are emptied. This removes their contribution all together thus eliminating the errors which would occur if readout was performed during the decay of these peaks. The half lives of peaks 3, 4, and 5 are sufficiently long at room temperature, 0.5, 7, and 80 years, respectively, that they contribute little to the fading process. Burgkhardt et al. (33) determined that LiF faded only 5% following storage at room temperature for 50 days. During their investigation, they utilized the pre- and post-irradiation annealing procedures recommended by Harshaw.

Dose rate dependence is a concern with the use of any radiation dosimeter. Hsu and Weng (34) reported that they observed a slight dependence in the response of powdered LiF for low exposure rates. Most investigators, however, have concluded that, for dose rates up to 10^{11} rad/sec, LiF shows no significant dose rate dependence (30,35). Hence, there should be negligible error induced in calibration curve data (system readout versus dose) obtained by TLD irradiation at varying dose rates.

The actual handling procedures used when picking up and moving TLDs can induce errors in subsequent measurements. Cox et al. (36) showed that rough handling of TLDs, through the use of tweezers, resulted in scratches on the detector's surfaces. This significantly reduced the integrated TL output (area under the glow curve) corresponding to a constant exposure. They recommended the use of a vacuum handling tool. An alternate method, used in this work, was to cover the tips of a pair of tweezers with plastic heat-shrinkable tubing. The tubing extended approximately 3 mm beyond the tips of the tweezers. This procedure eliminated both surface abrasion and TLD compression.

During TLD readout, the desired radiation induced signal is obtained along with a non-radiation induced signal. This non-radiation induced TL is often referred to as triboluminescence or chemiluminescence. Strictly speaking, triboluminescence refers to that portion of a TLD's emission due to mechanical stress or fracture of the crystalline structure. Chemiluminescence refers to a signal produced by a reaction between the TLD and its environment during the readout process. The emission of non-radiation induced TL typically occurs at temperatures above that at which the main glow peak appears (30). For this reason, the readout of a TLD should be performed at as low a temperature as possible which permits readout of the main glow peak. Additionally, the readout of LiF TLDs in a nitrogen atmosphere greatly inhibits the emission of this undesirable signal. Hence, nitrogen is normally flowed through the TLD chamber during readout.

7.0 Experimental Procedures

To reduce systematic errors, each TLD was handled, annealed, irradiated, and read in as careful and consistent a manner as possible. The TLDs were always moved utilizing the special tweezers described in Section 6.0. Care was taken so that the dosimeters, were not dropped, placed on a soiled surface, or exposed to fluorescent light following irradiation. These precautions were necessary to insure that the results obtained in this work were both reproducible and the best achievable.

7.1 Dosimeter Irradiations

In order to evaluate the photon counting TLD analyzer system, some means by which the dosimeters could be given precise doses had to be devised. The TLD irradiation device shown in Fig. 13 provided this capability. The 2.4 cm thick stryofoam platform was chosen as the TLD support device because of its transparent nature with respect to gamma-ray interaction. Moreover, the platform was suspended at least 2 meters from the nearest reflecting surface. Under these conditions, it was assumed that the absorbed dose at the location of the TLD could be calculated using the model of a point source in an infinite non-attenuating medium. Additionally, during irradiation, the TLDs were encapsulated in stainless steel sleeves (0.318 cm O.D., 0.142 cm I.D.) with wall mass thicknesses of 0.693 g/cm^2. Thus, the absorbed dose calculations were made assuming charged particle equilibrium and gamma-ray attenuation

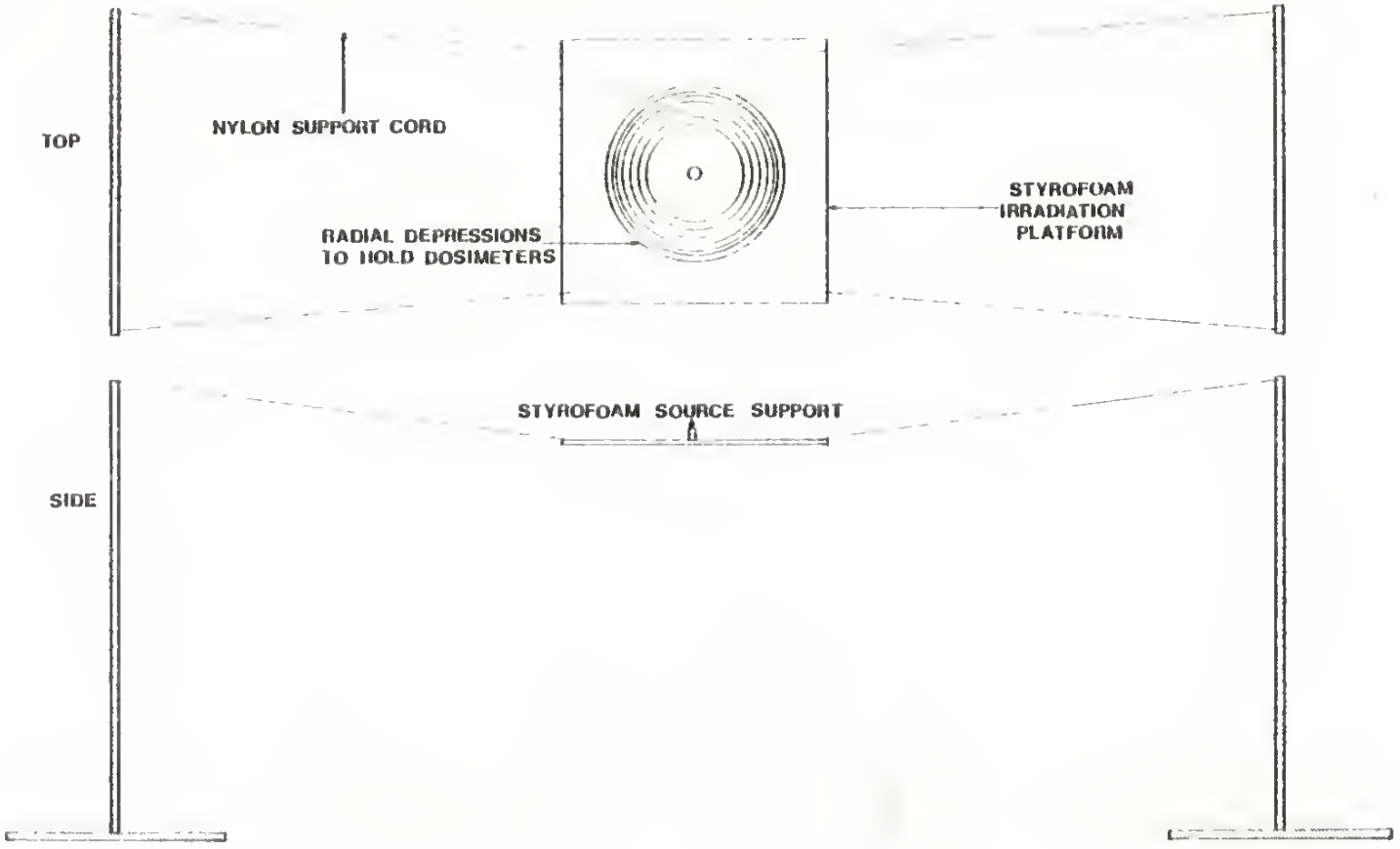

Fig. 13. Diagram showing the irradiation device designed for use with thermoluminescent dosimeters (TLDs).

only in the sleeve. Absorbed doses are therefore reported as rads in stainless steel. The ^{137}Cs source utilized had a strength of $3.0 \pm .1$ mCi. It was mounted in a styrofoam support positioned above the center of a series of slight radial depressions. The TLDs, when placed in the same depression, could be given equivalent doses. Identically, dosimeters placed at different radii could be given a variety of doses during the same irradiation period. The relatively weak strength of this gamma-ray source limited the doses that could be obtained during reasonable irradiation periods to about 5 rads. In order to achieve higher doses, an alternate facility was utilized.

The KSU Gammacell-220 is an irradiation device capable of irradiating samples to very high doses. Inside the irradiation chamber, TLDs could be given doses at an approximate rate of 620 rads/sec by exposure to a ^{60}Co gamma-ray source. This enabled the acquisition of high dose TLD data utilizing very short irradiation times. The TLDs were placed in a sample loader which required a finite amount of time to enter and leave the irradiation chamber. It was determined that the dosimeters received approximately 36.5 rads during these entrance and exit times. Therefore, it was necessary to adjust the total dose the TLDs received while in the chamber by this amount. The use of the ^{137}Cs source and the Gammacell-220 enabled the acquisition of data over the entire dynamic range of the photon counting TLD analyzer. This was essential in determining the upper and lower dose limits of this instrument.

7.2 Annealing Procedures

Prior to and following their irradiation, each TLD underwent an annealing process. This included the new, unused TLDs since a pre-irradiation annealing was required to remove any charge stored in the dosimeters resulting from natural background radiation. Likewise, the preparation of TLDs for reuse consisted of a pre-irradiation annealing. The pre-irradiation procedure utilized consisted of the following steps: (1) the TLDs were placed in a pyrex petri dish which was then (2) placed in a 400 °C oven for one hour, (3) cooled for ten minutes on an asbestos pad in a draft free drawer, (4) placed in a 100 °C oven for two hours, and finally (5) cooled to room temperature in the manner specified in step (3). TLDs were annealed in the pyrex dishes because of the tendency of most other materials to form an oxide when heated to high temperatures. This oxide could contaminate the dosimeters resulting in erroneous measurements. The post-irradiation annealing consisted of heating the TLDs in a 100 °C oven for ten minutes followed by cooling to room temperature as specified in the pre-irradiation annealing. Readout of the TLDs followed immediately.

7.3 Dosimeter Readout Techniques

The readout of TLDs was accomplished by heating them at a constant rate and counting the photons emitted. Since, as noted in Section 2.2, the shape of the glow peak is dependent on the heating rate experienced by the TLD during readout, two different heating rates were utilized to investigate their effect on the dynamic range of the photon

counting TLD analyzer. The slow heat cycle (see Fig. 14) consisted of heating the TLD planchet at a rate of 12.5 °C/sec. By gating the PAR photon counter on at 130 °C and off at 250 °C, the area under the main glow peak was measured and displayed by the counter at the end of the readout as integrated counts. The fast heat cycle (see Fig. 15) consisted of heating the TLD planchet at a rate of 24.7 °C/sec. For this cycle, however, the PAR photon counter was gated on at 150 °C and off at 280 °C. These higher temperatures were necessary as the finite thermal conductivity of the dosimeter caused its temperature to lag that of the planchet resulting in the glow peak's occurrence at a higher planchet temperature.

The height of each TLD's glow peak was also measured during its readout. Both the analog and digital peak heights were determined from the TLD's respective glow curve. The analog glow curve was obtained by connecting a Varian Model 9176 recorder to the PAR photon counter's ratemeter output. Digital glow curves were measured using the TMC model 402 MCA. The TLD's glow curve was recorded in both of these ways to serve as a check on the fast pulse to slow pulse interface provided by the Ortec Model 450 amplifier. Pulses from the PAR system were shaped by the Ortec amplifier to meet the MCA's input requirements. The analog curves were recorded directly without an interface, and hence could be used to verify the accuracy of the digital data. Digital curves were desirable since they lended themselves to numerical processing more readily than did the analog curves.

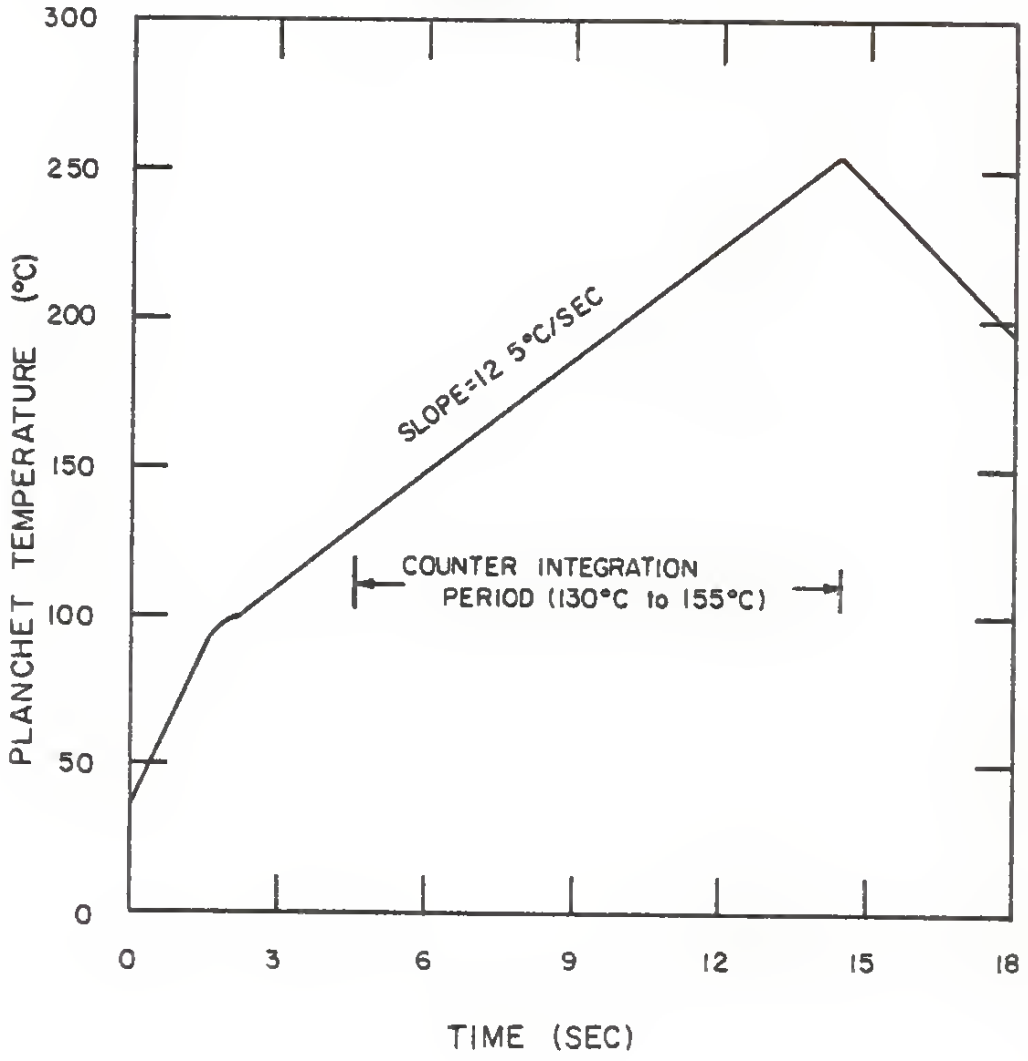

Fig. 14. Slow-heat readout cycle used in conjunction with group 1 TLDs.

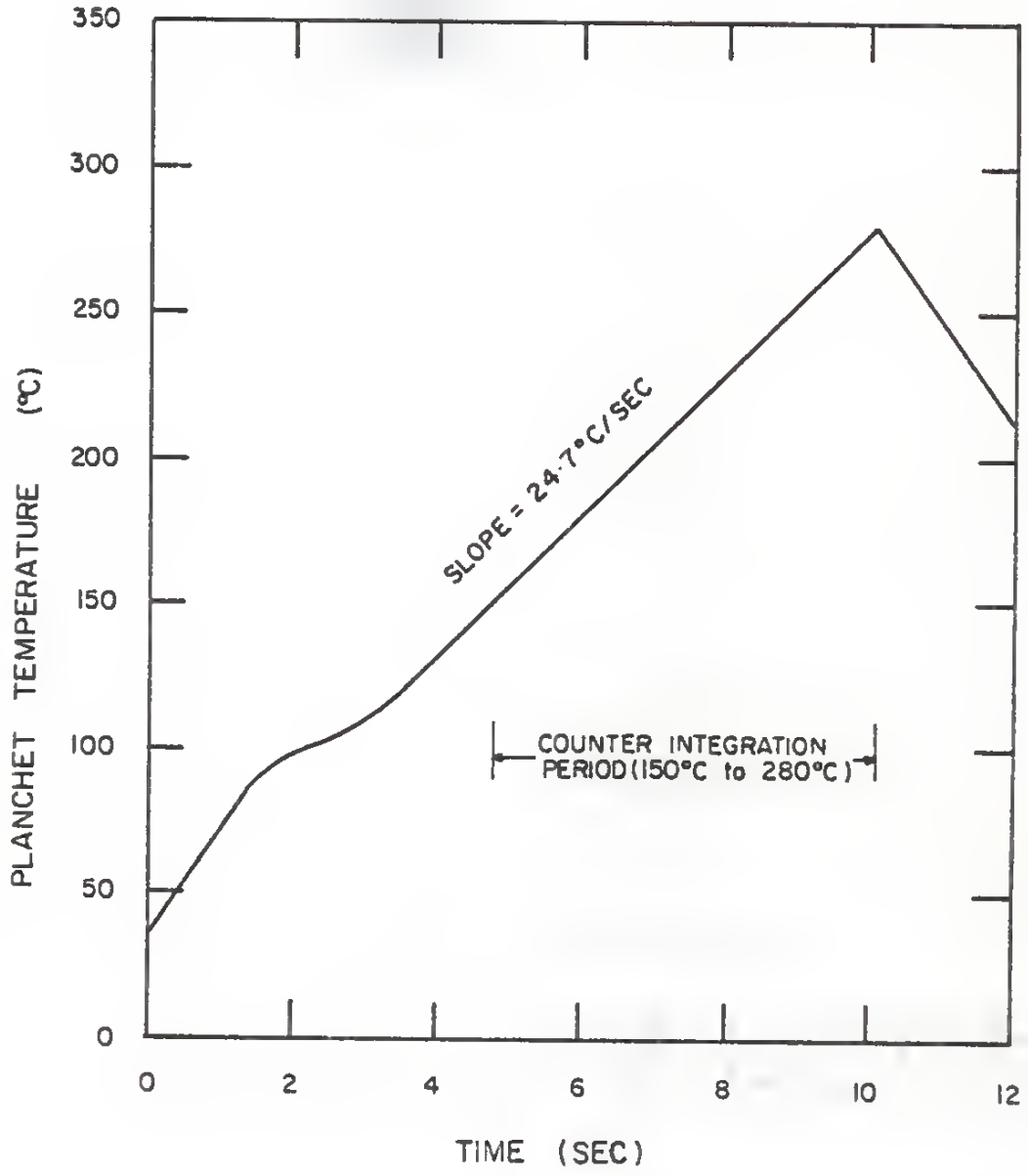

Fig. 15. Fast-heat readout cycle used in conjunction with group 2 TLDs.

Each TLD was heated in the same manner twice with the second readout being interpreted as background. The second readout of a TLD exposed to radiation will be composed of PMT dark noise, light from the hot planchet, non-radiation induced TL and radiation induced TL which was not released during the first readout. At moderate dose levels, this readout is much smaller than the first, however, at low-dose levels, it can be on the same order of magnitude. For this reason, the second readout is typically subtracted from the first to obtain a net readout. Although this procedure results in the subtraction of some radiation induced signal, the benefits are apparent as the non-radiation induced signal is much larger at low doses.

Since non-radiation induced TL from a dosimeter can be a significant contributer to the background observed at low doses, the TLDs were heated in a nitrogen atmosphere. The dosimeter readout chamber was purged of air during readout by a constant flow of nitrogen through it. Sufficient time was allowed after changing dosimeters in the readout chamber for the nitrogen to expel the air introduced by opening the TLD sample drawer. This procedure assured that the background reading would be as low as possible.

7.4 Sensitivity Selection

Sort irradiations were performed to evaluate the sensitivity of each TLD relative to the mean of the set of dosimeters. Two sets, each consisting of 130 new TLDs (Harshaw TLD-100 1x1x6 mm high sensitivity rods), were annealed and irradiated for four hours on the

styrofoam irradiator at a radial distance of 25.32 cm. No sleeves were utilized since an accurate dose measurement was not necessary. The sets were constructed by numbering the TLDs directly as they were removed, in groups of twenty, from the Harshaw-supplied capsules. Each TLD retained its identity throughout the remaining experiments.

The first sort irradiation was performed twice on the entire group of 130 dosimeters. The slow-heat readout procedure was used for both sets of readouts which were subsequently labeled as sorts 1A and 1B. The second group of dosimeters were heated using the fast heating rate and was labeled as sort 2. Readout procedures described in Section 7.3 were used.

From these data, two groups of 100 TLDs each were assembled as those dosimeters with sensitivities nearest the mean of their respective sort groups. Group 1 (from sort 1B) dosimeters were always subjected to the slow-heat readout cycle while those in group 2 (from sort 2) were always heated using the fast heating rate. The dosimeters in each group were then annealed and given a wide range of doses so that calibration curves could be obtained for the system.

7.5 Calibration Curves

Measurement of absolute doses with TLDs requires the determination of a calibration curve for each particular readout system. Additionally, the calibration data can be used to determine the system's linear range of readout versus dose.

Since the low-dose characteristics of this system were of special interest, the low-dose region was thoroughly investigated. For the calibration study, each group of 100 TLDs was further divided into 20 sub-groups of 5 TLDs each. The first 10 sub-groups in both groups 1 and 2 were given doses from 0.11 mrad to 67.1 mrad. For group 1 TLDS, this process was performed twice. The same experiments were performed three times for group 2 TLDs. Between each irradiation, the annealing procedures described in Section 7.2. were adhered to. The remainder of the TLDs in both groups were then given doses up to 656 rads to investigate the upper-dose portion of the calibration curves.

7.6 High Sensitivity Ribbons

The photon counting TLD analyzer system was designed to measure low doses by utilizing the improved low-level light detection capabilities that photon counting offers over those exhibited by conventional dc-type systems. Lower doses can, obviously, be measured by using TLDs with larger masses since they emit more TL per unit dose. This was investigated using a number of larger TLDs (Harshaw TLD-100 1/8 x 1/8 x 0.035" high sensitivity ribbons). They were annealed, irradiated, and their TL emitted compared to that obtained from the smaller rods. The doses given the ribbons were approximate because they were not encapsulated in the stainless steel sleeves. However, since only the TL per unit dose was being compared, exact values of

absorbed dose were not important. Additionally, sensitivity selection was not performed on these dosimeters. They were processed using the fast heating rate readout cycle.

8.0 Discussion of Results

Sufficient data were collected to thoroughly investigate the characteristics of the photon counting TLD analyzer system. They were obtained in the form of two integrated count measurements and two glow curves (analog and digital) for each dosimeter readout cycle. Since over 700 anneal/irradiate/readout processes were performed, it was necessary to include in this work only that raw data deemed essential. This resulted in the omission of the data collected in the sort irradiations and reduced the total amount of raw data by one-half. All of the data utilized in the optimization and calibration of the system are included in Appendix B.

8.1 Sensitivity Selection

8.1.1 Integrated Count Approach

The net integrated count readouts for the three sort irradiations, performed to determine the relative sensitivity of individual TLDs, are shown in Figs. 16-18. Since the purpose of these irradiations was to select a group of TLDs with similar sensitivities, limits were drawn on these figures to include the 100 dosimeters with the most closely matched sensitivities. For the TLDs in sorts 1A and 1B, these limits corresponded to $\pm$ 6% of the mean net readout. The mean net readouts for sorts 1A and 1B exhibited very good consistency and were calculated to be 24,501 and 24,390 counts, respectively. This indicated that the anneal, irradiation, and readout procedures utilized did not appreciably affect the sensitivities of the TLDs. These values were

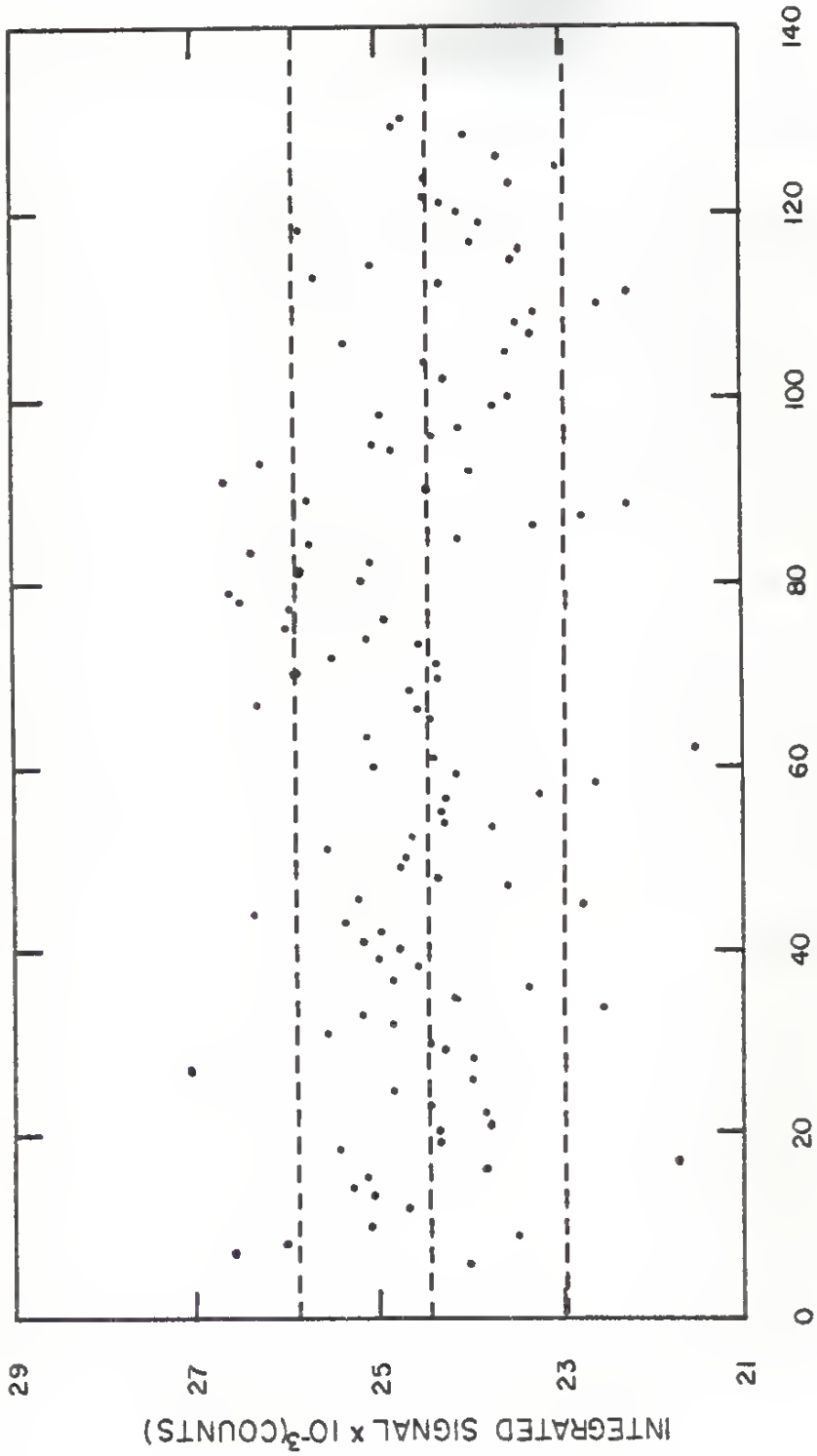

Fig. 16. Variation in the sensitivities of sort 1A TLDs for a uniform dose and slow-heat readout cycle.

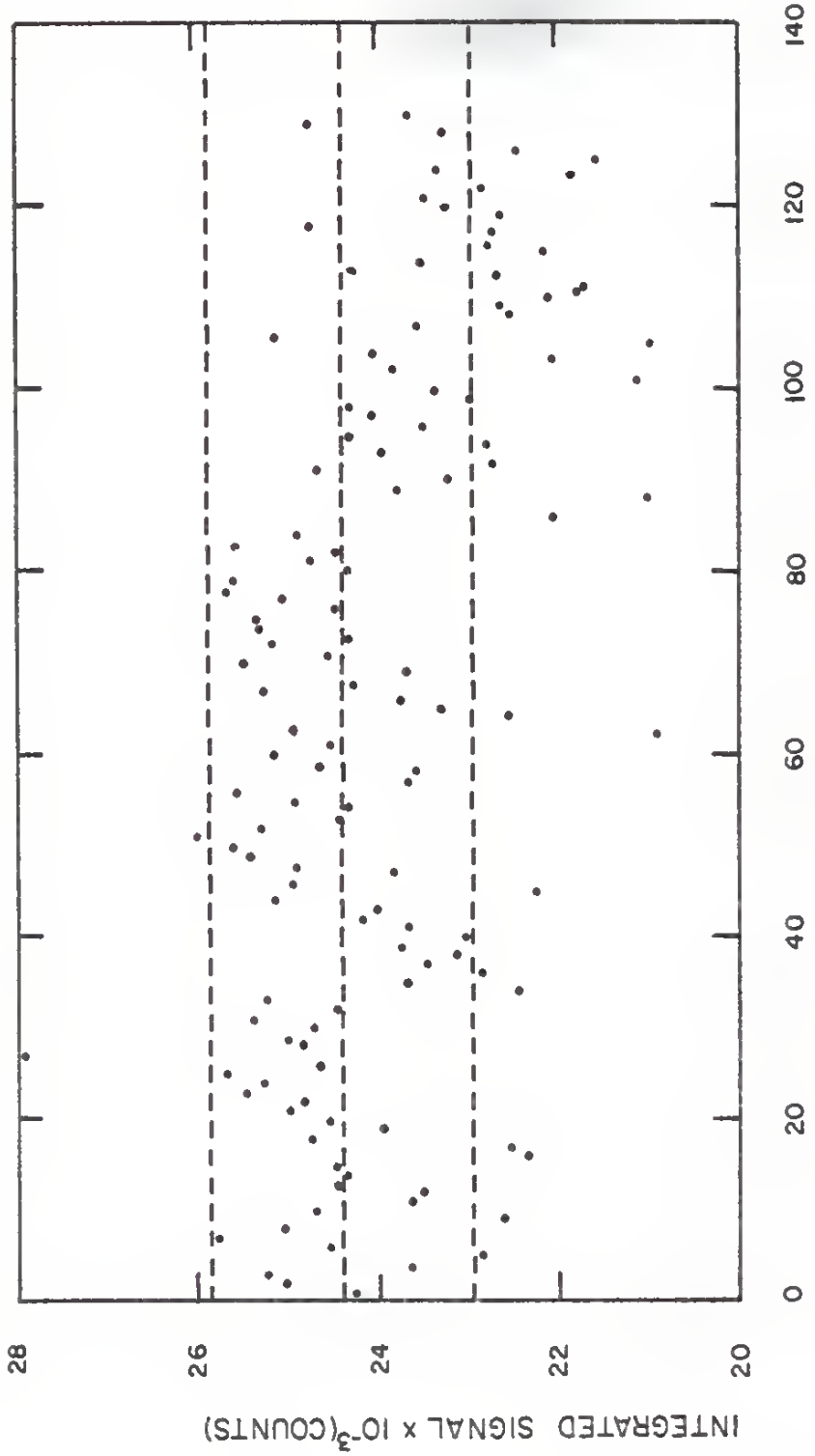

Fig. 17. Variation in the sensitivities of sort 1B TLDs for a uniform dose and slow-heat readout cycle.

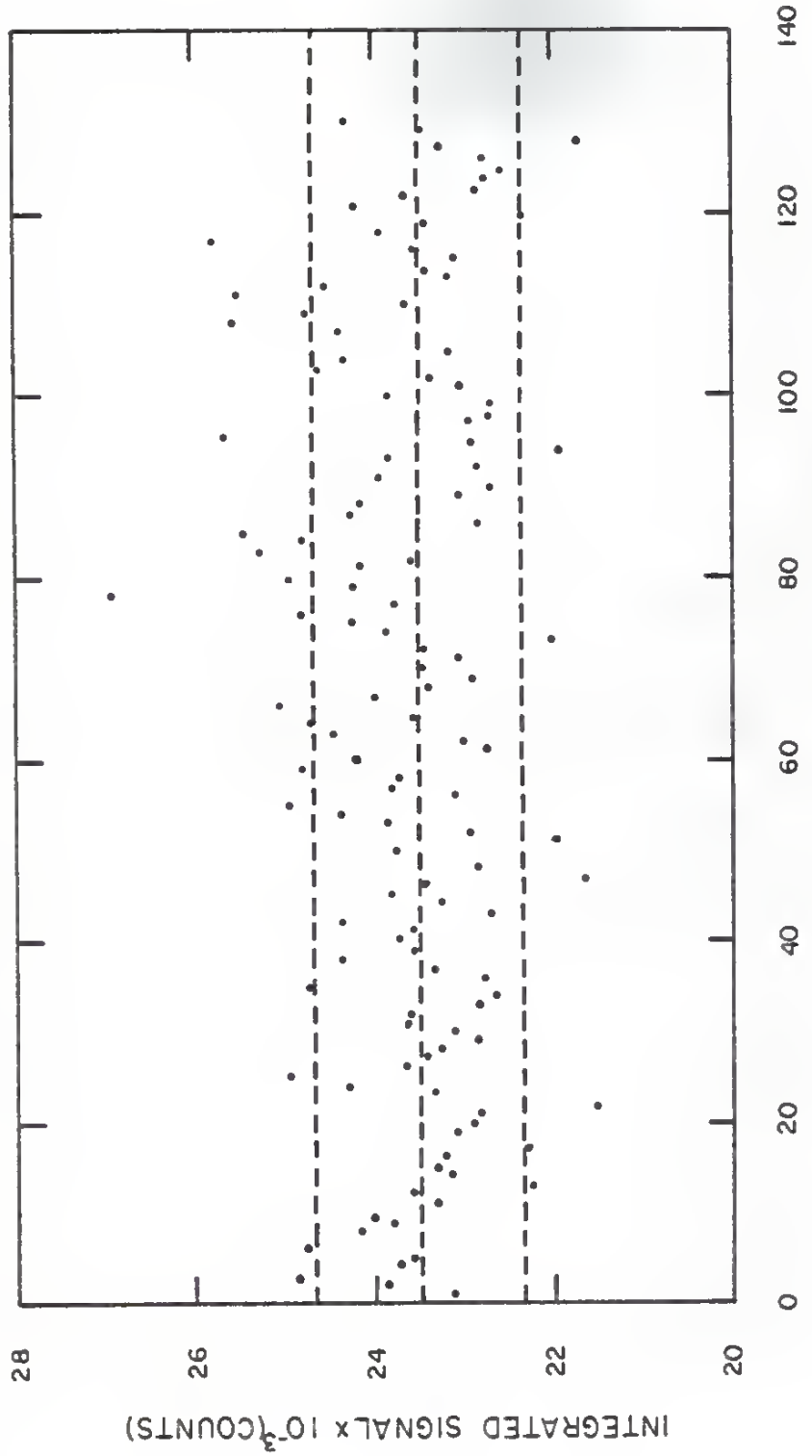

Fig. 18. Variation in the sensitivities of sort 2 TLDs for a uniform dose and fast-heat readout cycle.

calculated using only those readouts within the 6% limits. The mean values for the entire group of 130 TLDs were calculated and found to agree within 2%.

If the data shown in Figs. 16 and 17 are considered qualitatively, definite trends are apparent. The group of TLDs numbered 70-85 tended to have sensitivities consistently above the mean. Those in the group numbered 90-130, however, tended to exhibit sensitivities below the mean. This indicated that the scatter in the data about the mean was due to actual variations in sensitivity among the dosimeters and not caused by some inconsistency in the readout process or instrumentation. Moreover, since TLDs were numbered as they were removed from the capsules supplied by Harshaw, a correlation existed between the sensitivities of the TLDs and the capsules from which they came. Therefore, because of the process used to manufacture and package these TLDs, the ones sharing the same capsule had similar sensitivities which, in some instances, differed from those of other capsules.

It can also be qualitatively noted from the data in Figs. 16 and 17 that those TLDs with sensitivities which varied widely from the mean tended to do so consistently. This suggests the application of a sort correction factor to force the dosimeter's readouts to the mean. This would reduce the spread in data obtained in subsequent measurements. This correction factor might also be applied to those readouts near the mean. However, it was apparent that this would do little to improve the spread in the data obtained using these TLDs in later

measurements. A number of the TLDs with readouts above the mean in sort 1A had readouts below the mean in sort 1B and vice versa. Hence, the correction factor might worsen the spread in the data for TLDs with readouts near the mean. Based on these data, the 3.20% standard deviation calculated for the 100 selected TLDs in sort 1B could not be improved upon in subsequent measurements by the application of a sort correction factor. However, had it been necessary to utilize all 130 TLDs, applying sort correction factors to those with widely varying sensitivities would have improved the data. In this work, sufficient dosimeters were available to simply not use those with widely varying sensitivities.

The 130 TLDs comprising sort 2 tended to have sensitivities which were not as varied as those in sorts 1A and 1B. The standard deviation for the 100 selected dosimeters was only 2.36%. The mean readout for this group was 23,498 counts. The limits drawn on Fig. 18 are 5% as compared to the 6% limits necessary in sorts 1A and 1B. As was the case for sort 1B TLDs, the 100 sort 2 TLDs selected were renumbered consecutively.

8.1.2 Glow-Peak Height Approach

Since the height of the peak in a TLD's glow curve is proportional to dose (in the same manner as is the area under the glow curve), it can be used as a measure of the dosimeter's response to radiation. An analysis of the glow-peak height data taken in the sort irradiations revealed results similar to those obtained using the integrated count

approach. The standard deviations, however, tended to be higher. For example, the mean analog peak height for the group of 100 TLDs selected in sort 1B was 96.4 mV with a standard deviation of 4.20%. The mean digital peak height for this same group was 8,759 cps with a standard deviation of 4.21%. These values for standard deviations should be compared to that of 3.20% as calculated for the same group of TLDs using the net integrated count data. It was apparent that the integral count data were more consistent than were the glow-peak height.

8.2 System Calibration

8.2.1 Integrated Count Approach

It is necessary, before using TLDs to make dose determinations, that a calibration curve be constructed. The departure of this curve from linearity can be used to define the readout system's dynamic range. Summaries of the data taken for both the slow- and fast-heat readout cycles (groups 1 and 2, respectively) are listed in Tables IV-VI as mean net readouts and standard deviations for each irradiation. A comparison of these quantities for each irradiation (i.e., for each trial) indicated that they agreed fairly well. The comparison was better at higher doses where the standard deviations were smaller. For this reason, the irradiation of five dosimeters at a single time was considered sufficient to give a valid indication of net readout and standard deviation at higher doses. For the low-dose measurements, five TLDs were irradiated and read more than once for each dose investigated. These data were combined and are presented as mean net readout and standard deviation for each dose investigated

Table IV. Summary of the irradiation results for system calibration using both the fast and slow readout cycles.

	Fast Heat Rate						Slow Heat Rate			
	Trial 1		Trial 2		Trial 3		Trial 1		Trial 2	
Dose (mrad)	Average Signal (counts)	Standard Deviation (%)	Average Signal (counts)	Standard Deviation (%)	Average Signal (counts)	Standard Deviation (%)	Average Signal (counts)	Standard Deviation (%)	Average Signal (counts)	Standard Deviation (%)
0.11	33.6	210	16.4	301	58.2	179	163.6	43.4	51.2	125
0.31	134.6	38.6	161.4	36.5	127.6	69.8	161.0	75.3	171.6	68.2
0.61	258.4	18.8	276.6	17.8	240.2	35.0	312.4	19.3	345.4	22.0
0.94	405.0	14.2	438.2	12.8	426.5	24.7	512.0	10.5	479.8	10.8
1.62	661.8	4.14	717.8	13.1	740.0	16.8	921.3	6.88	825.0	6.54
2.18	--	--	1,040	5.76	1,025	8.59	1,092	7.55	1,055	8.28
4.82	2,230	2.93	2,219	5.71	2,210	3.56	2,271	8.06	2,205	4.55
8.50	3,795	1.75	3,939	2.99	4,046	4.22	4,295	1.99	4,194	5.86
18.7	8,129	3.09	8,365	3.57	8,278	3.25	8,875	1.82	9,035	2.77
67.1	28,469	5.06	30,191	2.89	29,408	1.09	30,122	3.28	30,497	2.43

Table V. Calibration curve data for the photon counting TLD analyzer system utilizing the slow-heat readout cycle.

Dose (rad)	Number of Measurements	Average Signal (Counts)	Standard Deviation (Counts)	Standard Deviation (%)
1.1×10^{-4}	10	107.4	87.07	81.1
3.1×10^{-4}	10	166.3	112.5	67.6
6.1×10^{-4}	10	328.9	66.92	20.3
9.4×10^{-4}	10	495.9	52.71	10.6
1.62×10^{-3}	9	867.8	74.39	8.57
2.18×10^{-3}	10	1073	82.42	7.68
4.82×10^{-3}	10	2238	143.5	6.41
8.50×10^{-3}	10	4244	181.4	4.27
18.7×10^{-3}	10	8,964	220.0	2.45
67.1×10^{-3}	10	30,310	847.1	2.79
.208	5	104,574	2,247	2.15
.570	5	285,402	7,049	2.47
1.26	5	629,370	8,298	1.32
4.49	5	2,246,486	60,069	2.67
36.5	5	17,081,200	463,597	2.71
88.2	5	43,193,436	1,471,985	3.45
140	5	62,869,246	1,632,261	2.60
192	5	80,824,636	1,860,198	2.30
243	5	96,641,092	621,914	0.64
346	5	120,591,902	2,362,069	1.96
450	5	140,206,318	2,612,730	1.86
656	5	162,849,574	2,651,221	1.63

Table VI. Calibration curve data for the photon counting TLD analyzer system utilizing the fast-heat readout cycle.

Dose (rad)	Number of Measurements	Average Signal (Counts)	Standard Deviation (Counts)	Standard Deviation (%)
1.1×10^{-4}	15	36.07	74.49	206
3.1×10^{-4}	15	141.2	65.24	46.2
6.1×10^{-4}	15	258.4	60.21	23.3
9.4×10^{-4}	14	423.0	69.08	16.3
1.62×10^{-3}	15	706.5	91.14	12.9
2.18×10^{-3}	10	1,032	71.40	6.92
4.82×10^{-3}	15	2,220	87.52	3.94
8.50×10^{-3}	15	3,927	157.8	4.02
18.7×10^{-3}	15	8,258	272.6	3.30
67.1×10^{-3}	15	29,356	1,170	3.99
.215	5	95,388	1,053	1.10
.586	5	273,384	4,279	1.57
1.29	5	555,706	8,120	1.46
4.63	5	2,023,006	23,649	1.17
36.5	5	16,252,498	201,782	1.24
88.2	5	36,035,852	677,464	1.88
140	5	50,775,744	1,624,732	3.20
346	4	82,974,528	918,281	1.11
656	5	105,971,084	1,037,184	0.98

in Tables V and VI. Calibration curves, based upon the values in these tables, are shown in Figs. 19 and 20 for both heat cycles. The error bars on these figures are $\pm$ 1 standard deviation and indicate the reproducibility of the data. The high dose portions of these calibration curves are shown in Figs. 21 and 22. It was determined by their departure from linearity that the system's dynamic range extended to nominally 100 rads for the slow-heat readout cycle and to nominally 40 rads for the fast-heat readout cycle.

The major factor influencing the lower dynamic range of a system is reproducibility. Figure 23 illustrates the behavior of this factor in the form of standard deviation as a function of dose. The data measured using the slow-heat readout cycle tended to retain better reproducibility to lower doses than did the fast-heat readout cycle derived data. The relatively low SNRs associated with this dose range are the primary factors affecting reproducibility. Hence, an explanation for the differences in the reproducibilities for the two readout cycles is suggested. A slope of 500 counts/mrad for the slow-heat readout cycle and a slope of 437 counts/mrad for the fast-heat readout cycle were calculated from the linear least-squares fits to the calibration curves. The 14% more counts measured per mrad using the slow-heat readout cycle improved the SNR and therefore, improved the reproducibility over that obtained utilizing the fast-heat readout cycle. This difference in signal measured per unit dose was attributed to the finite thermal conductivity of the TLD. More of the crystal reached a sufficiently high temperature to release the trapped charges during the slow-heat readout than the fast-heat readout.

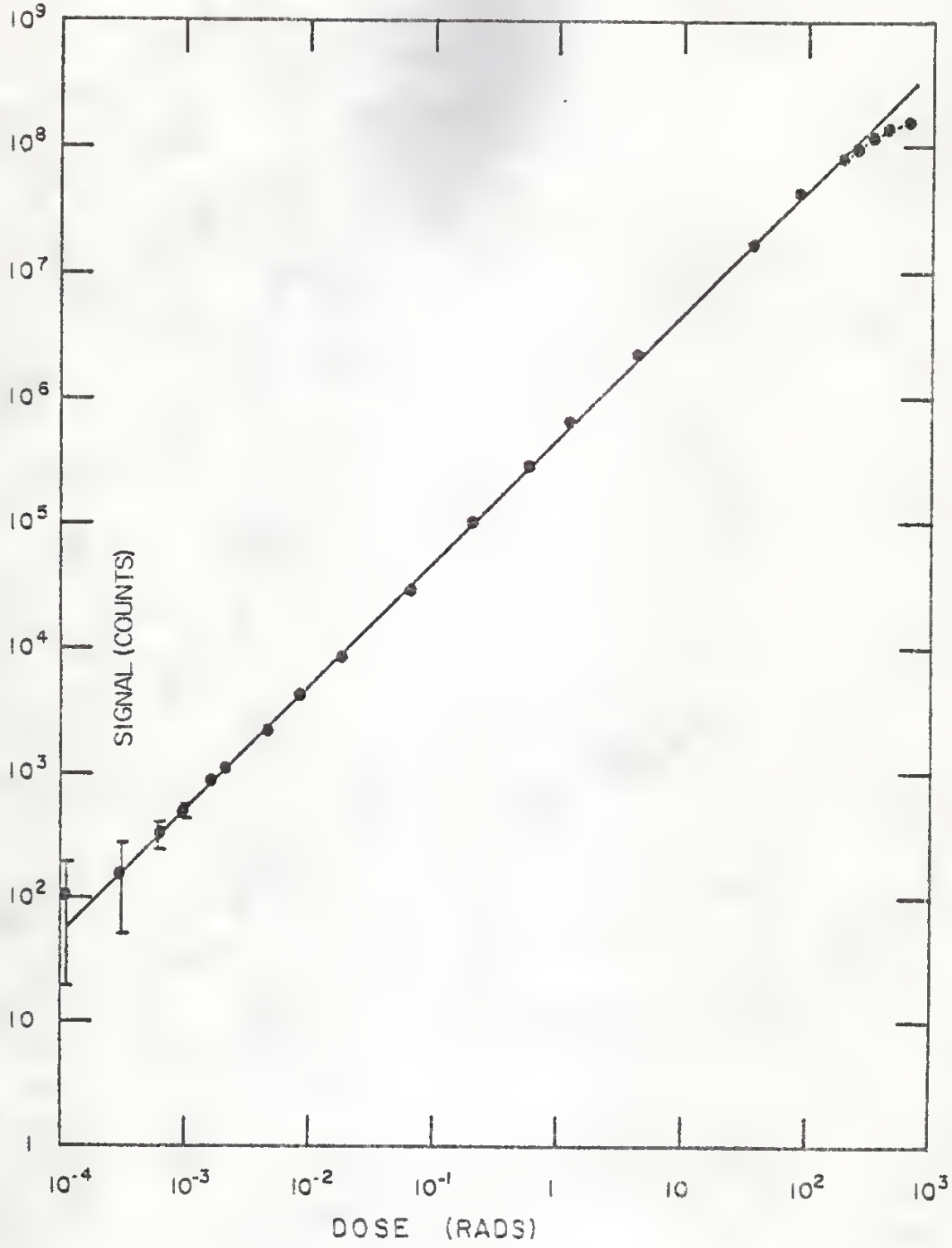

Fig. 19. Calibration curve for the photon counting TLD analyzer utilizing the slow-heat readout cycle. The signal quantity was obtained by subtracting the second readout from the first. The absorbed dose corresponds to rads in stainless steel and the straight line is linear least-squares fit to the data.

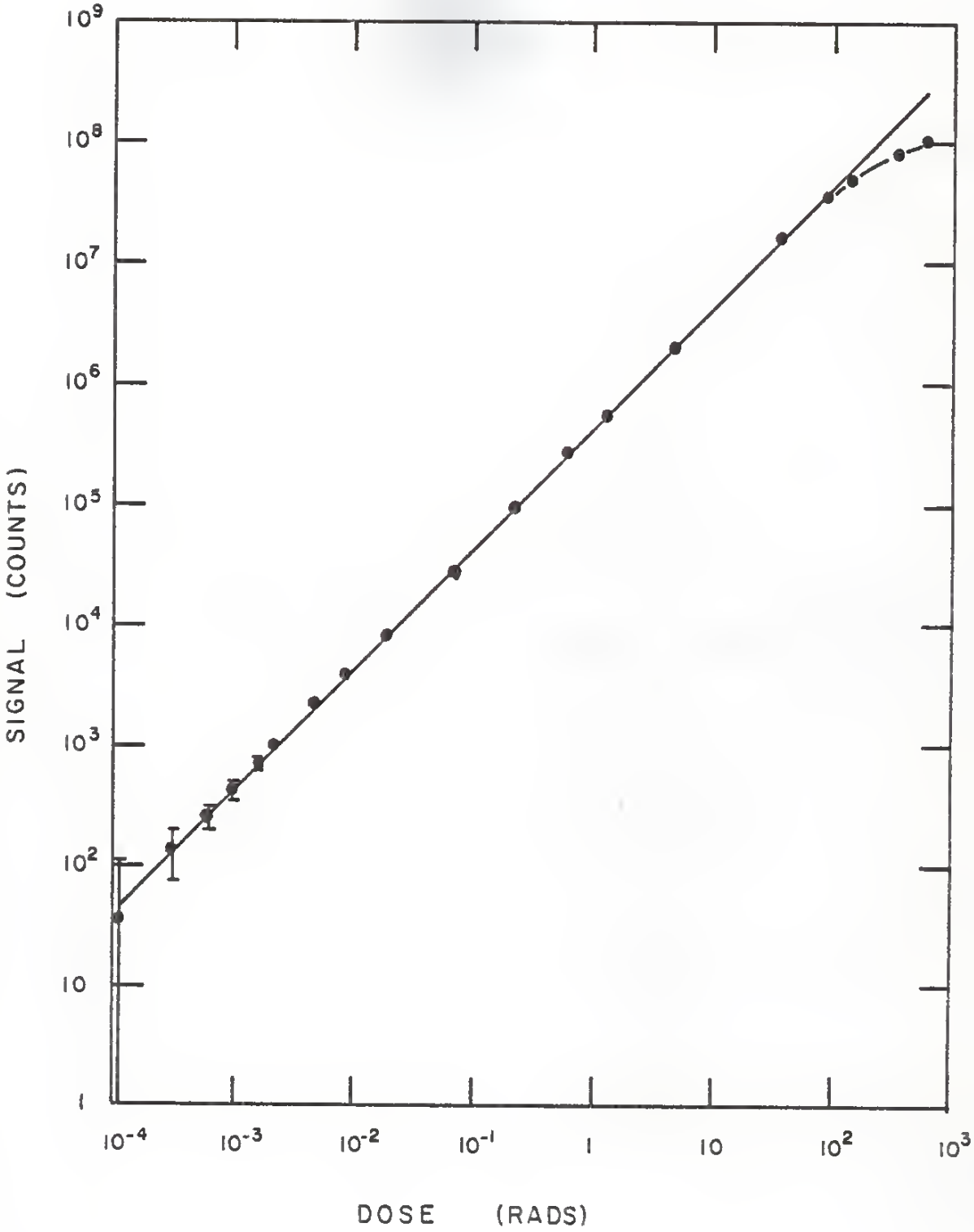

Fig. 20. Calibration curve for the photon counting TLD analyzer utilizing the fast-heat readout cycle. The signal quantity was obtained by subtracting the second readout from the first. The absorbed dose corresponds to rads in stainless steel and the straight line is a linear least squares fit to the data.

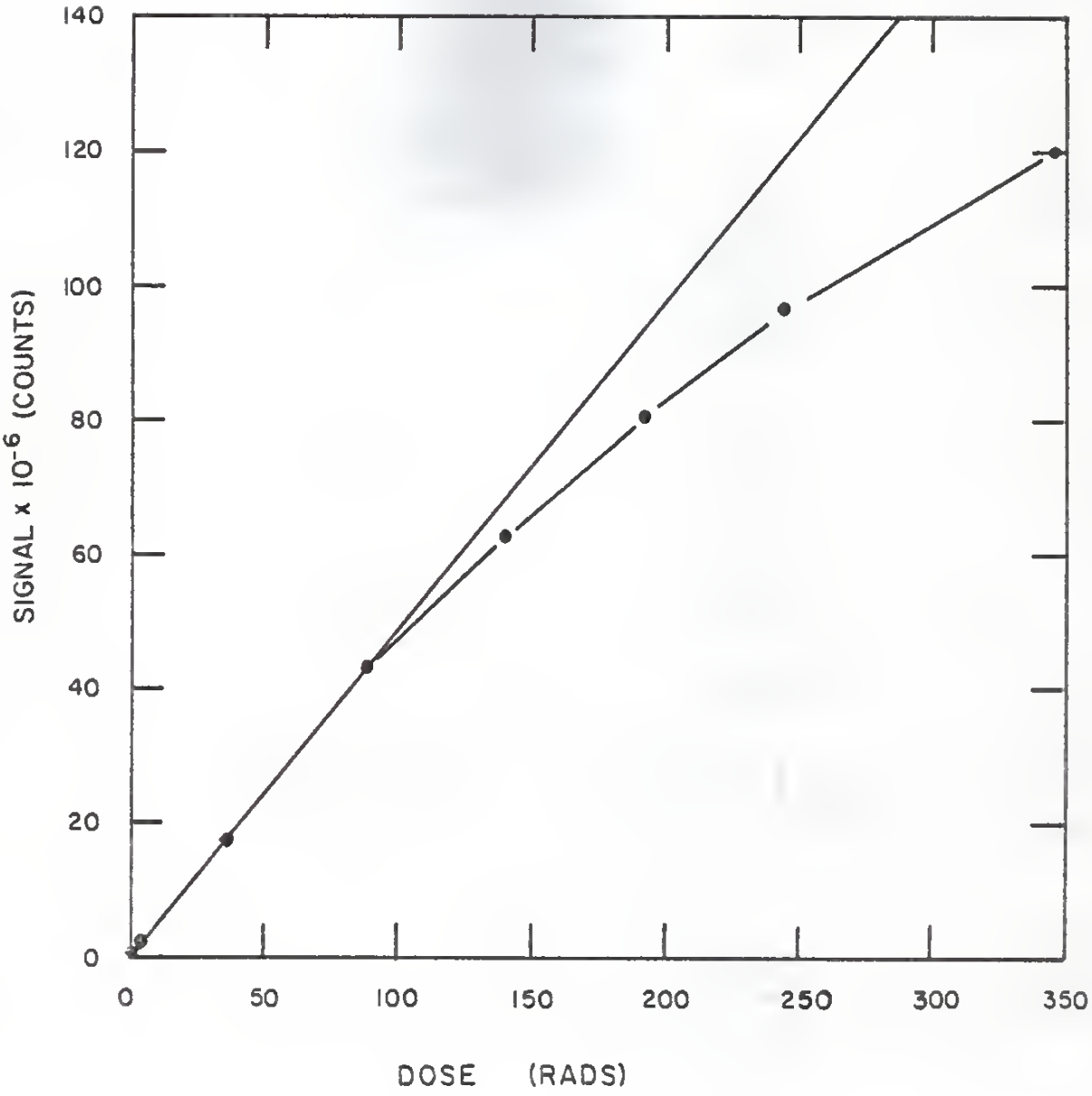

Fig. 21. Illustration of the photon counting TLD analyzer's upper dynamic range utilizing the slow-heat readout cycle. Dose is rads in stainless steel and the straight line is the linear least-squares fit to the linear portion of the calibration curve (straight line segments added for visual clarity).

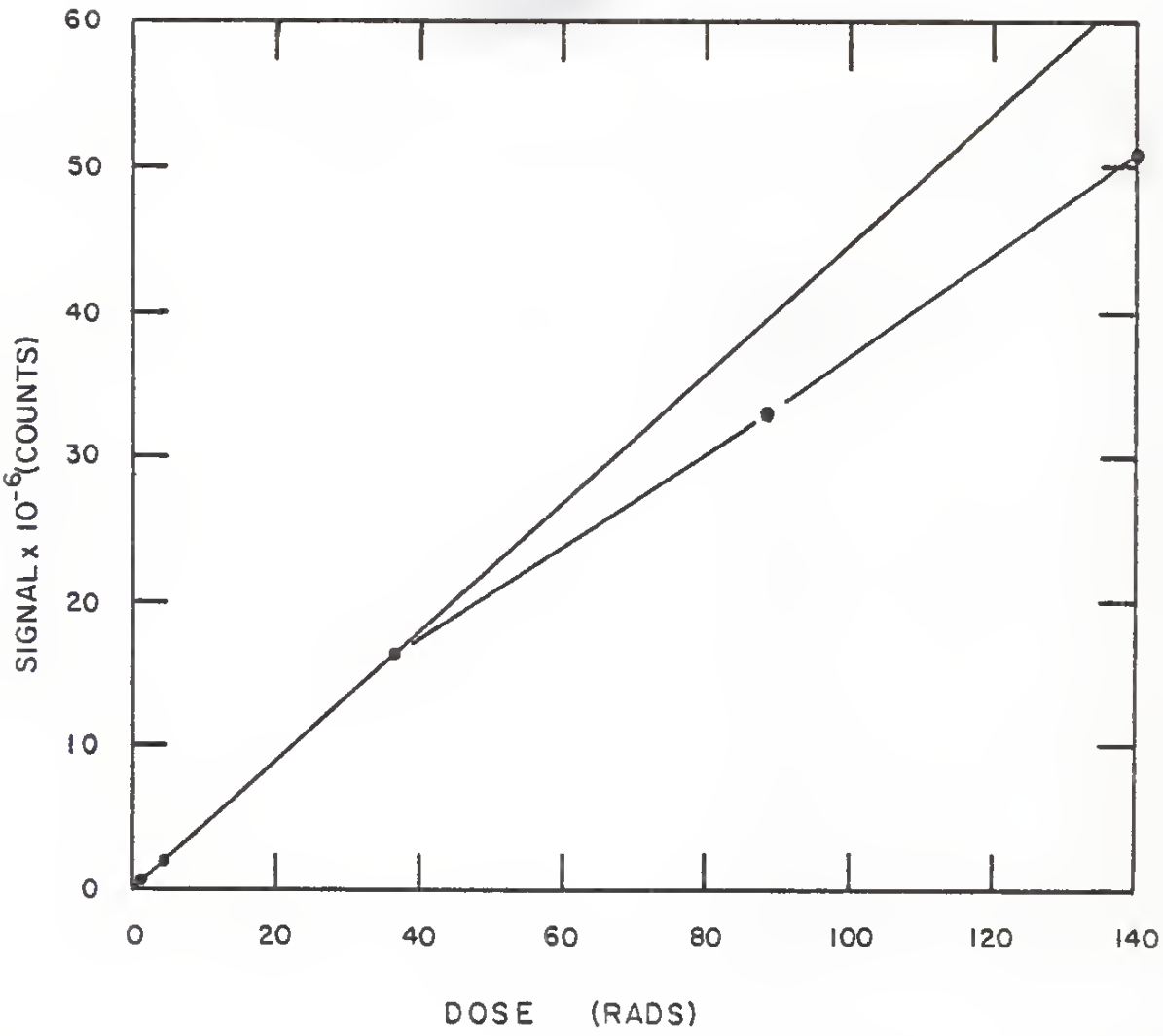

Fig. 22. Illustration of the photon counting TLD analyzer's upper dynamic range utilizing the fast-neat readout cycle. Dose is rads in stainless steel and the straight line is the linear least-squares fit to the linear portion of the calibration curve (straight line segments added for visual clarity).

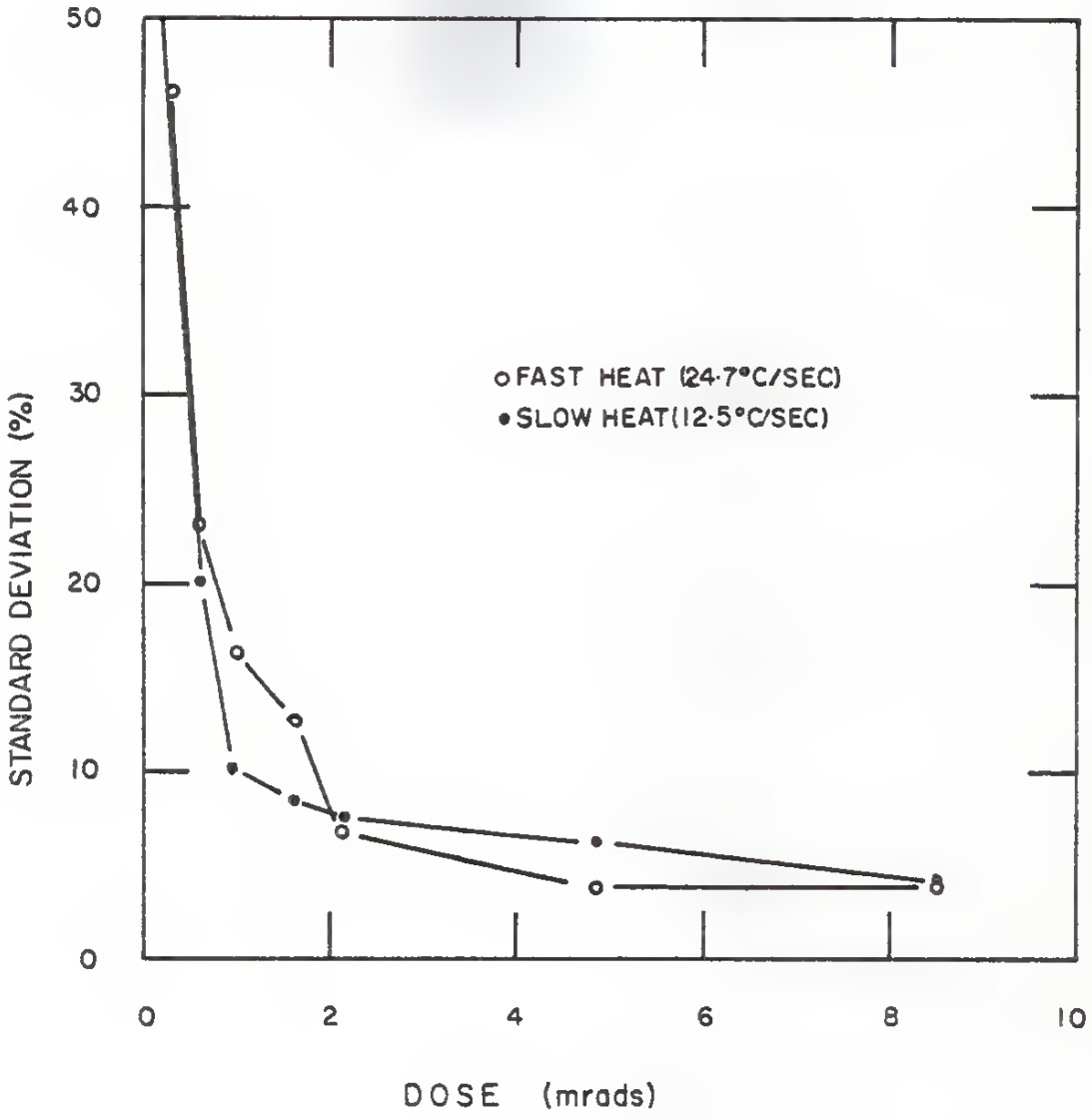

Fig. 23. Reproducibility of dose determinations (mrads in stainless steel) utilizing the photon counting TLD analyzer in conjunction with the second readout subtraction technique (straight line segments added for visual clarity).

At low doses, the TLD's second readout of approximately 700 counts was composed largely of PMT dark noise. The PMT dark noise rate was measured to be about 50 cps. Since the slow-heat readout cycle had a duration (during which the counter was active) of 10 sec, the PMT dark noise contribution was the dominant source of photons measured during the second readout. The second readout, as determined using the fast-heat readout cycle, was about the same as that obtained using the slow-heat readout cycle. However, it had a duration of only 5 sec. Thus, the PMT dark noise contributed only 250 counts. The remaining portion of the signal must have been due to contributions from radiation induced TL not liberated during the first readout as well as increased non-radiation induced TL and planchet radiation because of the higher planchet temperatures reached.

Proper photon counter gating was necessary in order to obtain reproducible dose measurements. The shape of the glow peak and its variation with dose determined the temperature interval over which the counter was active during the readout process. Figures 24 and 25 depict this relationship for both the slow- and fast-heat readout cycles. As the dose to the TLD was increased, the leading and trailing edges of its glow peak occurred at lower and higher temperatures, respectively. Therefore, it was important that the counter integration period be long enough to obtain the area of the entire glow peak. Otherwise, the linearity of the calibration curve would be limited by loss of counts rather than pulse pile-up at high doses. Additionally, short integration periods prevented the background levels from obscuring the desired signal at

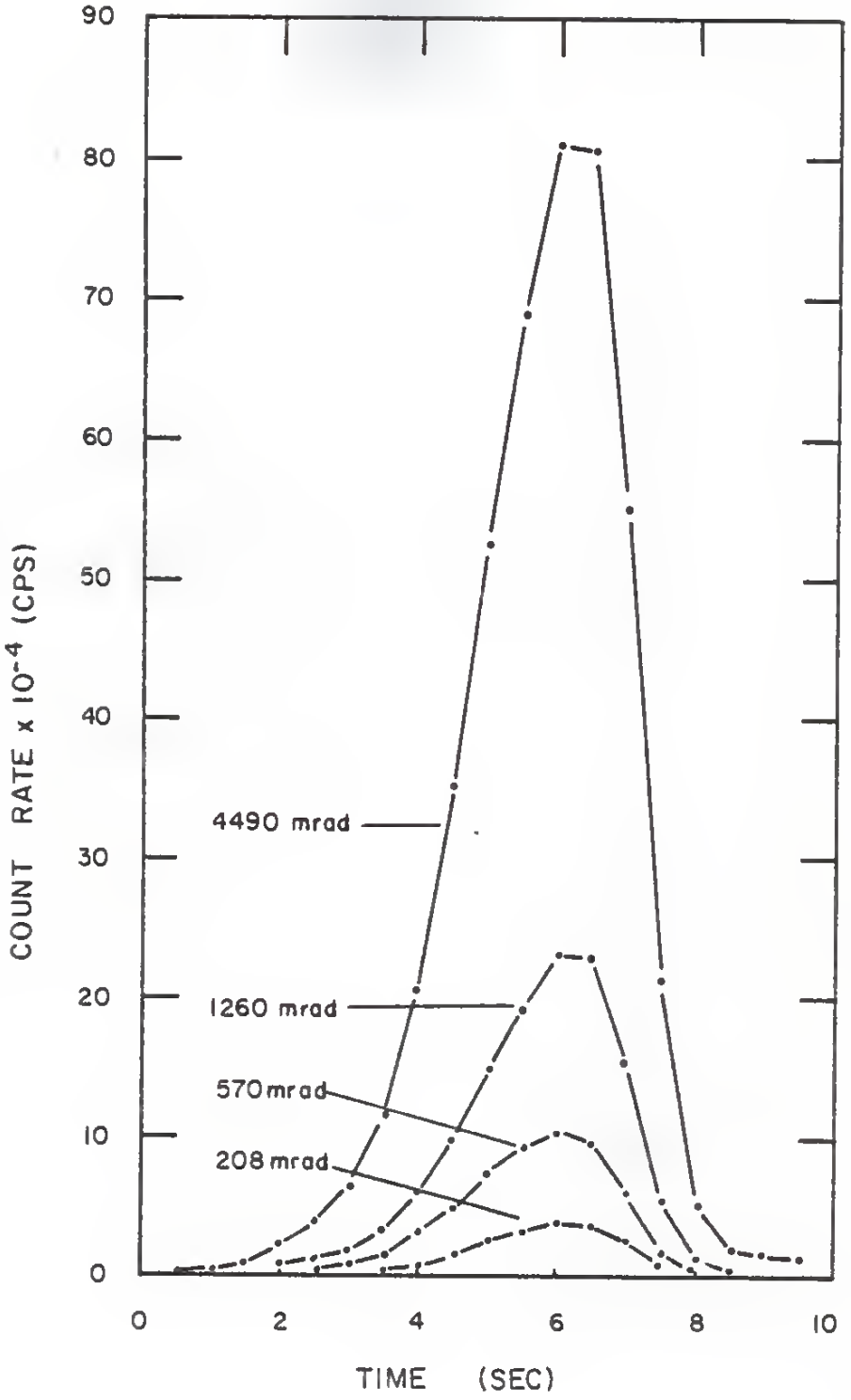

Fig. 24. Variation of glow curve shape with dose (mrads in stainless steel). Data were obtained digitally utilizing the slow-heat readout cycle where time = 0 corresponds to 130 °C (straight line segments added for visual clarity).

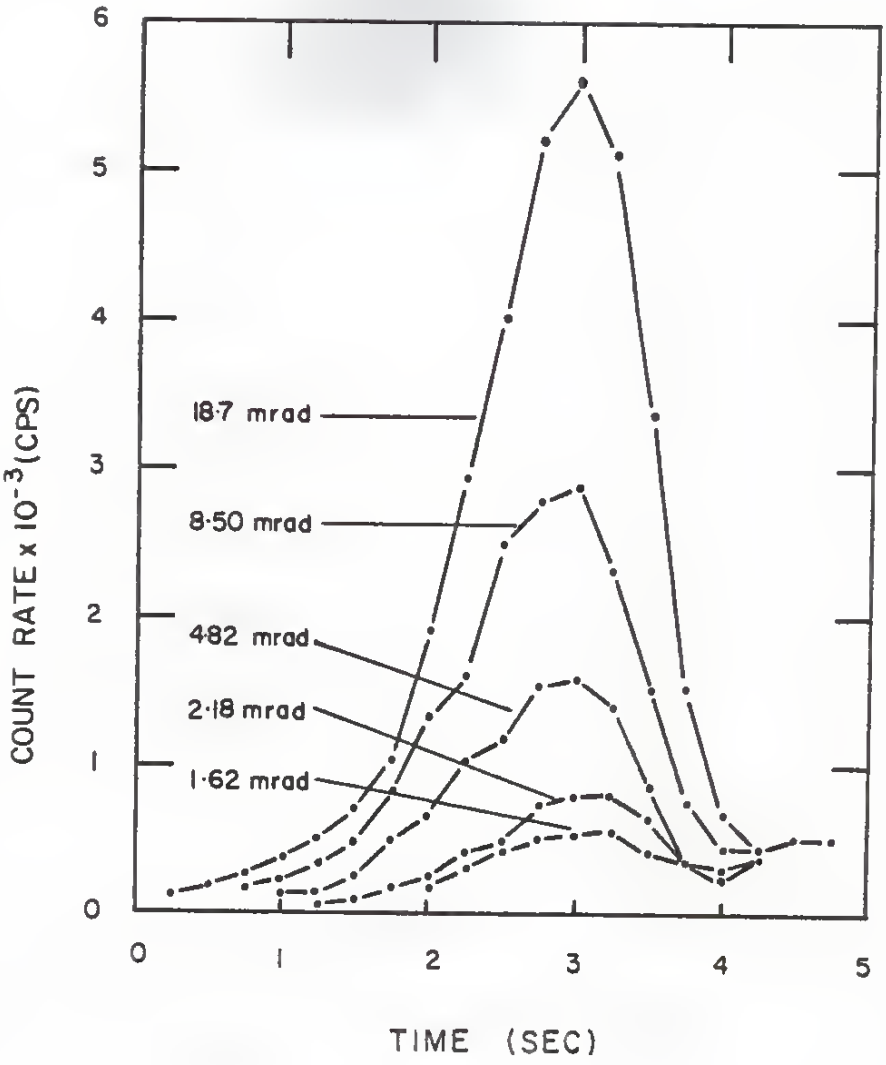

Fig. 25. Variation of glow curve shape with dose (mrads in stainless steel). Data were obtained digitally utilizing the fast-heat readout cycle where time = 0 corresponds to 150 °C (straight line segments added for visual clarity).

low-dose levels. Figure 26 illustrates the effect of heating rate on the shape of the glow peak. For comparison, the slow-heat glow peak was adjusted so that its peak occurred at the same time as the fast-heat glow peak. It was inferred from this figure that the fast-heat calibration data became nonlinear at a lower dose than did the slow-heat calibration data.

8.2.2 Glow-Peak Height Approach

As was the case for integrated count data, a calibration curve can be constructed utilizing glow-peak height data. These measurements, made simultaneous with the integrated count measurements, are summarized in Table VII. The resulting calibration curves are shown in Figs. 27 and 28 for both digital and analog peak height data as well as for both readout cycles. The standard deviation error bars were omitted from these figures only for visual clarity and were included in Table VII. They illustrated that these data were not as reproducible as the integrated count data. Additionally, the peak heights could not be determined from the glow curves of TLDs given doses below 1.5 mrads. The least-squares slope of the analog peak height calibration curves were calculated to be 1.91 mV/mrad and 3.03 mV/mrad for the slow- and fast-heat readout cycles, respectively. The PAR ratemeter transfer function was calculated as the slope of the digital peak height data versus the linear peak height data to be 94.7 cps/mV. Thus, the analog glow-peak calibration curve slopes became 181 cps/mrad for the slow-heat readout cycle and 286 cps/mrad for the fast-heat readout cycle. The value of 20 MHz as the maximum linear count rate (see Section 5.2)

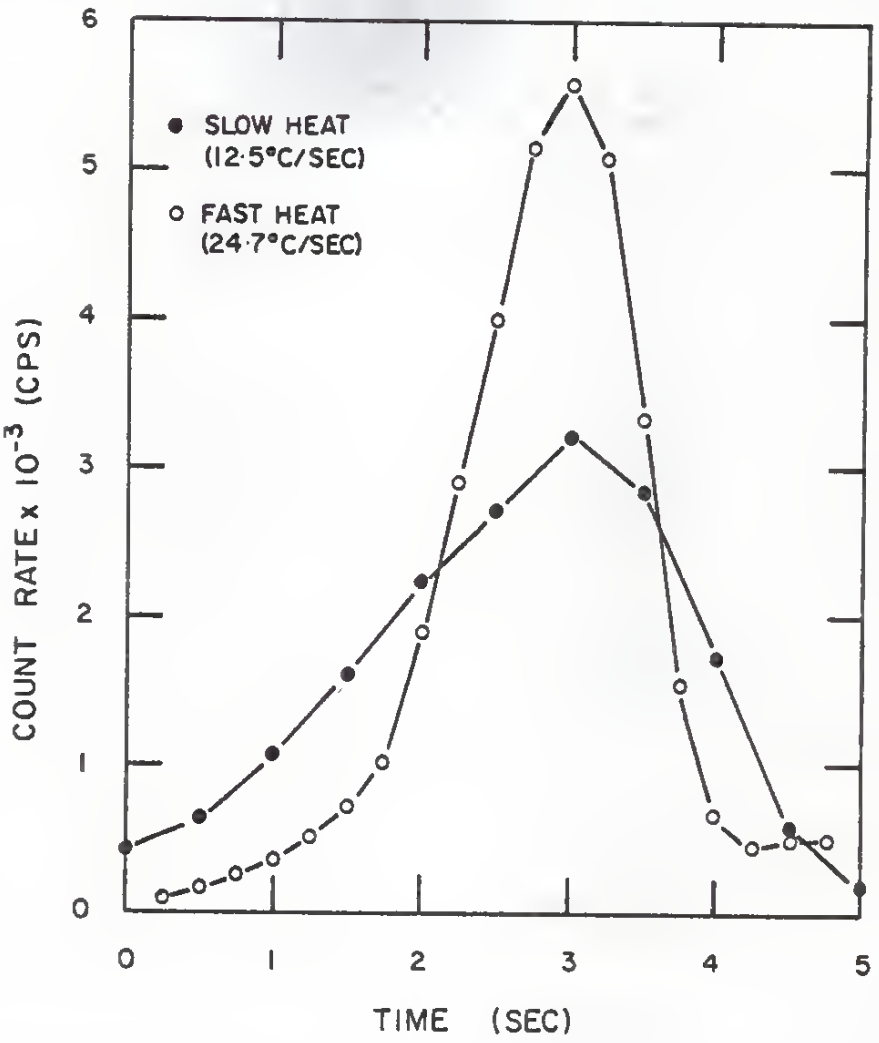

Fig. 26. Glow curve variation with dosimeter heating rate for TLDs given the same dose of 18.7 mrads in stainless steel. The slow-heat peak was adjusted so that it occurred at the same time as the fast-heat peak (straight line segments added for visual clarity).

Table VII. Glow-peak height calibration data for the photon counting TLD analyzer system.

Slow Heat Rate					Fast Heat Rate				
	Analog		Digital			Analog		Digital	
Dose (mrad)	Mean Peak Height (mV)	Standard Deviation (%)	Mean Peak Height (cps)	Standard Deviation (%)	Dose (mrad)	Mean Peak Height (mV)	Standard Deviation (%)	Mean Peak Height (cps)	Standard Deviation (%)
1.62	3.68	13.5	344.8	8.04	1.62	6.34	11.6	622.1	6.26
2.18	5.16	13.2	463.4	7.79	2.18	8.41	11.2	820.5	10.0
4.82	9.97	9.00	891.0	6.48	4.82	16.86	6.44	1,586	6.28
8.50	17.63	5.06	1,597	3.95	8.50	28.08	7.80	2,673	7.79
18.7	35.72	4.08	3,256	4.36	18.7	58.54	7.92	5,411	6.07
67.1	117.7	3.06	10,429	5.30	67.1	198.9	9.12	17,571	8.13
208	430.1	4.44	37,920	4.07	215	693.6	5.30	123,690	2.56
570	1,151	3.78	106,316	3.93	586	1,916	2.40	181,568	3.39
1,260	2,424	2.05	227,352	1.90	1,290	3,932	2.99	395,094	10.3
4,490	8,596	3.45	813,608	2.99	4,630	14,014	0.93	-	-

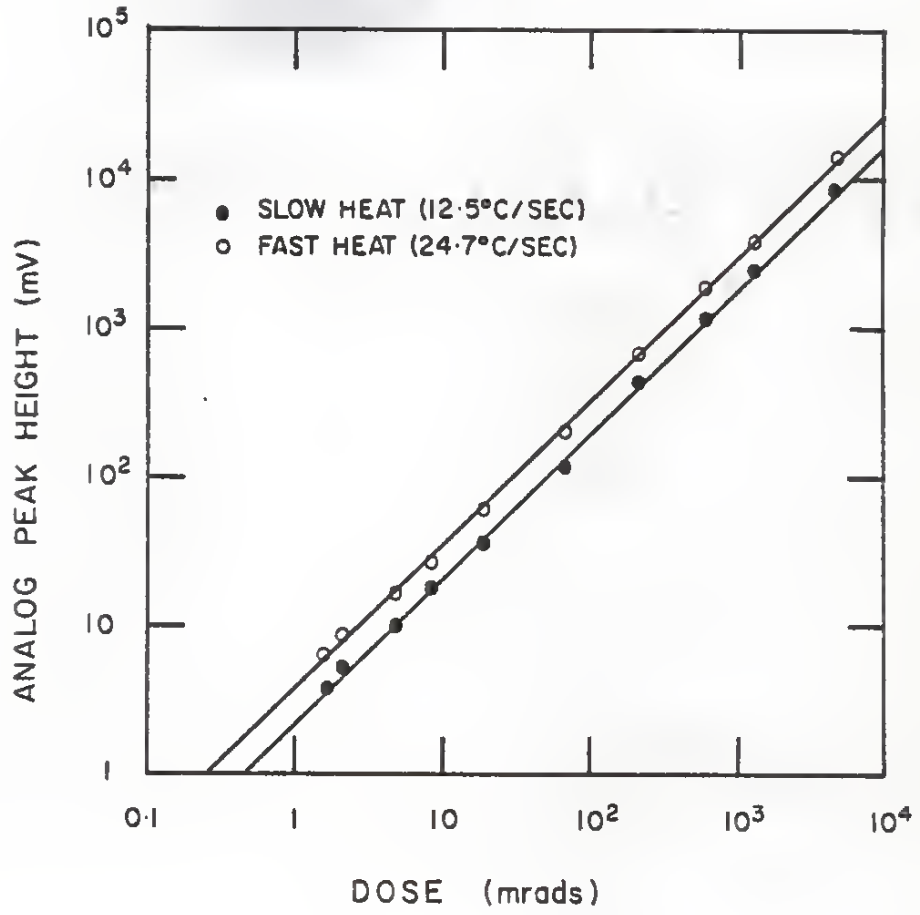

Fig. 27. Calibration curves for the two heat cycles obtained utilizing the PAR discriminator's ratemeter output. Absorbed dose is mrads in stainless steel with the straight lines resulting from the linear least-squares fits to the data.

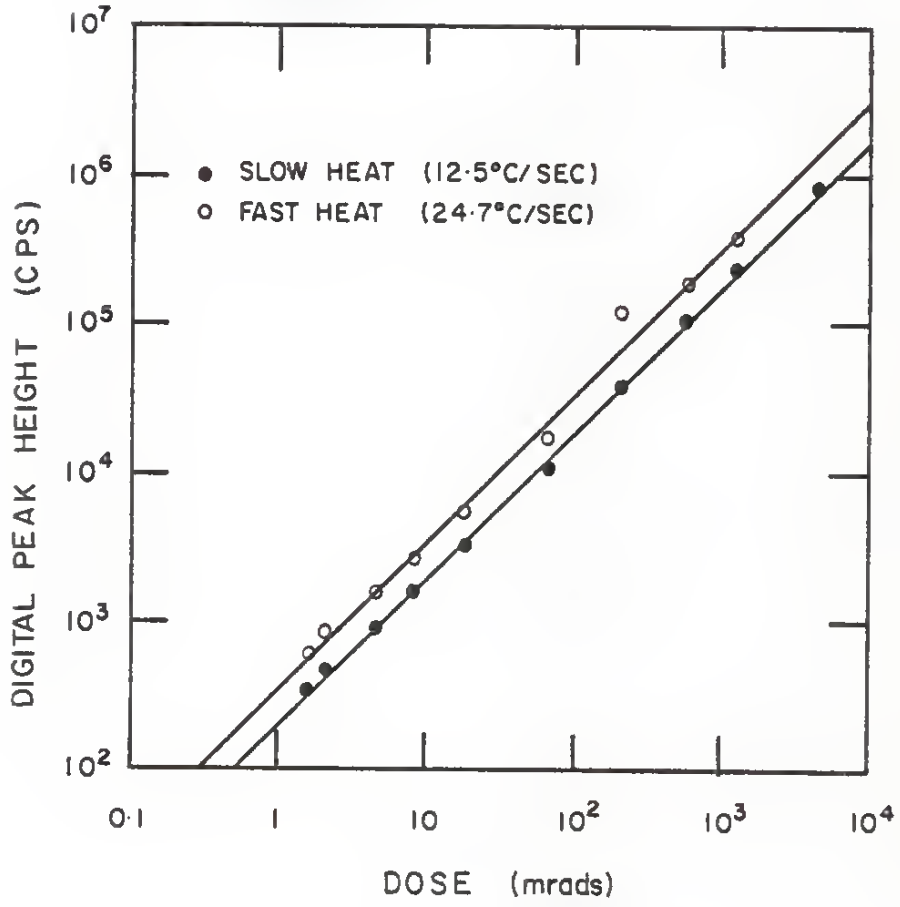

Fig. 28. Calibration curves for the two heat cycles obtained digitally utilizing the photon counting TLD analyzer. Absorbed dose is mrads in stainless steel with the straight lines resulting from linear least-squares fits to the data.

was then used to approximate the maximum measureable dose. It was 110 rads for the slow-heat readout cycle and 70 rads for the fast-heat readout cycle. These values compared fairly well to those determined earlier of 100 rads and 40 rads.

As was apparent from the data in Table VII, the glow-peak height calibration curves exhibited consistently poorer reproducibility than did the integrated count curves. This was a direct result of the strong glow-peak height dependence on heating rate as shown in Fig. 26. Variations in heating rates between the readout of TLDs induced systematic differences between subsequent peak-height measurements. This was not necessarily an indication of variations in the planchet heating rate due to imprecise control circuits although it may have been a contributing factor. It more likely was caused by differences in the thermal contact existing between the individual dosimeters and the heating planchet. Thus, individual placement of TLDs on the planchet as well as differences in their surface conditions may have induced variations in the peak-height data.

8.3 Single Readout Procedure

The process of heating individual TLDs twice was very time consuming. Moreover, it may be impractical if large numbers of dosimeters are being utilized. It was, therefore, of interest to investigate the low-dose characteristics of this system utilizing only the first readout. The second readouts for the first 50 dosimeters in each group were averaged. Values of 754 and 836 counts were obtained for the slow- and fast-heating rates. The results obtained through the subtraction

of these constant background values were tabulated in Table VIII. At higher doses, the second readout was relatively insignificant compared to the first. Hence, the difference between subtraction of a constant or the second readout was found to be small. It was in the reproducibility of low-dose measurements where significant differences were noted. The reproducibility of measurements using this constant background subtraction analysis is shown in Fig. 29 as a function of dose. When figs. 29 and 23 were compared, it was apparent that, above 5 mrad, the curves were essentially the same. Below this point, the constant background subtraction analysis resulted in poorer reproducibility than did the two readout analysis. This indicated that each dosimeter had a certain amount of spurious signal due entirely to its own characteristics and history. It could also be indicative of slight variations in the readout cycle. Although not noticeable in a few readouts taken over a short time span, its effect would tend to increase over relatively longer periods.

8.4 Dose Determination Using Second Readouts

One of the disadvantages of thermoluminescent dosimetry is the destruction of dose information which occurs during the readout of a TLD. Thus, it is of interest to investigate the second readout to determine if it contains any useful dose information. For doses below about 1 rad, the second readouts were essentially the same regardless of the dose given the TLD. However, at higher doses, the second readout increased as the dose increased. Table IX summarizes

Table VIII. Calibration data for the photon counting TLD analyzer system utilizing the single readout (constant background subtraction) technique.

Slow Heat Rate				Fast Heat Rate			
Dose (mrad)	Number of Measurements	Average Signal (Counts)	Standard Deviation (%)	Dose (mrad)	Number of Measurements	Averge Signal (Counts)	Standard Deviation (%)
0.11	10	146.2	52.1	0.11	15	51.3	171
0.31	10	234.6	38.4	0.31	15	171.3	45.3
0.61	10	363.4	21.3	0.61	15	272.4	32.3
0.94	10	466.0	22.6	0.94	15	458.9	38.2
1.62	9	835.7	10.5	1.62	15	787.3	14.8
2.18	10	1,035	10.3	2.18	10	967.4	9.21
4.82	10	2,238	3.88	4.82	15	2,164	5.57
8.50	10	4,269	4.26	8.50	15	3,894	4.07
18.7	10	8,924	3.11	18.7	15	8,229	3.04
67.1	10	30,281	2.98	67.1	15	29,330	3.93
208	5	104,542	2.18	215	5	95,270	1.06
570	5	285,506	2.44	586	5	273,220	1.54
1,260	5	629,900	1.29	1,290	5	555,648	1.47
4,490	5	2,249,674	2.66	4,630	5	2,023,582	1.17
36,500	5	17,104,804	2.71	36,500	5	16,261,154	1.24
88,200	5	43,253,602	3.47	88,200	5	36,060,644	1.87
140,000	5	63,076,605	2.61	140,000	5	50,828,170	3.19
192,000	5	81,141,822	2.28	--	--	--	--
243,000	5	97,156,236	0.62	--	--	--	--
346,000	5	121,362,784	1.98	346,000	4	83,143,452	1.12
450,000	5	141,408,226	1.80	--	--	--	--
656,000	5	164,980,354	1.58	656,000	5	106,447,588	1.04

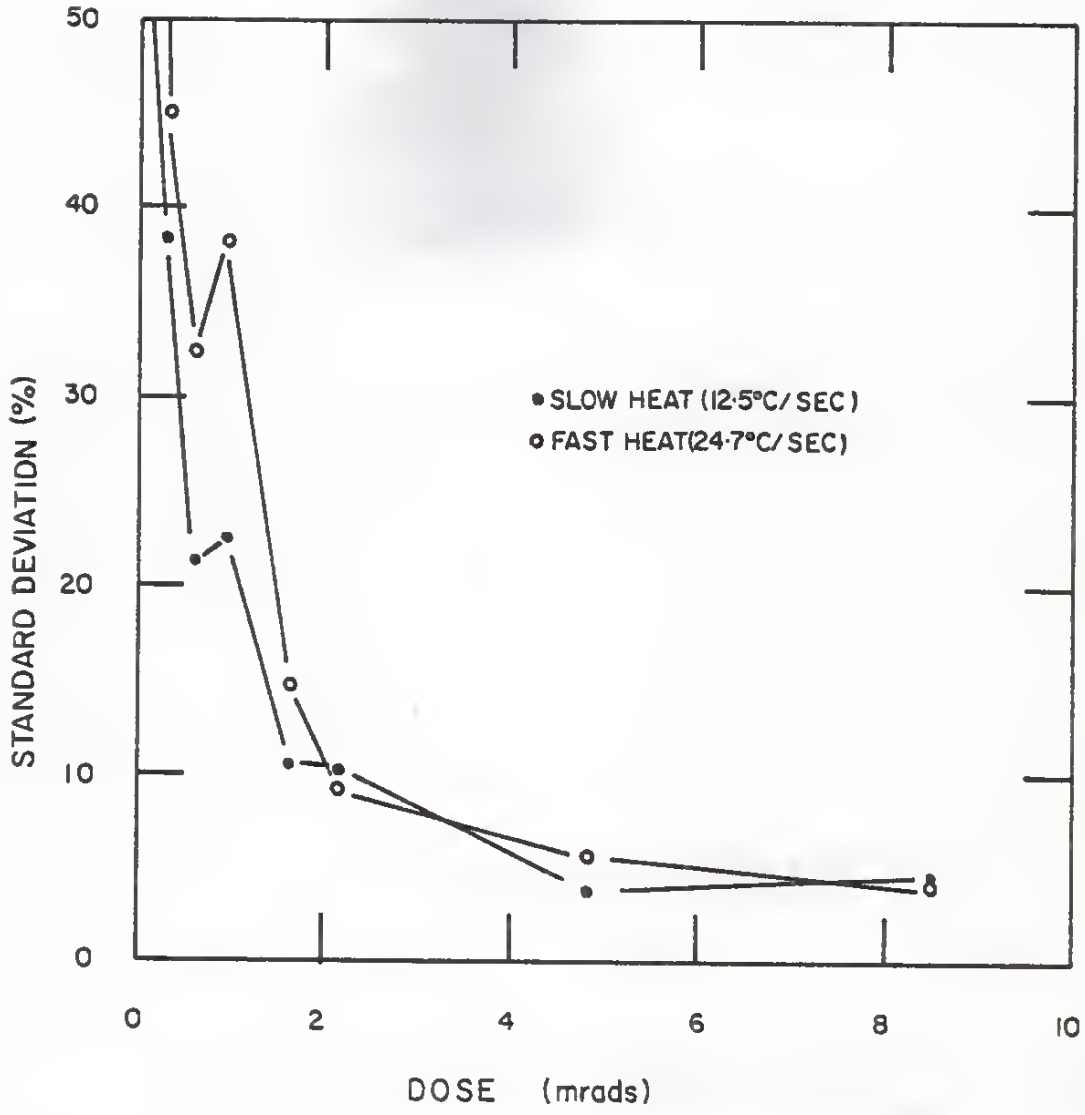

Fig. 29. Reproducibility of dose determinations (mrads in stainless steel) utilizing the photon counting TLD analyzer in conjunction with the constant background subtraction technique (straight line segments added for visual clarity).

Table IX. Variation of net second TLD readout (constant subtracted from second readout) with dose.

Slow Heat Rate			Fast Heat Rate		
Dose (rads)	Average Net Second Readout (Counts)	Standard Deviation (%)	Dose (rads)	Average Net Second Readout (Counts)	Standard Deviation (%)
1.26	530	49.9	-	-	-
4.49	3,188	18.3	4.63	576	47.8
36.5	23,604	14.4	36.5	8,656	11.9
88.2	66,166	14.4	88.2	24,792	21.2
140	207,360	9.15	140	52,426	18.2
192	317,186	9.18	-	-	-
243	515,144	19.3	-	-	-
346	770,882	12.9	346	168,924	10.6
450	1,201,908	18.4	-	-	-
656	2,130,780	9.76	656	476,504	20.7

the second readouts obtained for TLDs given doses above 1 rad. The average backgrounds determined earlier were subtracted from these second readouts to obtain the net second readout. Figure 30 illustrates the behavior of this quantity as a function of dose. The relationship exhibited appeared to be linear although the associated errors were relatively large. Thus, the second readouts were composed primarily of radiation induced TL which was not released during the first heating. Since the second readout was much smaller than the first, the range of the system could be increased to significantly higher doses if the errors could be reduced. Further study of this may allow improvements in these errors through variations in the readout cycle.

8.5 Comparison of Rods and Ribbons

The TL emitted by a heated TLD is as dependent on its mass as on the dose it received. Hence, lower doses can be measured using larger TLDs. High sensitivity ribbons supplied by Harshaw are 60% more massive than the rods used in the experiments discussed above and therefore can be expected to emit more TL per unit dose than the rods. Table X summarizes the data taken with these ribbons. Their effect on the system's readout is illustrated in Fig. 31 where these data are plotted with similar rod data. The least-squares slope of the line obtained using data from ribbon irradiations was calculated to be 860 counts/mrad and that of the rods to be 460 counts/mrad. Although these slopes were expected to differ by the same percentage as their masses, they did not. The ribbons were thinner than the rods, hence their thermal

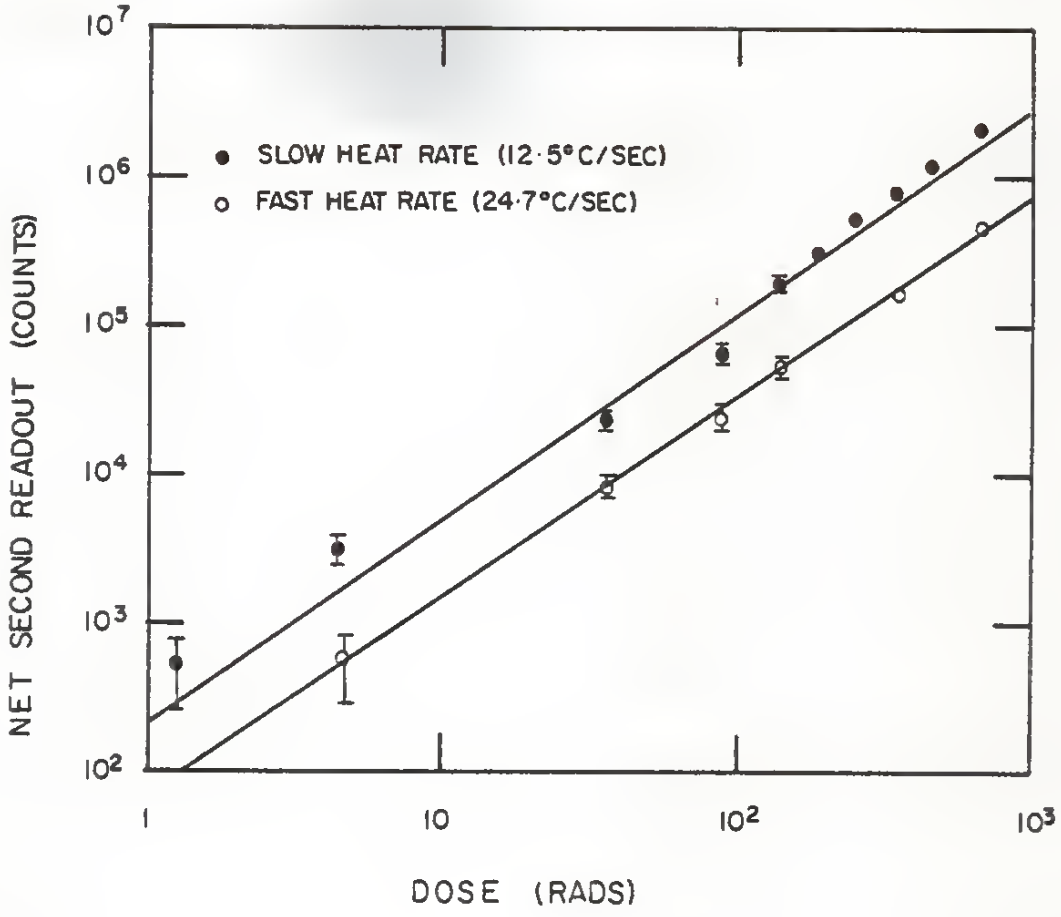

Fig. 30. Variation of the TLD net second readout with dose (rads in stainless steel). The net second readout quantity was obtained by subtraction of a constant background from the TLD's second readout. The straight line results from the linear least-squares fit to the data.

Table X. Calibration curve data utilizing larger TLD ribbons analyzed on the photon counting TLD analyzer using the fast-heat readout cycle.

Dose (mrad)	Number of Measurements	Average Signal (counts)	Standard Deviation (%)
0.61	4	657.5	9.66
0.94	5	950.6	8.65
1.62	4	1,425	8.74
2.18	5	2,036	6.68
4.82	4	4,443	1.53
8.50	5	7,359	2.67
18.7	2	16,142	5.06

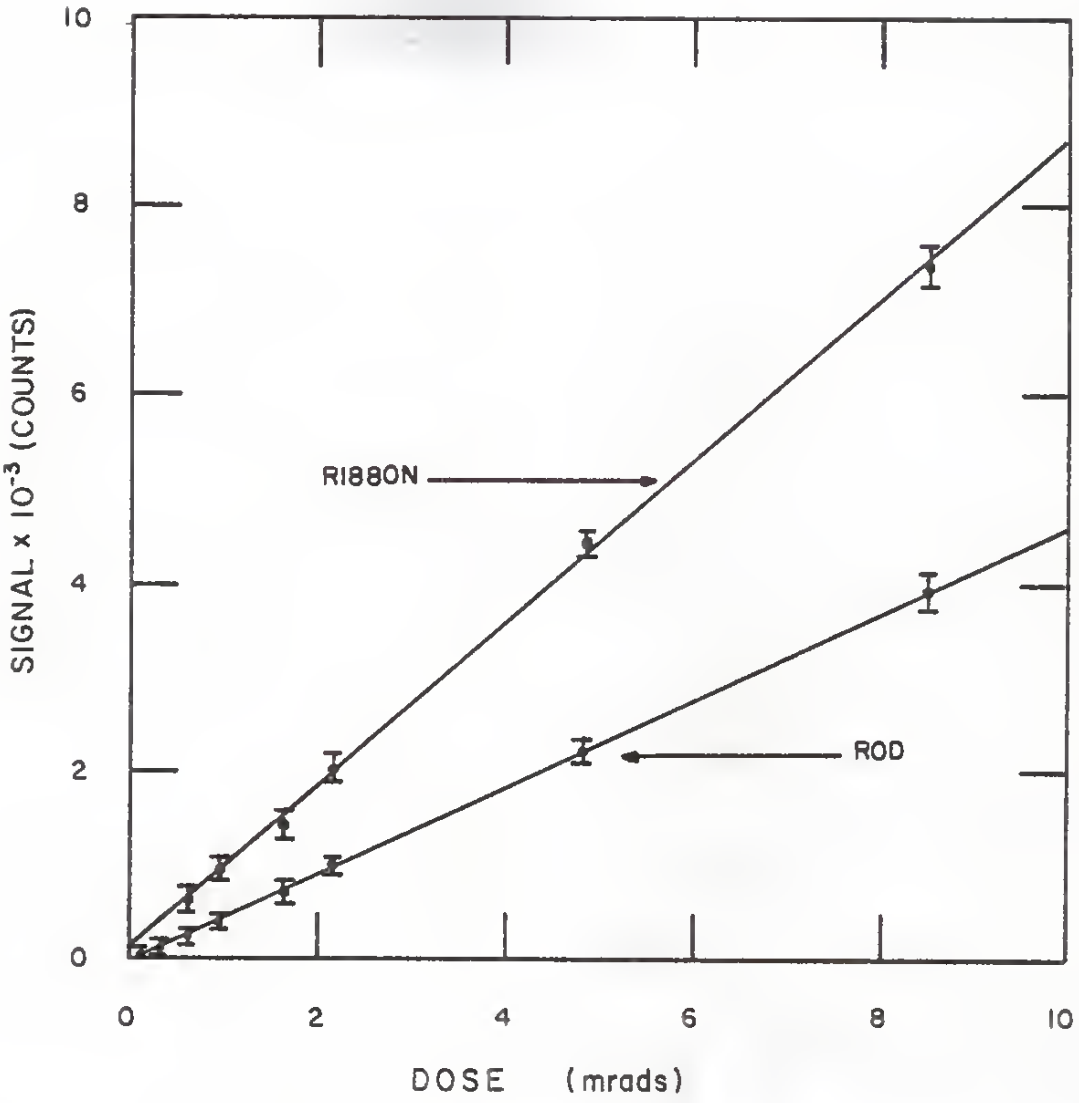

Fig. 31. Comparison of the signal obtained utilizing the photon counting TLD analyzer (fast-heat readout cycle) in conjunction with LiF (TLD-100) high sensitivity ribbons and rods. Dose is mrads in stainless steel and the straight lines result from linear least-squares fits to the data.

conductivity did not limit the heating of crystal as greatly as did the thermal conductivity of the rods. As a result, the radiation induced TL was more completely released from the ribbons than the rods. If the slope of the slow-heat readout calibration curve for the rods is compared to that of the ribbons (which were heated utilizing the fast-heat readout), a difference of 70% is noted, much closer to the 60% predicted.

9.0 Conclusions

The reproducibility of dose determinations using TLDs is as dependent on the techniques used during annealing and readout as it is on the system used for their readout. Therefore, no conclusions can be made on the performance of the photon counting TLD analysis system developed in this work without first stressing the importance of careful technique. Although the actual procedures utilized in the annealing process, for example, are important, reproducibility is more contingent upon consistency in these procedures. The dosimetry techniques recommended and utilized in this work may, then, be tailored to individual situations with little effect on the validity of the system's characteristics as described here, provided that consistency is maintained.

New LiF TLDs as received from the manufacturer exhibit a relatively wide range of sensitivities. For this reason, sensitivity selection should be utilized to identify those dosimeters with sensitivities either much less than or greater than the mean. These can then be either discarded from the set or used in conjunction with a sort correction factor. Some degradation of the precision with which dose determinations can be made utilizing any type of TLD analyzer system must be expected if this selection is not done. As manufacturing techniques improve, this requirement may be relaxed if all dosimeters can be delivered with sensitivities guaranteed to be within a small percentage of some nominal value.

One of the most important characteristics observed in the operation of the photon counting TLD analyzer was its excellent stability. This was indicated by the reduced affect of PMT fatigue. Very often, with dc-type TLD analyzers, fatigue causes a significant decrease in the system's output when a group of dosimeters given doses even less than 1 rad are processed. This has been observed in a commercial system operated at KSU as well as at other institutions. The photon counting system, on the other hand, was illuminated continuously for 8 hours with light from an LED whose photon emission rate corresponded to that observed from a TLD irradiated to approximately 100 rads and exhibited no decrease in its output. Because of this improvement alone, it seems it would be desirable to use neutral density optical filters in conjunction with the photon counting TLD analyzer system to measure doses currently outside its upper dynamic range.

TLDs are currently being used in personnel dosimetry work in an attempt to measure doses slightly above background. The errors in these measurements tend to be very large regardless of the dosimeter utilized. The use of this photon counting TLD analyzer would enable dose determinations as low as 1 mrad (in stainless steel) with a reproducibility error of nominally 10%. Additionally, a dose of 600 μrad is measurable with an error of 20%. Above about 10 mrad, the error becomes less than 3%. This system has a range which should certainly be sufficient for personnel dosimetry since it extends to 100 rads. For extreme accident situations, however, where the dose

level might exceed this, the second readout analysis could be used as an indication of the higher dose level. The photon counting system also showed itself applicable as a high volume dosimetry service tool. This was apparent as little degradation of its reproducibility was exhibited when both a fast readout cycle and a single heating readout process were utilized.

The photon counting TLD analysis system examined in this work was shown to have a number of significant advantages over dc-type systems. These were of such importance that its major disadvantage, i.e., its limited upper range, could be tolerated. In fact, significant work could be economically spent in its extension through both second readout techniques and neutral density optical filters.

10.0 Suggestions for Further Study

Following the completion of virtually any research project, proposals for additional study become apparent. There are basically two areas in which suggestions for further study have evolved from this work. The first of these involves research into TLD characteristics.

Sensitivity variations among TLDs appear to limit the accuracy with which dose measurements can be made. Although these variations between individual dosimeters degrade reproducibility in dose measurements, actual variations in the response of a single TLD to identical doses are important. This was illustrated when the application a sort correction factor failed to improve the scatter of data with sensitivities near the mean for a particular set. Hence, further research into the variation in response of a single TLD seems necessary. A possible procedure would be the irradiation and readout of a small number of dosimeters a large number of times to determine the distribution of their individual responses. These TLDs should be given low doses to minimize variations which might be induced by radiation damage. This is an obvious application for the photon counting TLD analyzer.

Another TLD characteristic which requires further research concerns the linearity of second readouts with higher doses. If the increased background, i.e., the second readout, is due to a higher temperature glow peak, then an obvious range extension for the photon counting system would be to make the second readout heat cycle extend

to higher temperatures to release more TL. This would, of course, be contingent upon the first readout exceeding the system's linearity. By releasing more TL, the accuracy with which second readout dose determinations could be made might improve.

The second area in which further study is necessary concerns improvements on and applications of the photon counting TLD analyzer. An obvious improvement in the system's upper range might be realized using neutral density optical filters. A circuit could be built allowing the microprocessor to mechanically insert a filter into the optical path of the TLD's emission once it sensed a certain photon emission rate was being exceeded. Various software techniques could then be used to account for the filter's presence and then display the desired quantity.

The lower range of the photon counting TLD analyzer might be improved upon by changing the PMT optimization procedure to weight SNR more heavily. This could be done in two ways. The most obvious is to set the discriminator level towards the upper end of the plateau in the integral pulse height distribution instead of in the center. The other is to weight the PMT voltage optimization constant with some power of NS^2R instead of simply NS^2R. It is absolutely necessary to repeat the fatigue test to insure that no degradation in the system's fatigue characteristics have been induced. This should be done regardless of which of the two suggestions are utilized.

Areas in which the photon counting TLD analyzer might be applied should also be investigated. Neutron dosimetry is an obvious area where the system's application might be beneficial. Another important

area would be its application in conjunction with dosimeter materials other than LiF which are more sensitive to radiation, i.e., emit greater amounts of TL per unit dose, such as CaF_2.

11.0 Acknowledgements

The author wishes to express his sincere appreciation to Dr. G. G. Simons for his guidance and encouragement throughout this research and especially for his diligence in reviewing it. Special thanks are also extended to Argonne National Laboratory for loaning Kansas State University much of the instrumentation utilized in the construction of this system, and to the KSU Engineering Experiment Station for funding the remainder. Financial support provided by the Department of Nuclear Engineering is gratefully acknowledged.

Finally, the author wishes to thank his wife, Janelle, for her love and understanding and to express his appreciation for the encouragement and support of his parents, John and Betty Hanna, without which this would not have been possible.

References

1. K. K. Shvarts, Z. A. Grant, E. A. Nemiro, M. M. Grube, and D. J. Gubatova, "Physical Principles of Thermoluminescent Dosimetry and Parameters of the Applied Detectors," Fourth Int. Conf. Lum. Dos., Krakow-Poland, 1 (1974).

2. M. J. Aitken, J. C. Alldred, and J. Thompson, "A Photon-Ratemeter System for Low-Level Thermoluminescence Measurements," Proc. Sec. Int. Conf. Lum. Dos., Gatlinburg, 248 (1968).

3. Per Spanne, "Comparison of Photon Counting and Charge Integration as Signal Registration Methods in Low-Dose TL Measurements," Fourth Int. Conf. Lum. Dos., Krakow-Poland, 597 (1974).

4. R. H. Schneider, W. P. Kirk, J. F. Steiner, Jr., and H. J. L. Rechen, "Photon Counter for the Measurement of Thermoluminescence," Rev. Sci. Instr. 39, 1369 (1968).

5. J. B. Lasky, D. W. Pearson, and P. R. Moran, "A Photon Counting System for Thermoluminescent Dosimetry," USAEC Report COO-1105-188 (1973).

6. T. Niewiadomski, "Determination of Optimum Conditions for Photon Counting in Thermoluminescence Measurements," IAEA-SM-160, 199 (1972).

7. T. Schlesinger, A. Avni, and Y. Feige, "Photon Counting as Applied to Thermoluminescence Dosimetry," Riso Report 249 (Danish Atomic Energy Commission Establishment, Riso), 226 (1971).

8. J. T. Randall and M. H. F. Wilkins, Proc. Roy. Soc. (London) A184, 365 (1945).

9. Toshiyuki Nakajima, "Theoretical Consideration on Thermoluminescence Response," J. Appl. Phys. 48, 4880 (1977).

10. W. Fichtner and W. Hacker, "Time Resolution of Ge Avalanche Photodiodes Operating as Photon Counters in Delayed Coincidence," Rev. Sci. Instr. 47, 374 (1976).

11. G. A. Morton, "Photon Counting," Appl. Opt. 7, 1 (1968).

12. D. J. Fegan, and P. G. Craven, "Low-Noise Photon Counting System Using the Photosil Detector," J. Phys. E: Sci. Instr. 10, 510 (1977).

13. M. O. Scully and M. Sargent III, "The Concept of the Photon," Physics Today, 38 (March 1972).

14. RCA Corp., Phototubes and Photocells Manual, Technical Series PT-60, Lancaster, Pa.

15. M. L. Franklin, G. Horlick, and H. V. Malmstadt, "Basic and Practical Considerations in Utilizing Photon Counting for Quantitative Spectrochemical Methods," Analytical Chemistry 41, 2 (1969).

16. H. V. Malmstadt, M. L. Franklin, and G. Horlick, "Photon Counting for Spectrophotometry," Analytical Chemistry 44, 63A (1972).

17. J. S. Gethner and G. W. Flynn, "Evaluation of Photomultiplier Tubes for Use in Photon Counting Correlation Spectroscopy," Rev. Sci. Instr. 46, 586 (1975).

18. Andrew T. Young, "Cosmic Ray Induced Dark Currents in Photomultipliers," Rev. Sci. Instr. 37 (1966).

19. R. Foord, R. Jones, C. J. Oliver, and E. R. Pike, "The Use of Photomultiplier Tubes for Photon Counting," Appl. Opt. 8, 1975 (1969).

20. R. Jones, C. J. Oliver, and E. R. Pike, "Experimental and Theoretical Comparison of Photon Counting and Current Measurements of Light Intensity," Appl. Opt. 10, 1673 (1971).

21. A. A. Cafolla, J. N. Carter, C. F. G. Delaney, and I. R. McDonald, "A Computation on Secondary Electron Emission Statistics and its Application to Single Electron Spectra in Photo- and Electron Multipliers," Nucl. Inatr. and Meth. 128, 157 (1975).

22. J. D. Ingle, Jr., and S. R. Crouch, "Critical Comparison of Photon Counting and Direct Current Measurement Techniques for Quantitative Spectrometric Methods," Analytical Chemistry 44, 785 (1972).

23. B. Leskovar and C. C. Lo, "Single Photoelectron Time Spread Measurement of Fast Photomultipliers," Nucl. Instr. and Meth. 123, 145 (1975).

24. B. Leskovar, C. C. Lo, P. R. Hartig, and K. Sauer, "Photon Counting System for Subnanosecond Fluorescence Lifetime Measurements," Rev. Sci. Instr. 47, 1113 (1976).

25. M. R. Zatzick, "Applying Digital Techniques to Photon Counting," Research/Development (Nov. 1970).

26. E. J. Darland, G. E. Leroi, and C. G. Enke, "Pulse (Photon) Counting: Determination of Optimum Measurement System Parameters," Analytical Chemistry 51, 240 (1979).

27. Max Garbuny, Optical Physics, Academic Press, New York (1965).

28. M. E. A. Robertson and W. B. Gilboy, "Techniques for Reducing Systematic Errors in TLD Readers," Fourth Int. Conf. Lum. Dos., Krakow-Poland, 691 (1974).

29. G. G. Simons and T. S. Huntsman, "Precision of LiF Thermoluminescent Dosimeters Using Sensitivity Selection," Argonne National Laboratory (Unpublished Technical Memo., ZPR-TM-200)(1975).

30. J. R. Cameron, N. Suntharalingan, and G. N. Kenney, Thermoluminescent Dosimetry, The University of Wisconsin Press (1968).

31. E. W. Mason, A. F. McKinlay, and I. Clark, "Cooling Rate Effects in Thermoluminescence Grade Lithium Fluoride. Implications for Practical Dosimetry," Phys. Med. Biol. 21, 60 (1976).

32. H. Vora, L. A. DeWerd, and T. G. Stoebe, "Influence of Lattice Defects on Thermoluminescence in LiF," Fourth Int. Conf. Lum. Dos., Krakow-Poland, 143 (1974).

33. B. Burgkhardt, R. Herrera, and E. Piesch, "Fading Characteristics of Different Thermoluminescent Dosimeters," Nucl. Instr. and Meth. 137, 41 (1976).

34. P. C. Hsu and P. S. Weng, "Calibration of Thermoluminescent Dosimeters for Low Exposure Rates," Nucl. Instr. and Meth. 138, 307 (1976).

35. Klaus Becker, Solid State Dosimetry, CRC Press (1973).

36. F. M. Cox, A. C. Lucas, and B. M. Kapsar, "The Reusability of Solid Thermoluminescent Dosimeters and its Relation to the Maintenance of TL Standards," Health Physics 30, 135 (1976).

Appendix A

Microprocessor Software

The software program described in this Appendix was utilized to control the operation of the photon counting TLD analyzer system. A flow diagram illustrating the basic approach used is shown in Fig. A-I. This program runs continuously following initiation and was written such that each TLD is heated twice. Additionally, a short beep is utilized to mark the occurrence of the beginning and ending of the photon counter's integration period. A series of short beeps followed by a constant buzz notifies the operator to replace the TLD. The constant buzz stops once the operator opens the sample drawer to change TLDs. The temperatures T_H and T_L control the counter integration period and are adjustable via the temperature comparator reference potentiometers. This program was written for RAM although only one memory location is utilized by it for temporary data storage. Hence it may be placed (at the same addresses) in ROM provided a temporary storage location is available in RAM. The software listing follows Fig. A-1.

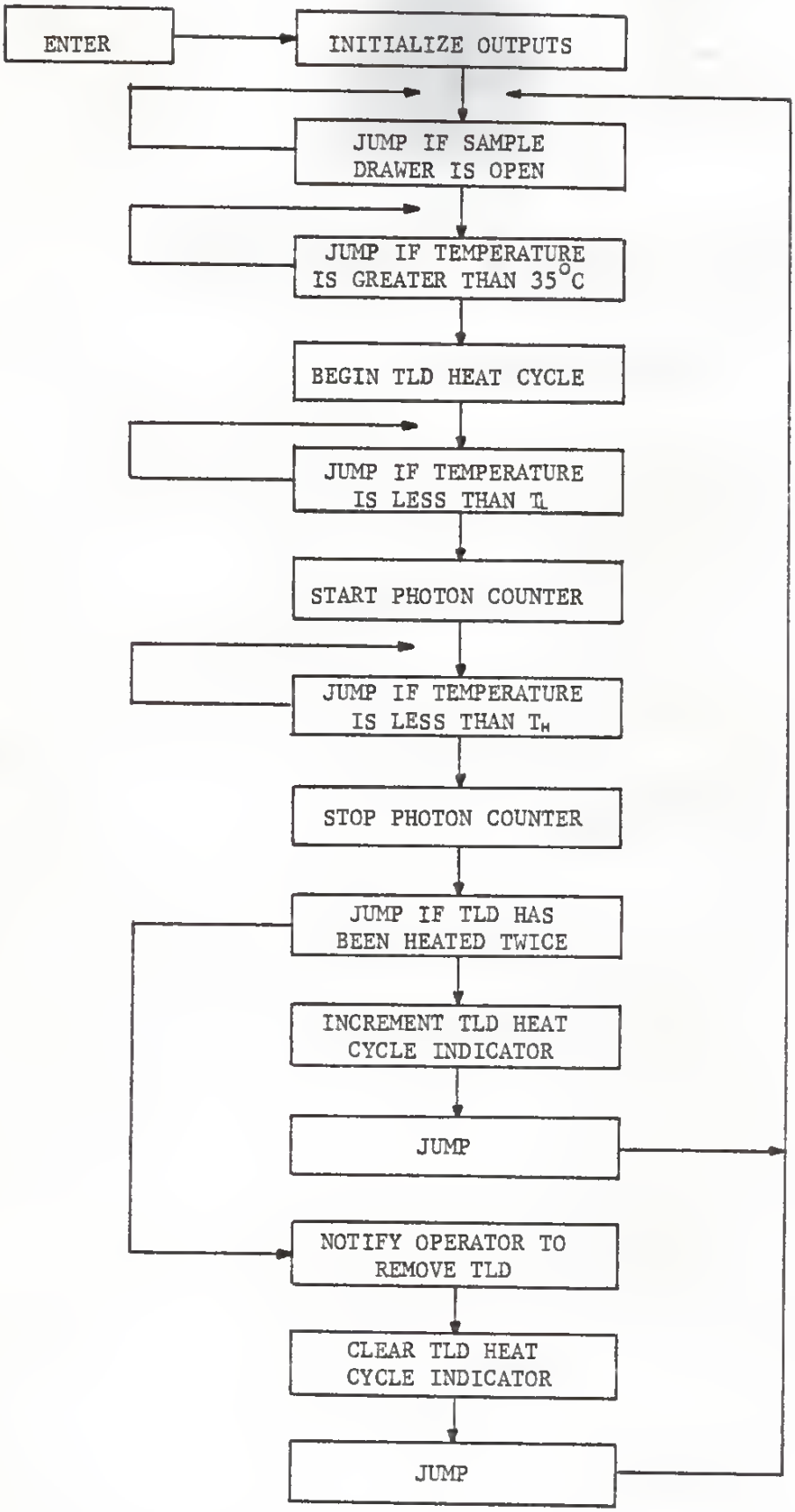

Fig. A-1. Microprocessor software flow diagram.

MEMORY LOCATION	MNEMONIC	OP CODE	COMMENTS
003-000	MVI A	076	Initialize outputs
-001	000	000	
-002	OUT	323	
-003	001	001	
-004	MVI B	006	Clear Cycle counter
-005	000	000	
-006	IN	333	Get drawer status
-007	004	004	
-010	RAR	037	
-011	JC	332	Jump if open
-012	006	006	
-013	003	003	
-014	RAR	037	
-015	JC	332	Jump if temperature greater than $35^{\circ}C$
-016	006	006	
-017	003	003	
-020	MVI A	076	Begin Heat Cycle
-021	020	020	
-022	OUT	323	
-023	001	001	
-024	CALL	315	Notify operator
-025	000	000	
-026	002	002	
-027	IN	333	
-030	004	004	
-031	ANI	346	
-032	010	010	
-033	JZ	312	Jump if temperature less than T_1
-034	027	027	
-035	003	003	
-036	MVI A	076	
-037	004	004	
-040	OUT	323	Reset counter
-041	001	001	
-042	MVI A	076	
-043	006	006	
-044	OUT	323	Start counter
-045	001	001	
-046	CALL	315	Notify operator
-047	150	150	
-050	002	002	
-051	IN	333	
-052	004	004	
-053	ANI	346	
-054	020	020	
-055	JZ	312	Jump if temperature less than T_h
-056	051	051	
-057	003	003	
-060	MVI A	076	
003-061	024	024	

MEMORY LOCATION	MNEMONIC	OP CODE	COMMENTS
003-062	OUT	323	Stop counter and Heat Cycle
-063	001	001	
-064	MVI A	076	
-065	000	000	
-066	OUT	323	Initialize outputs
-067	001	001	
-070	MOV A,B	170	
-071	CPI	376	
-072	000	000	
-073	JNZ	302	Jump if TLD read out twice
-074	105	105	
-075	003	003	
-076	CALL	315	Notify operator
-077	000	000	
-100	002	002	
-101	INR B	004	Increment Cycle counter
-102	JMP	303	
-103	006	006	
-104	003	003	
-105	DCR B	005	Decrement Cycle counter
-106	CALL	315	Notify operator
-107	050	050	
-110	002	002	
-111	JMP	303	Return for next Heat Cycle
-112	006	006	
003-113	003	003	
002-000	MVI A	076	
-001	010	010	
-002	OUT	323	Start Buzzer
-003	001	001	
-004	MVI C	016	
-005	030	030	
-006	CALL	315	Delay about ½ second
-007	277	277	
-010	000	000	
-011	DCR C	015	
-012	JNZ	302	
-013	006	006	
-014	002	002	
-015	MVI A	076	
-016	000	000	
-017	OUT	323	Stop Buzzer
-020	001	001	
002-021	RET	311	
002-050	MVI D	026	
-051	300	300	
-052	CALL	315	Alternate Buzzer ON and OFF
-053	000	000	
002-054	002	002	

MEMORY LOCATION	MNEMONIC	OP CODE	COMMENTS
002-055	CALL	315	
-056	277	277	
-057	000	000	
-060	DCR D	025	
-061	JNZ	302	
-062	055	055	
-063	002	002	
-064	IN	333	
-065	004	004	
-066	ANI	346	
-067	004	004	
-070	JNZ	302	Jump if temperature greater than 60°C
-071	050	050	
-072	002	002	
-073	MVI A	076	
-074	010	010	
-075	OUT	323	Turn Buzzer ON
-076	001	001	
-077	IN	333	
-100	004	004	
-101	RAR	037	
-102	JNC	322	Jump if drawer closed
-103	077	077	
-104	002	002	
-105	MVI A	076	
-106	000	000	
-107	OUT	323	Turn Buzzer OFF
-110	001	001	
002-011	RET	311	
002-150	MVI A	076	
-151	016	016	
-152	OUT	323	Turn Buzzer ON
-153	001	001	
-154	MVI C	016	
-155	030	030	
-156	CALL	315	Delay about ½ second
-157	277	277	
-160	000	000	
-161	DCR C	015	
-162	JNZ	302	
-163	156	156	
-164	002	002	
-165	MVI A	076	
-166	006	006	
-167	OUT	323	Turn Buzzer OFF
-170	001	001	
002-171	RET	311	

Appendix B

Raw Data

This Appendix contains a series of tabular compilations of the raw data taken for both optimization and calibration of the photon counting TLD analyzer system.

Table B-I. Data taken with PAR photon counting system for construction of integral pulse-height distributions.

PMT VOLTAGE (volts)	DISCRIMINATOR LEVEL (mV)	5 min COUNT (DARK)	5 min COUNT (LED-0.3uA)	SIGNAL (COUNTS)
	0.2	15,978	139,877	123,899
	0.3	14,882	135,757	120,875
	0.4	13,778	132,490	118,712
	0.5	12,771	128,107	115,336
	0.6	12,874	124,730	111,856
1950	0.7	12,294	120,678	108,384
	0.8	11,689	115,872	104,183
	0.9	11,236	107,855	96,619
	1.0	10,547	103,533	92,986
	1.2	9,270	89,588	80,318
	1.5	6,363	55,366	49,003
	0.2	17,621	144,569	126,948
	0.4	15,565	136,421	120,856
	0.5	14,477	134,165	119,688
	0.6	14,211	131,211	117,000
2000	0.8	12,873	124,066	111,193
	1.0	12,578	117,922	105,344
	1.2	11,938	107,551	95,613
	1.5	10,053	91,934	81,881
	1.8	7,968	65,809	57,841
	0.2	18,769	147,971	129,202
	0.4	17,070	141,825	124,755
	0.6	15,630	136,126	120,496
	0.8	15,046	130,781	115,735
2050	1.0	13,993	125,080	111,087
	1.2	13,454	120,259	106,805
	1.5	12,353	111,845	99,492
	1.8	11,528	100,929	89,401
	2.1	8,817	66,312	57,495
	0.2	22,094	153,662	131,568
	0.4	17,760	144,040	126,280
	0.6	17,128	139,429	122,301
	0.8	16,477	135,487	119,010
	1.0	15,620	131,218	115,598
2100	1.2	14,600	127,277	112,677
	1.5	14,058	122,519	108,461
	1.8	13,196	116,161	102,965
	2.1	12,064	104,793	92,729
	2.4	10,548	89,744	79,196
	2.7	8,651	67,336	58,658

Table B-I continued

PMT VOLTAGE (volts)	DISCRIMINATOR LEVEL (mV)	5 min COUNT (DARK)	5 min COUNT (LED-0.3uA)	SIGNAL (COUNTS)
	0.2	24,674	157,768	133,094
	0.4	20,797	148,084	127,287
	0.6	18,750	144,727	125,977
	0.8	18,491	139,999	121,508
	1.0	17,243	136,232	118,989
	1.2	17,062	133,756	116,694
2150	1.5	16,036	129,551	113,515
	1.8	14,693	124,028	109,335
	2.1	14,322	118,492	104,170
	2.4	13,473	111,060	97,587
	2.7	11,890	101,115	89,225
	3.0	10,598	84,086	73,488
	4.0	9,384	61,114	51,730
	0.2	29,625	162,812	133,187
	0.4	21,817	152,041	130,224
	0.6	20,067	146,558	126,491
	0.8	19,439	144,550	125,111
	1.0	19,066	141,343	122,277
	1.2	18,271	139,361	121,090
2200	1.5	17,558	134,724	117,166
	1.8	16,600	131,727	115,127
	2.1	15,968	127,194	111,226
	2.4	15,722	121,520	105,798
	2.7	14,583	115,019	100,436
	3.0	14,124	108,054	93,930
	4.0	12,633	98,821	86,188
	0.4	27,124	160,974	133,850
	0.6	23,474	152,411	128,937
	0.8	21,886	149,374	127,488
	1.0	20,872	145,915	125,043
	1.2	20,158	143,716	123,558
2250	1.5	19,621	139,893	120,272
	1.8	19,132	137,340	118,208
	2.1	18,693	133,818	115,125
	2.4	17,659	130,894	113,235
	3.0	16,568	120,723	104,155
	0.4	27,689	159,332	131,643
	0.8	24,342	153,188	128,956
	1.2	22,934	148,438	125,504
	1.5	21,876	145,110	123,234
	1.8	21,218	142,354	121,136
2300	2.1	20,622	141,017	120,395
	2.4	20,605	136,488	115,883
	3.0	18,978	130,087	111,109
	4.1	17,147	121,079	103,932
	5.1	16,025	108,245	92,220
	6.1	12,621	85,631	73,010

Table B-II. Data taken with PAR photon counting system to determine its linearity.

LED CURRENT (microamps)	COUNT RATE (cpm)
20.00	11,311,620
40.00	33,849,970
60.00	66,711,720
80.00	110,023,840
100.0	163,643,600
140.0	299,499,110
180.0	467,712,740
220.0	658,608,580
260.0	862,209,750
300.0	1,068,821,530
350.0	1,314,641,930
400.0	1,524,955,360
450.0	1,689,257,640
500.0	1,812,919,770
550.0	1,901,857,260
600.0	1,969,196,190
650.0	2,041,973,910
700.0	2,063,559,210

Table B-III. Data taken with PAR photon counting system to determine fatigue characteristics (PMT illuminated by LED (current = 150 μA), PMT at 2200 V, and discriminator level at 1.35 mV).

TIME	COUNT RATE (cps)
0.5min	5,541,719
2.5	5,534,565
4.5	5,526,913
6.5	5,521,636
8.5	5,518,085
10.5	5,515,911
12.5	5,515,456
14.5	5,515,897
19.5	5,518,123
24.5	5,519,066
29.5	5,519,256
34.5	5,517,991
39.5	5,518,128
44.5	5,518,190
49.5	5,517,452
54.5	5,517,183
59.5	5,516,551
1hr-05min	5,516,033
1-11	5,515,243
1-21	5,512,720
1-31	5,516,336
1-41	5,521,032
1-51	5,519,300
2-2.5	5,516,472
2-32.5	5,519,552
3-2.5	5,521,214
3-32.5	5,517,828
4-2.5	5,525,026
4-32.5	5,521,418
5-2.5	5,524,455
5-32.5	5,526,549
6-2.5	5,534,870
6-32.5	5,531,745
7-2.5	5,530,636
7-32.5	5,533,687
8-2.5	5,533,914

Table B-IV. Data taken with PAR photon counting system to determine fatigue characteristics (PMT illuminated by LED (current = 250 μA), PMT at 2200 V, and discriminator level at 1.35 mV).

TIME	COUNT RATE (cps)
0.5min	13,383,598
2.5	13,335,898
4.5	13,306,401
6.5	13,296,287
8.5	13,289,411
10.5	13,286,740
12.5	13,282,059
14.5	13,278,938
19.5	13,261,709
24.5	13,244,611
29.5	13,245,717
34.5	13,243,704
39.5	13,244,099
44.5	13,258,968
49.5	13,257,903
54.5	13,259,448
59.5	13,257,420
1hr-2.5min	13,256,370
1-32.5	13,253,142
2-2.5	13,255,199
2-32.5	13,257,667
3-2.5	13,251,648
3-32.5	13,248,315
4-2.5	13,263,419
4-32.5	13,265,186
5-2.5	13,258,543
5-32.5	13,264,455
6-2.5	13,264,205
6-32.5	13,253,911
7-2.5	13,258,127
7-32.5	13,252,576
8-2.5	13,251,822

Table B-V. Data taken with PAR photon counting system to determine fatigue characteristics (PMT illuminated by LED (current = 350 μA), PMT at 2200 V, and discriminator level at 1.35 mV).

TIME	COUNT RATE (cps)
0.5min	21,778,964
2.5	21,800,769
4.5	21,790,884
6.5	21,771,687
8.5	21,767,844
10.5	21,770,898
12.5	21,773,601
14.5	21,780,010
19.5	21,786,144
24.5	21,781,408
29.5	21,784,476
34.5	21,787,804
39.5	21,798,920
44.5	21,805,390
49.5	21,803,984
54.5	21,807,999
59.5	21,809,481
1hr-2.5min	21,808,648
1-32.5	21,822,577
2-2.5	21,814,946
2-32.5	21,807,567
3-2.5	21,804,714
3-32.5	21,805,414
4-2.5	21,814,016
4-32.5	21,828,445
5-2.5	21,834,233
5-32.5	21,841,177
6-2.5	21,841,445
6-32.5	21,837,075
7-2.5	21,838,373
7-32.5	21,839,452
8-2.5	21,840,531

Table B-VI. Calibration data for photon counting TLD analyzer using dosimeters in group 1 heated using the slow heat cycle (integral count analysis).

TLD NUMBER	DOSE (mrad)	TRIAL 1		TRIAL 2	
		FIRST READOUT (COUNTS)	SECOND READOUT (COUNTS)	FIRST READOUT (COUNTS)	SECOND READOUT (COUNTS)
1		1,009	750	816	858
2		946	800	792	755
3	0.11	868	783	884	780
4		943	827	825	787
5		1,002	790	920	801
6		1,018	723	1,179	832
7		1,005	872	845	793
8	0.31	998	717	1,004	891
9		923	868	1,051	822
10		945	904	921	804
11		1,245	837	1,158	741
12		1,054	726	1,231	800
13	0.61	1,109	848	1,104	848
14		1,124	822	1,109	786
15		1,013	750	1,030	730
16		1,421	855	1,122	723
17		1,080	659	1,248	704
18	0.94	1,348	823	1,156	668
19		1,228	705	1,269	785
20		1,175	650	1,156	672
21		1,640	716	1,605	832
22		1,604	759	1,450	595
23	1.62	--	--	1,724	823
24		1,548	632	1,483	705
25		1,680	680	1,576	758

Table B-VI continued

TLD NUMBER	DOSE (mrad)	TRIAL 1		TRIAL 2	
		FIRST READOUT (COUNTS)	SECOND READOUT (COUNTS)	FIRST READOUT (COUNTS)	SECOND READOUT (COUNTS)
26		1,834	637	1,858	734
27		1,700	580	1,698	618
28	2.18	1,909	783	1,784	858
29		1,801	800	1,907	772
30		1,569	554	1,833	824
31		3,004	494	3,051	781
32		3,116	810	2,947	836
33	4.82	2,880	789	2,986	852
34		2,928	564	2,947	786
35		2,920	835	3,144	797
36		4,893	459	5,223	952
37		5,046	824	4,874	970
38	8.50	4,958	644	5,444	878
39		4,900	664	4,918	805
40		5,056	788	4,925	811
41		9,732	604	10,027	670
42		9,582	780	9,995	851
43	18.7	9,589	646	9,736	726
44		9,338	590	10,045	957
45		9,311	555	9,426	758
46		31,903	923	31,952	931
47		31,683	649	31,396	699
48	67.1	30,947	514	31,666	738
49		29,866	589	30,030	831
50		29,521	633	31,388	748

Table B-VI continued

TLD NUMBER	DOSE (RAD)	FIRST READOUT (COUNTS)	SECOND READOUT (COUNTS)
51		103,510	720
52		106,650	660
53	0.208	106,260	760
54		107,740	800
55		102,320	670
56		280,890	880
57		294,240	850
58	0.570	285,270	950
59		278,400	950
60		292,500	660
61		621,030	1,610
62		638,740	940
63	1.26	623,500	1,400
64		632,230	1,100
65		637,770	1,370
66		2,224,000	4,870
67		2,258,910	3,440
68	4.49	2,334,490	3,550
69		2,263,900	4,150
70		2,170,840	3,700

Table B-VI continued

TLD NUMBER	TIME IN GAMMA CELL (SEC)	DOSE (RAD)	FIRST READOUT (COUNTS)	SECOND READOUT (COUNTS)
71			17,338,850	28,150
72			16,890,030	27,500
73	0	36.5	17,757,230	21,990
74			17,004,070	20,350
75			16,537,610	23,800
76			41,655,900	66,090
77			41,883,520	71,250
78	5	88.2	44,402,540	77,130
79			45,061,510	68,560
80			43,268,310	51,570
71			63,469,930	201,700
72			62,022,450	186,080
73	10	140	65,296,230	237,790
74			63,604,438	203,450
75			60,993,750	211,550
76			80,729,110	327,820
77			78,649,200	325,870
78	15	192	82,314,500	356,980
79			83,506,130	282,790
80			80,513,940	296,240
81			96,680,010	518,290
82			96,567,040	461,010
83	20	243	97,033,460	518,940
84			98,046,220	407,980
85			97,458,220	673,270
86			121,119,550	727,250
87			120,810,640	861,040
88	30	346	121,820,820	640,900
89			124,876,510	879,930
90			118,190,170	749,060
91			141,920,800	1,362,230
92			140,350,530	917,020
93	40	450	138,888,570	1,477,510
94			145,525,820	1,103,920
95			140,359,180	1,152,630
96			163,403,470	2,370,010
97			165,104,300	2,325,000
98	60	656	166,801,670	2,091,250
99			168,052,750	1,923,170
100			161,543,350	1,948,240

Table B-VII. Calibration data for photon counting TLD analyzer using dosimeters in group 2 heated using the slow heat cycle (integral count analysis).

TLD NUMBER	DOSE (mrad)	TRIAL 1		TRIAL 2		TRIAL 3	
		FIRST READOUT (COUNTS)	SECOND READOUT (COUNTS)	FIRST READOUT (COUNTS)	SECOND READOUT (COUNTS)	FIRST READOUT (COUNTS)	SECOND READOUT (COUNTS)
1		926	807	801	847	777	642
2		916	971	834	820	917	925
3	0.11	774	710	938	906	784	701
4		987	925	973	885	759	845
5		960	982	970	976	988	821
6		1,003	938	1,097	905	976	731
7		884	708	1,040	806	1,013	963
8	0.31	1,130	935	1,159	980	1,018	938
9		1,009	885	999	893	943	742
10		951	838	988	892	893	831
11		1,164	978	1,238	942	1,028	850
12		1,040	756	1,010	810	1,082	801
13	0.61	1,138	831	1,128	863	1,011	796
14		1,038	805	1,201	912	1,020	859
15		1,077	795	1,285	952	1,160	794
16		1,321	992	1,280	778	1,206	896
17		1,095	648	1,050	671	--	--
18	0.94	1,570	1,100	1,566	1,186	1,228	806
19		1,070	702	1,379	925	1,240	832
20		1,550	1,139	1,355	879	1,213	647
21		1,437	807	1,740	1,022	1,516	872
22		1,637	967	1,729	1,009	1,510	815
23	1.62	1,725	1,084	1,633	785	1,508	645
24		1,752	1,052	1,606	1,023	1,695	813
25		1,698	1,030	1,738	1,018	1,420	804

Table B-VII continued

TLD NUMBER	DOSE (mrad)	TRIAL 1		TRIAL 2		TRIAL 3	
		FIRST READOUT (COUNTS)	SECOND READOUT (COUNTS)	FIRST READOUT (COUNTS)	SECOND READOUT (COUNTS)	FIRST READOUT (COUNTS)	SECOND READOUT (COUNTS)
26		--	--	1,857	812	1,774	783
27		--	--	1,762	749	1,689	573
28	2.18	--	--	1,839	854	1,835	931
29		--	--	1,796	780	1,696	689
30		--	--	2,000	860	1,782	676
31		2,828	614	2,861	646	2,924	699
32		3,038	860	2,943	780	2,926	784
33	4.82	3,145	875	3,090	792	3,184	865
34		2,966	644	2,933	888	2,902	777
35		3,118	952	3,203	827	2,927	688
36		4,946	1,177	4,892	875	5,065	809
37		4,649	956	4,698	822	4,800	670
38	8.50	4,630	815	4,808	1,012	4,724	682
39		4,584	724	4,823	729	4,631	620
40		4,550	712	4,665	755	4,481	688
41		8,953	740	8,947	768	9,063	789
42		9,152	1,138	9,272	981	9,264	730
43	18.7	9,347	853	9,338	790	9,134	714
44		8,699	884	8,811	781	8,600	770
45		8,889	778	9,459	681	9,040	706
46		29,617	1,056	31,348	898	30,086	719
47		30,159	737	30,690	744	29,524	583
48	67.1	26,869	909	31,581	799	30,449	701
49		30,127	864	29,518	723	30,014	692
50		30,193	1,053	31,819	838	30,488	825

Table B-VII continued

TLD NUMBER	DOSE (RAD)	FIRST READOUT (COUNTS)	SECOND READOUT (COUNTS)
51		97,060	660
52		94,720	750
53	0.215	96,880	640
54		96,470	770
55		95,400	770
56		268,890	740
57		270,280	760
58	0.586	277,640	630
59		275,540	600
60		277,930	630
61		561,720	800
62		566,780	780
63	1.29	556,450	820
64		551,150	760
65		546,320	730
66		2,045,790	1,500
67		2,053,540	1,300
68	4.63	2,006,620	1,780
69		2,002,110	1,450
70		2,014,030	1,030

Table B-VII continued

TLD NUMBER	TIME IN GAMMA CELL (SEC)	DOSE (RAD)	FIRST READOUT (COUNTS)	SECOND READOUT (COUNTS)
71			16,533,240	9,890
72			16,203,000	7,720
73	0	36.5	16,384,670	9,800
74			16,008,100	9,640
75			16,180,940	10,410
76			35,431,950	22,360
77			36,815,640	27,790
78	5	88.2	35,829,680	29,870
79			35,482,200	30,070
80			36,747,930	18,050
81			51,366,680	50,430
82			49,092,890	63,190
83	10	140	49,842,960	42,680
84			50,535,240	63,320
85			53,307,260	46,690
91			--	--
92			82,246,490	152,340
93	30	346	83,465,130	162,640
94			82,556,110	170,000
95			84,309,420	194,460
96			105,361,300	438,400
97			107,112,400	620,090
98	60	656	106,885,730	497,440
99			107,680,770	481,660
100			105,201,920	349,110

Table B-VIII. Calibration data for photon counting TLD analyzer using dosimeters in group 1 heated using the slow heat cycle (glow-peak height analysis).

TLD NUMBER	TRIAL 1		TRIAL 2	
	ANALOG PEAK HEIGHT (mV)	DIGITAL PEAK HEIGHT (cps)	ANALOG PEAK HEIGHT (mV)	DIGITAL PEAK HEIGHT (cps)
21	9.60	338	10.3	364
22	9.20	302	10.3	384
23	9.70	338	11.0	364
24	10.1	330	10.2	314
25	10.4	382	10.0	332
26	12.8	506	11.8	454
27	11.4	506	10.8	440
28	12.5	458	11.4	414
29	10.9	446	11.8	522
30	10.8	428	11.4	460
31	17.0	908	16.8	864
32	15.6	848	16.6	952
33	15.2	840	15.0	810
34	17.1	878	16.0	880
35	17.8	1,004	16.6	926
36	23.8	1,672	--	1,640
37	23.8	1,608	23.1	1,510
38	23.0	1,526	25.5	1,530
39	23.5	1,630	24.5	1,636
40	23.8	1,546	25.3	1,674
41	42.4	3,378	44.2	3,266
42	42.0	3,224	44.0	3,414
43	41.1	3,216	39.6	3,034
44	42.4	3,264	43.2	3,464
45	40.6	3,042	41.7	3,258
46	--	10,536	127	9,132
47	123	10,726	129	10,824
48	123	10,792	127	10,694
49	--	--	118	9,944
50	121	10,538	125	10,676

Table B-IX. Calibration data for photon counting TLD analyzer using dosimeters in group 2 heated using the fast heat cycle (glow-peak height analysis).

TLD NUMBER	TRIAL 1		TRIAL 2		TRIAL 3	
	ANALOG PEAK HEIGHT (mV)	DIGITAL PEAK HEIGHT (cps)	ANALOG PEAK HEIGHT (mV)	DIGITAL PEAK HEIGHT (cps)	ANALOG PEAK HEIGHT (mV)	DIGITAL PEAK HEIGHT (cps)
21	12.9	644	12.2	612	12.4	648
22	13.8	716	12.3	604	13.0	588
23	13.0	584	12.5	616	12.1	584
24	13.8	636	12.5	648	14.0	656
25	13.2	644	11.8	576	11.6	576
26	14.2	796	14.3	804	14.0	772
27	14.4	808	13.8	752	15.8	804
28	14.4	788	14.3	764	14.3	772
29	16.4	976	14.5	792	17.0	1,032
30	14.9	844	15.5	868	14.3	736
31	--	1,488	21.5	1,424	22.8	1,580
32	23.4	1,560	23.8	1,512	23.5	1,576
33	24.2	1,608	24.1	1,700	24.0	1,700
34	24.2	1,768	23.3	1,612	22.0	1,500
35	22.3	1,500	25.0	1,724	21.5	1,536
36	34.0	2,624	36.8	2,816	36.8	2,880
37	31.3	2,304	36.8	2,884	34.0	2,636
38	35.0	2,744	35.5	2,716	33.4	2,600
39	31.8	2,440	37.2	3,028	33.5	2,528
40	30.0	2,332	35.5	2,832	35.6	2,732
41	62.0	5,296	68.7	5,532	63.0	5,236
42	65.5	5,556	72.1	5,964	70.8	5,688
43	65.0	5,352	70.5	5,836	60.3	4,968
44	58.0	4,980	67.0	5,496	62.0	5,324
45	56.5	4,772	66.5	5,572	66.2	5,592
46	189	16,524	223	19,052	211	18,072
47	190	16,320	215	18,304	214	17,968
48	162	14,188	221	18,784	211	17,920
49	192	16,348	218	18,484	182	15,784
50	216	18,388	226	19,392	209	18,040

Table B-X. Calibration data for photon counting TLD analyzer for both the slow and fast heat cycles (glow peak height analysis).

TLD NUMBER	SLOW HEAT RATE		FAST HEAT RATE	
	ANALOG PEAK HEIGHT (mV)	DIGITAL PEAK HEIGHT (cps)	ANALOG PEAK HEIGHT (mV)	DIGITAL PEAK HEIGHT (cps)
51	--	3,826	70.0	--
52	--	3,872	64.0	--
53	--	3,874	73.0	12,660
54	45.0	3,870	73.0	12,416
55	42.3	3,518	70.0	12,032
56	--	10,292	188	17,388
57	119	11,158	192	18,048
58	112	10,414	200	18,960
59	112	10,288	191	18,560
60	120	11,006	190	17,828
61	--	22,636	385	46,615
62	241	23,276	412	39,312
63	237	22,098	394	37,468
64	246	22,746	396	37,184
65	248	22,920	382	36,968
66	837	79,232	1,420	--
67	861	82,488	1,390	--
68	904	84,992	1,410	--
69	870	80,820	1,400	--
70	829	79,272	1,390	--

Table B-XI. Data taken with large LiF ribbons (TLD-100, 1/8 x 1/8 x .035").

TLD NUMBER	DOSE (mrad)	FIRST READOUT (COUNTS)	SECOND READOUT (COUNTS)
1		1,419	755
2		1,183	561
3	0.61	1,175	575
4		1,812	1,068
5		--	--
6		1,746	889
7		1,632	744
8	0.94	1,701	704
9		1,890	829
10		1,726	776
11		--	--
12		2,560	969
13	1.62	2,295	1,005
14		2,065	668
15		2,326	904
16		2,821	930
17		2,838	741
18	2.18	2,759	869
19		2,854	724
20		3,078	904
21		--	--
22		5,180	762
23	4.82	5,334	791
24		5,295	905
25		5,412	991
26		7,971	857
27		7,965	777
28	8.50	8,255	742
29		8,347	916
30		8,331	781
31		16,445	880
32	18.7	17,476	757

DEVELOPMENT AND OPTIMIZATION OF A THERMOLUMINESCENT DOSIMETER (TLD) ANALYZER SYSTEM FOR LOW-DOSE MEASUREMENTS UTILIZING PHOTON COUNTING TECHNIQUES

by

DONALD WADE HANNA

B.S., Kansas State University, 1978

AN ABSTRACT OF A MASTER'S THESIS

submitted in partial fulfillment of the

requirements for the degree

MASTER OF SCIENCE

Department of Nuclear Engineering

KANSAS STATE UNIVERSITY
Manhattan, Kansas

1979

ABSTRACT

A thermoluminescent dosimeter (TLD) analyzer system utilizing photon counting techniques for signal registration was designed and evaluated for its low-dose measurement capabilities. A procedure is described whereby the photomultiplier tube applied voltage and the pulse-height discriminator level were optimized using signal-to-noise ratio (SNR) and stability as criteria. The system was operated under microprocessor control in order to minimize systematic readout errors. Additional errors were reduced by careful consideration of consistency in TLD handling and annealing procedures. Two TLD heating rates (12.5 °C/sec and 24.7 °C/sec) were investigated to determine their effect on reproducibility, at low doses, and system linearity, at high doses. The best data were obtained using the slower heating rate readout cycle. Although, little degradation of the system's characteristics were observed when the fast heating rate readout cycle was employed. The photon counting TLD analyzer's response to LiF (Harshaw Chemical Co. TLD-100) 1 x 1 x 6 mm high sensitivity rods irradiated to 1 mrad (in stainless steel) by a ^{137}Cs gamma-ray source exhibited reproducibility with a standard deviation of 10%. The system's reproducibility at a dose of 0.6 mrads had a standard deviation of 20% whereas doses above 10 mrad could be measured routinely and reproduced with a standard deviation of less than 3%. The dose at which the system's readout became nonlinear was 100 rads when the 12.5 °C/sec TLD heating rate was utilized. A comparison was made between these rods and larger

1/8 x 1/8 x 0.035" high sensitivity ribbons (Harshaw Chemical Co. TLD-100) concerning the light emitted per unit dose. It was concluded that the larger dosimeters emitted significantly more light and could, therefore, be utilized for lower dose measurements.